AMINOGLYCOSIDE-INDUCED MISTRANSLATION AND ITS CONSEQUENCES IN HIGHER EUKARYOTIC CELLS

Dissertation

zur

Erlangung der naturwissenschaftlichen Doktorwürde

(Dr. sc. nat.)

vorgelegt der

Mathematisch-naturwissenschaftlichen Fakultät

der

Universität Zürich

von

Stefan Duscha

aus

Deutschland

Promotionskomitee

Prof. Dr. Erik C. Böttger (Vorsitz)

Prof. Dr. Peter Sander

Prof. Dr. Roland K.O. Sigel

Zürich, 2015

Table of Contents

1 Acknowledgements

I am very obliged to all people who made this thesis possible. Without their supervision, support and help it would have been impossible.

First, I would like to thank Prof. Erik C. Böttger, who gave me the opportunity to do my thesis in his laboratory. Erik, I am deeply grateful, that you gave me the trust and freedom to accomplish own experiments and ideas. I highly appreciated your openness to new methods and questions, which made this thesis so exciting. Your guidance and input were a strong support to accomplish my PhD studies.

Next, I would like to thank the members of my committee Prof. Dr. Peter Sander and Prof. Dr. Roland K.O. Sigel. I greatly appreciated your support and the fruitful discussions during my studies.

I am deeply grateful to the former and current members of the Böttger group. I highly appreciated the supervision of Rashid Akbergenov and Dimitri Scherbakov, who were always helpful in solving problems and giving new ideas. I would like to thank Akshay Subramanian, for teaching me the secrets of ribosome purification, Tanja Matt, Martin Meyer, Heithem Boukari, Pietro Freihofer, Reda Juskeviciene, Youjin Teo, Thomas Schrepfer and last but not least Tanja Janusic. It was such a pleasure and great experience to work with you during the last years. I am also much obliged to Susanna Salas, who was always very supportive in administrative issues and during preparation of manuscripts.

Furthermore, I would like to thank the members of the other groups of the Institute for their help and support whenever it was necessary.

I also want to express my great appreciation to Prof. Jochen Schacht and his co-workers. This thesis greatly benefited by their provided ototoxicity data. Also I would like to thank Prof. Andrea Vasella, Prof. Venki Ramakrishnan and Prof. Richard Lee, collaborators of the Böttger group who developed new aminoglycosides, provided new insights into the ribosomal structure by crystallographic data and designed new spectinamide compounds, respectively. It was a great honor to be part of these successful collaborations.

The proteomics part of this thesis would not be possible without the excellent supervision from the staff of the Functional Genomic Center (FGCZ). I am very

obliged to Bernd Roschitzki who supervised my project, Claudia Fortes who helped me during sample preparation, Christian Trachsel and Jonas Grossmann who assisted me whenever I was in need.

Next, I would like to thank my parents who always supported me and helped me to be where I am now. Your unconditional support during hard times was invaluable for me and gave me the possibility to realize my dreams. I would like to thank my grandmother and grandfather, who unfortunately passed away 3 years ago, my brother Marcel, Yvonne and Henning for their mental support and sharing lots of happy hours. I also want to thank my other family part in Switzerland namely Melissa, Claudio, Anissa and Gian-Marco and in Peru namely Abraham, Carola, Gardenia, Omar, Azucena, Cesar and Catalina for the warm welcome you gave me and your heartiness.

Finally, I would like to dedicate my thesis to my wife Begonia. After we went through such a hard time, or love grew and made us stronger and happier. I am looking forward of spending my life with you and grow old and happy.

Te amo, Beguito!

2 Zusammenfassung

Das Ribosom ist der zentrale Ort der Proteinsynthese. Hier wird die genetische Information, die durch die messenger RNA kodiert wird in Polypeptidketten übersetzt, welche sich dann zu aktiven Proteinen falten. Die Beeinträchtigung der ribosomalen Translationsgenauigkeit führt zu Übersetzungsfehlern (Mistranslation), was fehlgefaltete und funktionsgestörte Proteine zur Folge hat.

Im Rahmen dieser Arbeit wurden die Auswirkungen der Mistranslation bei höheren Eukaryoten untersucht. Aminoglykoside wurden auf ihre Eigenschaft getestet die Translokation in Ribosomen höherer Eukaryoten zu hemmen und Übersetzungsfehler zu induzieren. Dazu wurden *in vitro* mittels Kaninchen Reticulozyten Lysat und *in vivo* mittels HEK293 Zellen duale Luciferase Assays etabliert. Das Aminoglykosid Geneticin zeigte in beiden Assays eine starke Induktion der Mistranslation. Im Gegensatz dazu induzierte das Aminoglykosid Hygromycin B keine Translationsfehler, obwohl die Inhibition der Translation vergleichbar mit derjenigen von Geneticin war. Die Bindungstelle von Hygromycin B in der ribosomalen Dekodierungsstelle ist einige Angström von der Geneticin Bindungsstelle entfernt. Mittels Kristallstruktur konnten unterschiedliche Konformationsänderungen der Nucleotide A1492 und A1493 gezeigt werden, welche entscheidend für die Decodierung sind. Um die zelluläre Reaktion auf Mistranslation zu untersuchen, wurde das Proteom von Geneticin und Hygromycin B behandelten HEK293 Zellen untersucht. Im Gegensatz zu Hygromycin B führte die Behandlung mit Geneticin zu einer ausgeprägten Aktivierung der *Unfolded Protein Response* im Endoplasmatischen Reticulum (erUPR) und der zytosolischen Hitzeschock-Antwort (zytoUPR). Daraus lässt sich schlussfolgern, dass Mistranslation in höheren Eukaryoten zur Fehlfaltung von Proteinen und zur Aktivierung der UPRs führt. Mehr als zwei Drittel der durch Geneticin induzierten Proteine sind Bestandteil des Proteinmetabolismus, d.b. Proteine welche bei der Proteinfaltung, Translation, Degradation, Transport und Signalübertragung bei proteotoxischen Stress involviert sind. Sowohl bei Hygromycin B als auch bei Geneticin behandelten Zellen, wurden Proteine der Proteinsynthese hochreguliert, was eine gemeinsame Reaktion auf die Inhibition der Translokation andeutet. Neben der gemeinsamen Induktion einiger Chaperone welche oxidativem Stress entgegenwirken, waren auch Schlüsselenzyme mitochondrialer metabolischer Aktivität herunterreguliert, was auf eine Rückkopplung

schliessen lässt, um die Menge mitochondrialer Sauerstoffradikale (ROS) zu verringern. Um oxidativem Stress direkt zu untersuchen, wurde die Bildung von ROS in HEK293 Zellen gemessen. Die Fähigkeit Sauerstoffradikale zu generieren korrelierte gut mit der Inhibition der zytosolischen Translation, wobei Geneticin und Hygromycin B die effektivsten ROS-Induktoren waren.

3 Summary

The ribosome is the central machinery in protein synthesis. Here, the genetic information encoded by the messenger RNA is translated into polypeptides, which fold into functional proteins. Impairment of ribosomal decoding accuracy results in mistranslation with the consequence of misfolded and non-functional proteins.

In this thesis the cellular response to mistranslation in higher eukaryotes was investigated. Aminoglycosides were studied for their efficacy to inhibit translation and to induce translation errors in ribosomes of higher eukaryotes. For this purpose *in vitro* and *in vivo* dual luciferase assays were established using rabbit reticulocyte lysate and HEK293 cells, respectively. Both *in vitro* and *in vivo*, the aminoglycoside geneticin was found to induce prominent read-through. In contrast, the aminoglycoside hygromycin B did not induce translational errors, although translation was inhibited comparable to geneticin. As per crystal structures the ribosomal binding site of hygromycin B is a few angstroms away from the binding site of geneticin, resulting in distinct conformational changes of key decoding nucleotides A1492 and A1493. To study the cellular response to mistranslation in HEK293 cells, quantitative proteome analyses were performed and the effect of geneticin and hygromycin B on the proteome was studied. In contrast to hygromycin B, geneticin treatment resulted in a prominent induction of the cytosolic heat shock response and the endoplasmatic reticulum unfolded protein response (erUPR), suggesting that mistranslation in higher eukaryotes leads to protein misfolding and to activation of UPRs. More than two thirds of the proteins upregulated by geneticin are involved in protein metabolism, *i.e.* protein folding, translation, degradation, protein transport and signal transduction. Geneticin and hygromycin B treated cells showed a common upregulation of components of the cytosolic translation machinery, indicating a mutual response to translation inhibition. In addition to a common minor subset of upregulated chaperones involved in scavenging of oxidative stress, key enzymes involved in mitochondrial metabolic activity were downregulated, pointing to a feedback mechanism to lower mitochondria-derived reactive oxygen species (ROS). To study ROS directly, we measured formation of oxidative stress in HEK293 cells. The ability to induce oxidative radicals correlated well with the drug's efficacy to inhibit cytosolic translation, with hygromycin B and geneticin as the most active ROS inducers.

4 Introduction

The correct conversion of genetic information into functional proteins is one of the most fundamental and complex processes in a cellular organism. The central apparatus for protein synthesis is a large ribonucleoprotein complex termed the ribosome. By using aminoacyl-transfer RNA (aa-tRNA) as substrates, the ribosome translates genetic information encoded by messenger RNA (mRNA) into polypeptides.

The ribosome consists of a small and a large subunit (Fig. 1). Decoding of the mRNA message into polypeptides takes place at the small ribosomal subunit. The functional sites of the small ribosomal subunit are the path for mRNA guidance during translation, the decoding center with the A-, the P- and E-sites. The A-site harbours the aminoacyl-tRNA, the P-site serves to bind the tRNA with the growing polypeptide chain (peptidyl-tRNA) and the E-site (Exit) is the place where the deacetylated tRNA leaves the ribosome. Analogous to the small ribosomal subunit, the large subunit has A, P and E- tRNA binding sites. The major functional sites of a large subunit are the peptidyl transferase center (PTC) where the amino-acid peptide bond is catalysed and the peptide exit tunnel where the growing polypeptide chain is released from the ribosome.

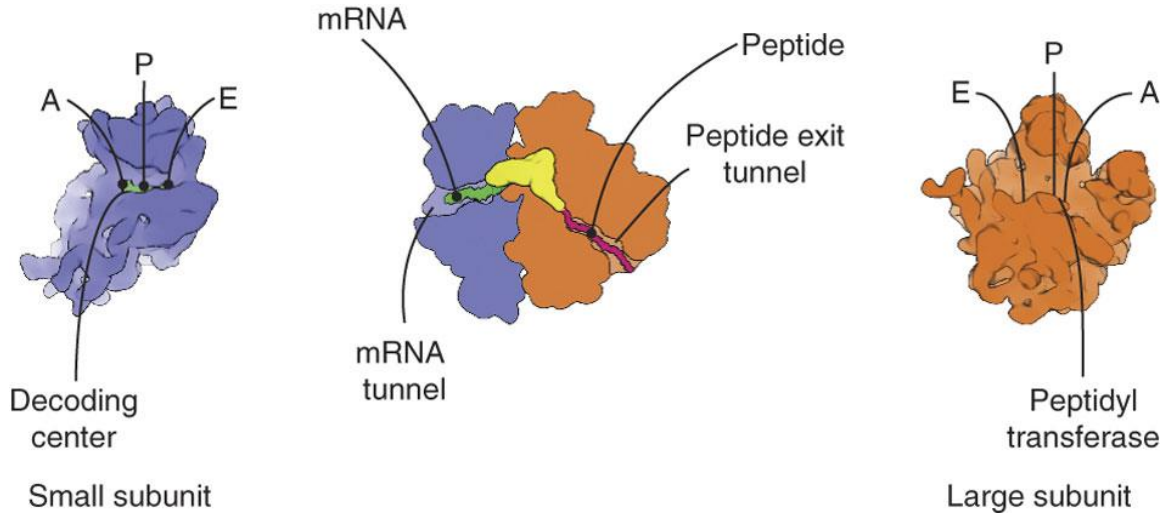

Fig. 1: The ribosomal core functions. The small and the large ribosomal subunits are shown in blue and ochre, respectively. The mRNA is shown in green, the tRNA bound to the ribosome in yellow and the emerging nascent polypeptide in pink. Adapted from (Melnikov, Ben-Shem et al. 2012).

4.1 The eukaryotic ribosome

Eukaryotic ribosomes are at least 40% larger than their prokaryotic counterpart because of additional ribosomal RNA (rRNA) elements and protein moieties (Spahn, Beckmann et al. 2001). The molecular weight of eukaryotic ribonucleoprotein-particles is around 4 MDa, in prokaryotes the molecular weight of the ribosome is about 2.5 MDa. The human large 60S subunit (50S in bacteria) comprises three rRNA molecules (25S, 5.8S and 5S) and 47 proteins. The small 40S subunit (30S in bacteria) is build-up of one 18S rRNA molecule and 33 proteins. Of the 80 ribosomal proteins in eukaryotes, there are 32 without homologs in bacterial ribosomes. Ribosomal proteins, which show homologies with their prokaryotic counterparts, usually have large eukaryote-specific extensions (Lecompte, Ripp et al. 2002). High-resolution ribosome crystal structures of lower eukaryotes (*Saccharomyces cerevisiae*, *Tetrahymena thermophila*) have been described (Ben-Shem, Garreau de Loubresse et al. 2011, Klinge, Voigts-Hoffmann et al. 2011, Weisser, Voigts-Hoffmann et al. 2013), as have been high-resolution crystal structures of *S. cerevisiae* 80S ribosomes in complex with distinct translation inhibitors (Garreau de Loubresse, Prokhorova et al. 2014). Recently the structure of the human 80S ribosome has been determined using high-resolution cryo-electron-microscopy density maps (Anger, Armache et al. 2013).

Although the eukaryotic and prokaryotic ribosomes differ in details of translational initiation, termination and regulation (Sonenberg and Hinnebusch 2009, Jackson, Hellen et al. 2010) the functional core of the ribosome is universally conserved (Fig. 2) (Schmeing and Ramakrishnan 2009). Functionally conserved regions of the core are the peptidyl transferase center (PTC) and the A-site of the decoding region. However, variations in the ribosomal RNA sequences exist. These rRNA variations are crucial for specificity of ribosomal inhibitors against bacterial ribosomes as opposed to eukaryotic ribosomes.

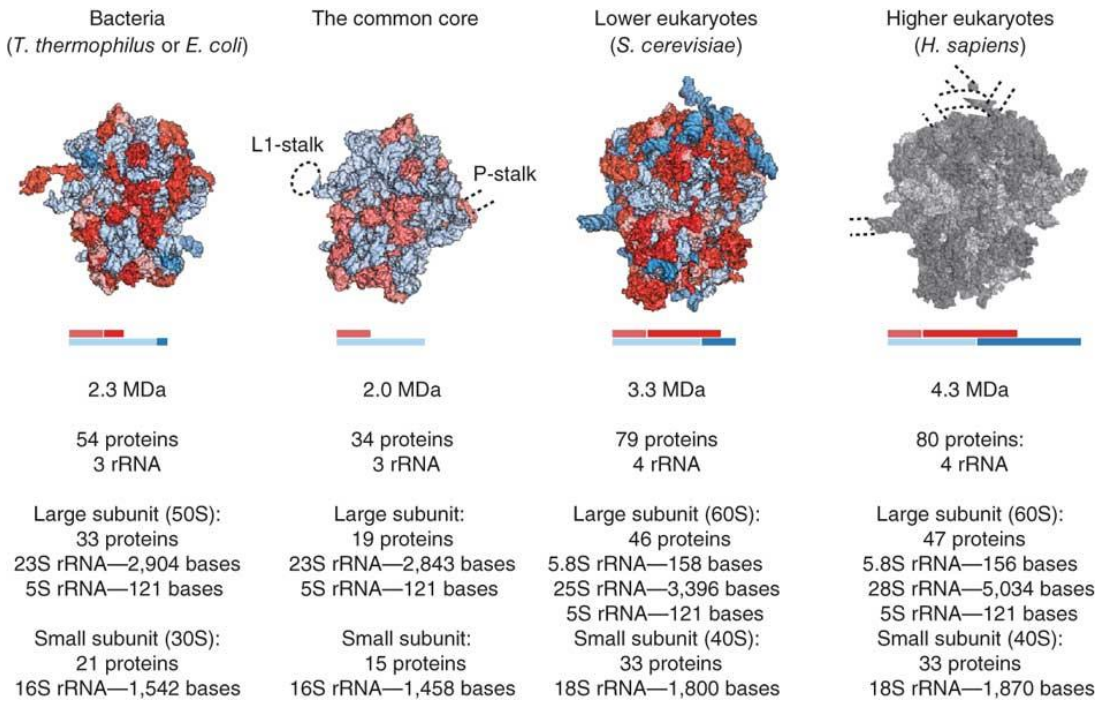

Fig. 2: Overview of bacterial and eukaryotic ribosomes. The common core is shown in light blue (RNA) and light red (protein). Both prokaryotes and eukaryotes have their specific set of additional proteins or extensions or insertions in conserved proteins (red) or extension moieties in rRNA (blue). In grey the predicted human 80S ribosome is shown. Dashed lines indicate the probable positions of the human-specific long rRNA expansion segments. Adapted from (Melnikov, Ben-Shem et al. 2012).

4.2 Protein synthesis in eukaryotes

In eukaryotes, translation is more complex compared to prokaryotes. Translation is initiated by the 43S pre-initiation complex (PIC) which is composed of the 40S subunit, the three initiation factors eIF1, eIF1A, eIF3 and a ternary complex (TC) consisting of initiator tRNA ($tRNA_i^{Met}$) and initiation factor eIF2-GTP (Fig. 3) (Jackson, Hellen et al. 2010). The messenger RNA (mRNA) is delivered to the 43S PIC by the eIF4F complex consisting of eIF4A, eIF4E and eIF4G bound to the mRNA. The resulting 48S complex scans an mRNA starting from the 5' end for the start codon. Hydrolysis of eIF2 bound GTP is triggered by eIF5, but inorganic phosphate is not released until the start codon is encountered and eIF1 is released (Algire, Maag et al. 2005). It is still unknown at which stage eIF5 joins the initiation complex. When a start codon is encountered the initiation complex switches from an open to a closed state. After release of eIF2 and eIF5, the large subunit joins the complex under the participation of eIF5B (Singh, Lee et al. 2006). eIF1A and eIF5B dissociate from the complex after GTP is hydrolysed by eIF5B. As a result, the initiator tRNA is located in

the P-site of the 80S complex and the A-site is vacant. At this stage the ribosome can enter the elongation cycle (Sonenberg and Hinnebusch 2009, Jackson, Hellen et al. 2010, Hinnebusch 2011).

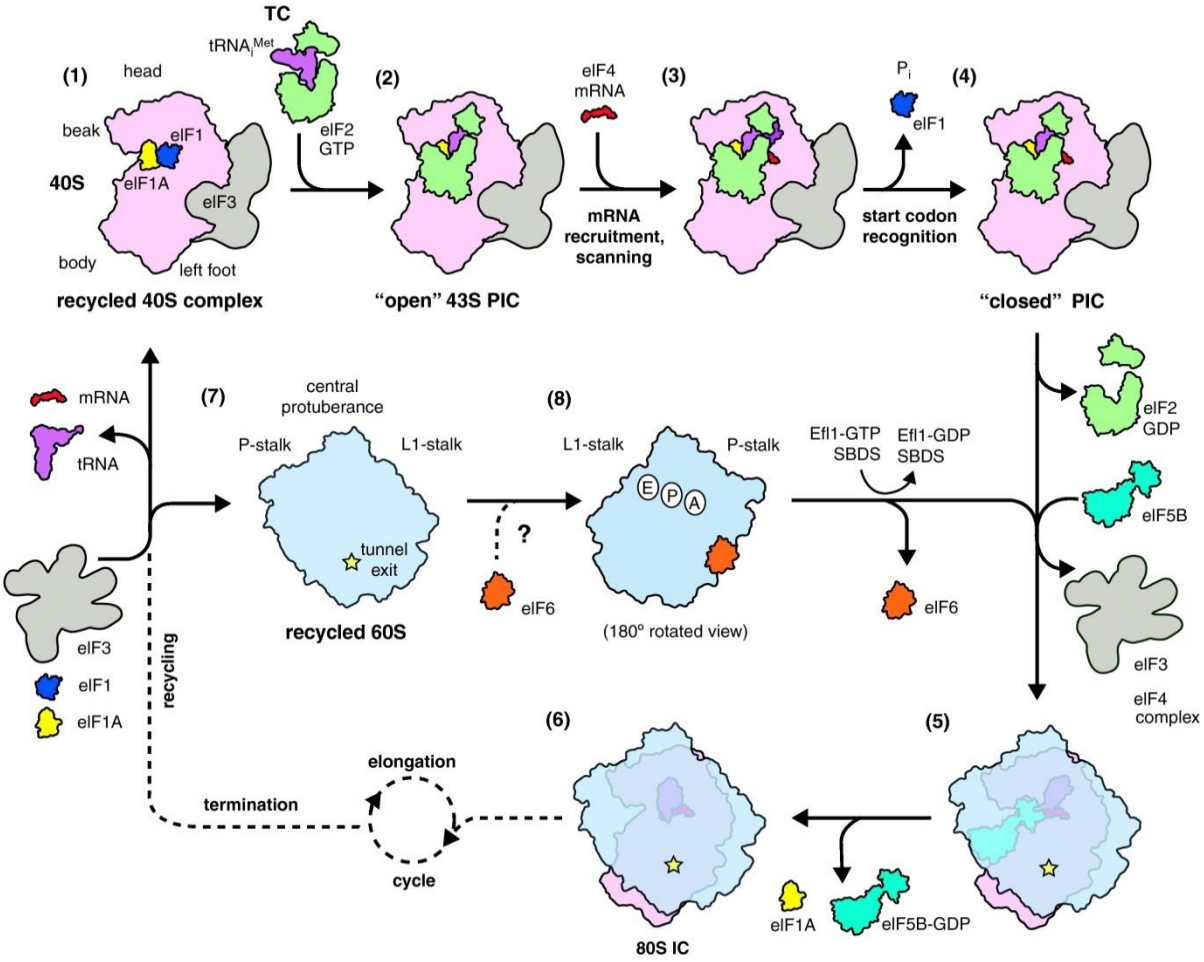

Fig. 3: Translation initiation in eukaryotes: (1)-(4) illustrates the formation of the 43S preinitiation complex (PIC) and scanning for the start codon. (5)-(6) shows the formation of the 80S initiation complex (IC), subsequently the 80S ribosome enters the elongation cycle. Adapted from (Voigts-Hoffmann, Klinge et al. 2012).

In bacteria, the initial aminoacyl-tRNA binding, codon recognition and GTPase activation has been investigated in detail. (Ogle, Brodersen et al. 2001, Schmeing, Voorhees et al. 2009, Jenner, Demeshkina et al. 2010, Voorhees, Schmeing et al. 2010, Schmeing, Voorhees et al. 2011). In eukaryotes these functions are expected to be similar, because of the universally conserved core. The eukaryotic elongation cycle starts when a ternary complex consisting of aminoacyl-tRNA, eEF1A and GTP binds to the ribosomal A-site (Fig. 4). Correct codon-anticodon interaction triggers GTP hydrolysis by eEF1A resulting in accommodation of the aminoacyl-tRNA in the A-site and eEF1A and GDP are released from the ribosome. After accommodation,

the peptide bond is formed rapidly with the P-site peptidyl-tRNA by the help of the PTC, which positions the substrates appropriately for catalysis. Structures of the PTC of *S. cerevisiae* 80S ribosomes and bacterial ribosomes are almost superimposable, suggesting that the peptide bond formation mechanism is universally conserved (Ben-Shem, Garreau de Loubresse et al. 2011). Subsequently, the A-site tRNA harbours the nascent peptide chain and the A- and P-site tRNAs transit into the hybrid state, i.e. the acceptor ends of these tRNAs move to

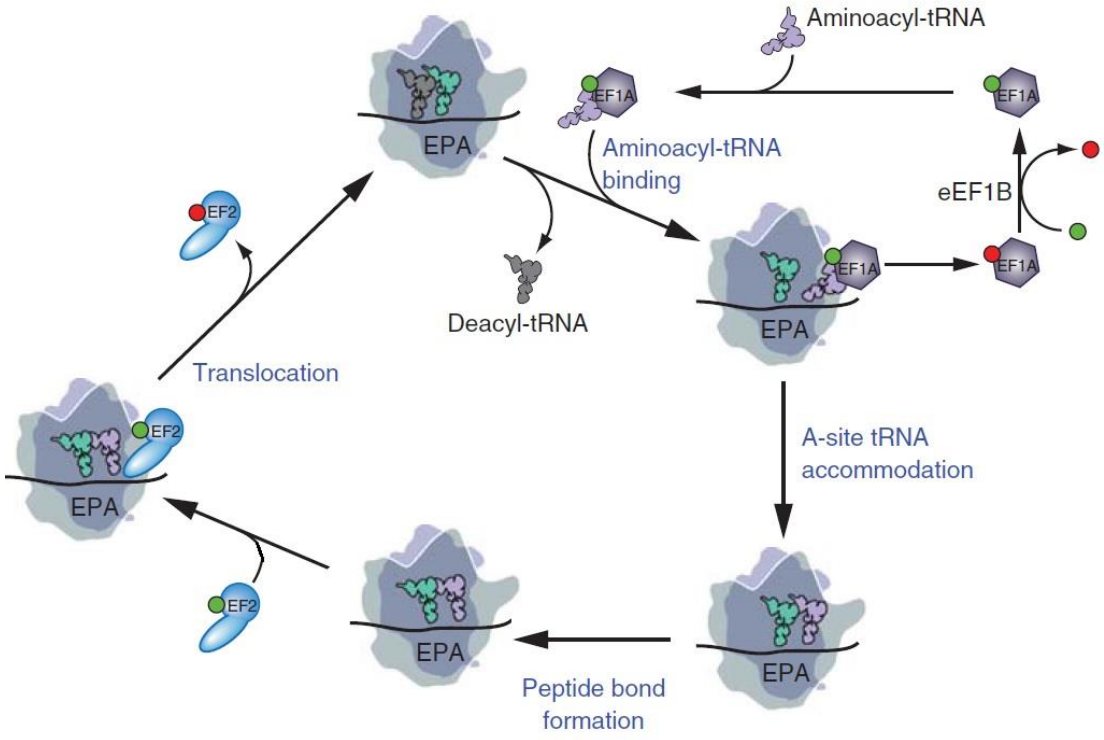

Fig. 4: The eukaryotic translation elongation cycle. The large ribosomal subunit is shown in light grey, the small subunit in dark grey. Accommodation of the tRNA, peptide bond formation and translocation are shown. Green ball denotes GTP, red ball denotes GDP. Adapted from (Dever and Green 2012).

the P- and E-sites, respectively. Then the ribosome translocates the peptidyl-tRNA into the P-site and the deacetylated tRNA into the E-site. This step is catalysed by factor eEF2-GTP. After GTP hydrolysis elongation factor G reveals interaction with its domain IV and mRNA, P-site tRNA and A-site suggesting that the factor prevents backwards movement of the tRNAs (Gao, Selmer et al. 2009). In bacteria, domain IV of the elongation factor was shown to be critical for the catalysis of translocation: deletion or mutation in domain IV results in the absence of translocation activity of elongation factor G (Rodnina, Savelsbergh et al. 1997, Martemyanov and Gudkov

1999). The deacetylated E-site tRNA is released from the ribosome and a new ternary complex binds to the A-site (Uemura, Aitken et al. 2010). This cycle continues until the ribosome encounters a stop codon (*i.e.* UAA, UAG, UGA). The peptide synthesis ends when the A-site encounters a stop-codon (Fig. 5). The stop codon sequence is recognized by a ternary complex consisting of the release factors eRF1, eRF3 and GTP, which binds in a pre-accommodated fashion. Upon hydrolysis of GTP, eRF3 is released (Frolova, Le Goff et al. 1996). The ATPase ABCE1/Rli1 binds to the ribosome and supports accommodation of eRF1. The nascent polypeptide chain is released by peptidyl-tRNA hydrolysis mediated by eRF1 in a highly discriminative fashion (Salas-Marco and Bedwell 2005). After ATP hydrolysis the subunits dissociate and can be reused in the next round of translation initiation (Dever and Green 2012).

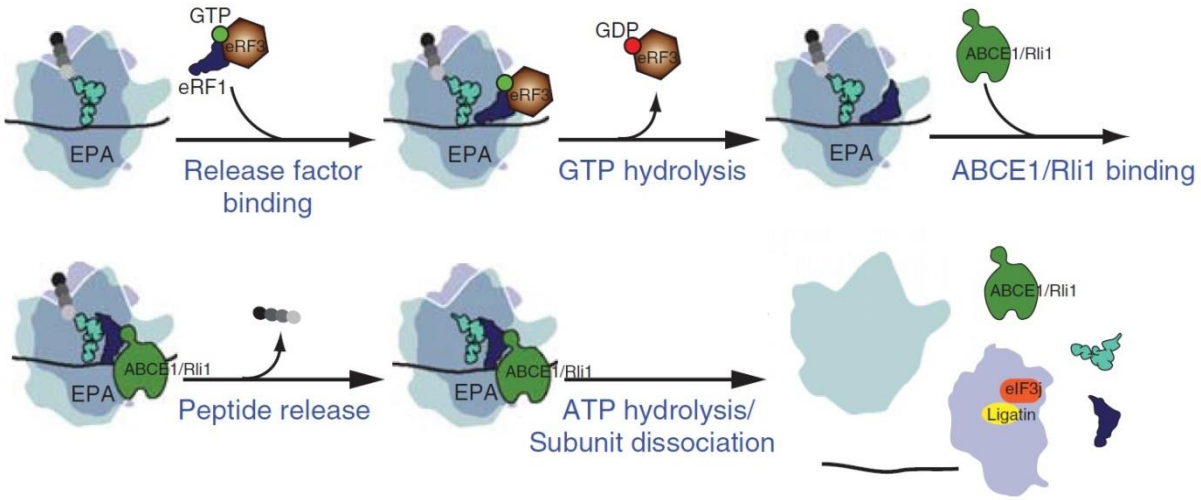

Fig. 5: Translation termination in eukaryotes. The large ribosomal subunit is shown in light grey, the small subunit in dark grey. Adapted from (Dever and Green 2012).

4.3 Ribosomal accuracy

Ribosomal accuracy is important because genes have evolved to encode for specific proteins with optimized function. The error frequency of ribosomal translation is estimated to be 1 in 10^3 to 10^4 (Edelmann and Gallant 1977, Bouadloun, Donner et al. 1983, Kramer and Farabaugh 2007). This level of accuracy is achieved by two consecutive selection steps (Fig. 6). The initial selection starts with codon-independent tRNA selection, where the ternary complex interacts labile with the ribosome (rate constants k_1 and k_{-1}). The codon-independence is supported by the

observation that cognate, near-cognate and non-cognate ternary complexes show the same rate of interaction with the ribosome.

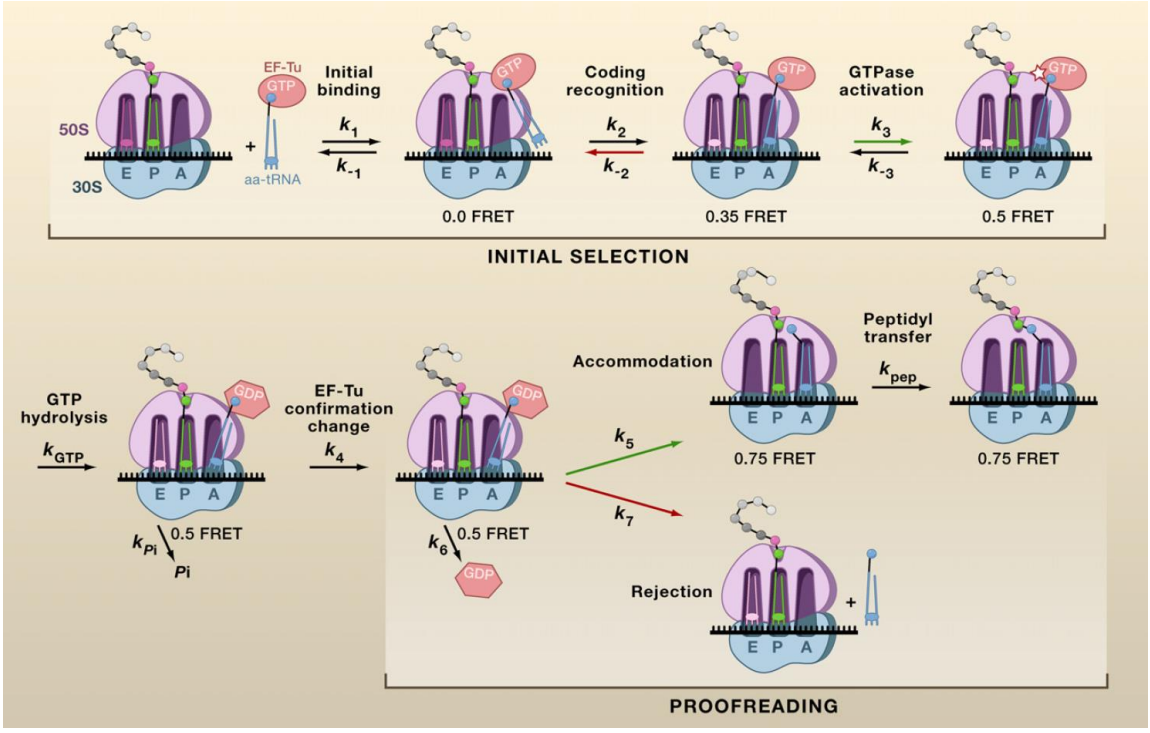

Fig. 6: The tRNA selection pathway. The stepwise process of tRNA selection is illustrated. The bacterial ribosome with its large subunit (magenta) and small subunit (cyan) is shown. Förster resonance energy transfer (FRET) values below the ribosome particles indicate distinct intermediate states of the ribosome. Green arrows indicate accelerated reaction rate for cognate tRNAs, whereas red arrows indicate accelerated reaction rates for near-cognate tRNAs. Adapted from (Zaher and Green 2009).

This process is rapid and readily reversible. This initial binding is fully dependent on the elongation factor of the ternary complex, suggesting an active mechanism for initial tRNA loading (Pape, Wintermeyer et al. 1998). The next step of tRNA selection is codon-dependent (Rodnina, Fricke et al. 1994). This step is observed for cognate and near-cognate tRNAs, but not for non-cognate ternary complexes (Pape, Wintermeyer et al. 1998). The rates of codon-recognition (k_2) for cognate and near-cognate tRNA complexes are similar; however, the dissociation rates (k_{-2}) are 1000-fold higher for near-cognate than for cognate tRNAs (Gromadski and Rodnina 2004). The difference in dissociation rates suggests an active involvement of the ribosome, by stabilizing correct cognate interactions. The difference in dissociation is larger than expected, in comparison to observed free energy of binding between cognate and near cognate tRNA codon-anticodon complexes in solution. The around 1000-

fold difference in free energy of binding for cognate and near-cognate tRNA species cannot be explained by the stability differences in the decoding helix (*i.e.* the interaction between mRNA codon and tRNA anticodon), rather the ribosome is actively involved in discrimination of cognate and near-cognate tRNAs. Binding of a cognate anticodon stem loop stabilizes a significant conformational change of the key decoding center nucleotides G530, A1492 and A1493 (Fig. 7). The two adenines move from an intrahelical position in helix 44 to an extrahelical position and G530 flips from a *syn*- to an *anti*-conformation (Ogle, Brodersen et al. 2001). As a result, the minor groove of the decoding helix is monitored for correct codon/anti-codon interaction. The A1492/1493 movement, stabilized by the cognate codon/anti-codon interaction, results in a global structural change of the small subunit, i.e. a more closed state of the small ribosomal subunit by rotating its head and shoulder domains. In contrast, near cognate codon/anti-codon interactions do not induce this closed confirmation.

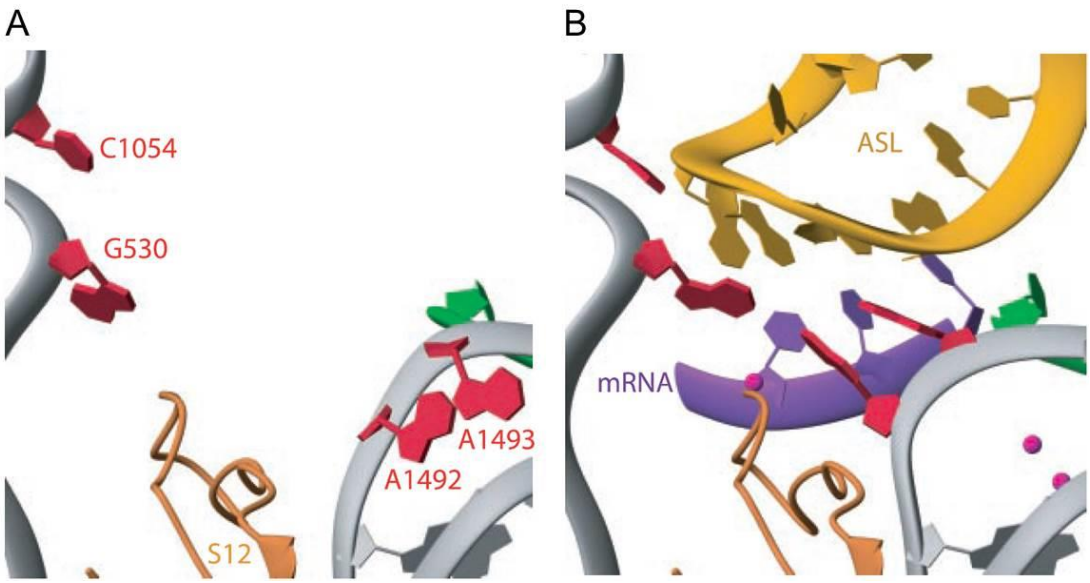

Fig. 7: Crystal structures of the bacterial A-site. (**A**) The vacant A-site is shown with the key decoding nucleotides A1492 and A1493 in intrahelical position of helix 44 and G530 in syn-conformation. (**B**) A mRNA codon (shown in purple) and a cognate anticodon stem loop (ASL, shown in yellow) interact with the A-site. The adenines 1492 and 1493 change their conformation to extrahelical position and G530 moves into an anti-conformation. By this conformational change the minor groove of the decoding helix is monitored for correct codon anticodon interaction. The ribosomal protein S12 is shown in orange. Adapted from (Ogle, Brodersen et al. 2001).

The subsequent steps of tRNA selection involve the elongation factor and GTP hydrolysis and establish the irreversible step necessary for proofreading. First, a

structural change the elongation factor is observed (k_3) which limits the rate of subsequent GTP hydrolysis (k_{GTP}) (Rodnina, Fricke et al. 1995). The following steps include inorganic-phosphate release (k_{Pi}), elongation factor change to GDP-bound state (k_4) and irreversible dissociation of the elongation factor from the aa-tRNA (k_6) (Pape, Wintermeyer et al. 1998). After dissociation of the elongation factor the critical branch point termed proofreading of the tRNA selection pathway is reached. The A-site associated tRNA either accommodates into the A-site (k_5) of the large subunit and participates in peptidyl transfer (k_{pep}), or is rejected from the ribosome (k_7). Notably, GTPase activation (k_3), and accommodation step (k_5) strongly depend on the properties of the decoding helix, which is formed by pairing between the codon and the anticodon (Pape, Wintermeyer et al. 1999).

4.4 Aminoglycosides and translation

Aminoglycosides form a large family of poly-cationic, water soluble antibacterial agents (Kotra, Haddad et al. 2000). Most aminoglycosides occur naturally and are isolated from actinomycetes *Streptomyces* (“-mycin” suffix) or *Micromonaspora* (“-micin” suffix) (Zembower, Noskin et al. 1998).

Aminoglycosides share as a common feature the neamine core, which is composed of a glucopyranosyl (ring I) glycosidically linked to position 4 of the 2-deoxystreptamine (2-DOS) (ring II) (Busscher, Rutjes et al. 2005). Additional sugars are attached to the 5’ or 6’ position of the 2-DOS. Representatives of the 4,5-disubstituted deoxystreptamines are paromomycin and neomycin (Fig. 8A). Members of the 4,6-disubstituted deoxystreptamines are geneticin, gentamicin C1a, kanamycin A, amikacin and tobramycin (Fig. 8C). Apramycin and hygromycin B have unique structures within the group of aminoglycosides. Apramycin has a bicyclic sugar moiety and a 4-monosubstituted 2-deoxystreptamine (Fig. 8B) (Matt, Ng et al. 2012). Hygromycin B has a dual ether linkage between its second and fourth rings, resulting in a third ring (Fig. 8D). The 2-deoxystreptamine ring I of hygromycin B is 5-monosubstituted, resulting in unique functional properties (Borovinskaya, Shoji et al. 2008).

Aminoglycosides target the rRNA of helix 44 located in the A-site of the small ribosomal subunit. As a result, aminoglycosides affect protein synthesis by inducing mistranslation and inhibition of the mRNA-tRNA complex translocation from the A to

the P-site (Davies, Gorini et al. 1965, Noller 1991, Spahn and Prescott 1996). Aminoglycosides are effective against both gram-positive and gram-negative bacteria. Anaerobic bacteria are not susceptible to aminoglycosides due to the lack of an oxygen dependent electron transport system, which delivers energy for the uptake of the drug (Rasmussen, Bush et al. 1997).

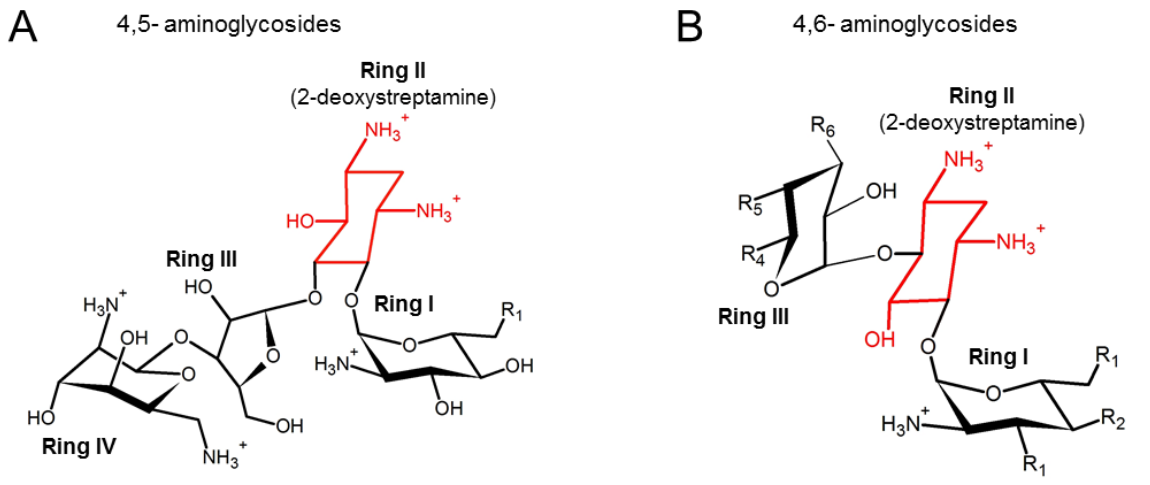

	R_1
Paromomycin	OH
Neomycin	NH_3

	R_1	R_2	R_3	R_4	R_5	R_6	R_7
Geneticin	NH_3	OH	OH	CH_3OH	H	CH_3OH	NH_2CH_3
Gentamicin C1a	NH_3	H	H	NH_3	H	CH_3OH	NH_2CH_3
Kanamycin A	OH	OH	OH	NH_3	CH_2OH	OH	NH_3
Amikacin	OH	OH	OH	NH_3	CH_2OH	OH	NH_3
Tobramycin	NH_3	H	OH	NH_3	CH_2OH	OH	NH_3

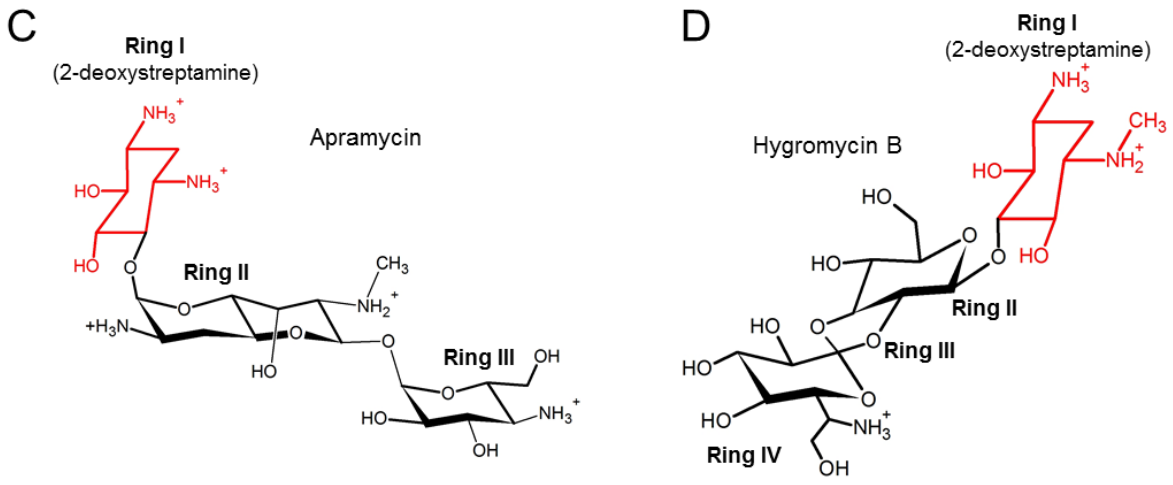

Fig. 8: Chemical structures of aminoglycosides. (**A**) 4,5-disubstituted aminoglycosides, (**B**) 4,6-aminoglycosides with corresponding substituents R_1-R_7 of ring I and III, note that amikacin has an additional (l)-α-hydroxy-γ-aminobutyric amide (L-HABA) chain at the C1 amino-group of ring II, (**C**) apramycin, (**D**) hygromycin B. The 2-deoxystreptamine ring is shown in red.

4.5 Interactions of aminoglycosides with the bacterial ribosome

The secondary structure of helix 44 of the 16S rRNA is shown in Fig. 10A. The bacterial A-site nucleotides are boxed in red. As a result of sequence variations in nucleotide positions 1408 and/or 1491 in helix 44, aminoglycosides have a higher affinity to bacterial than to eukaryotic ribosomes. The aminoglycoside drug binding

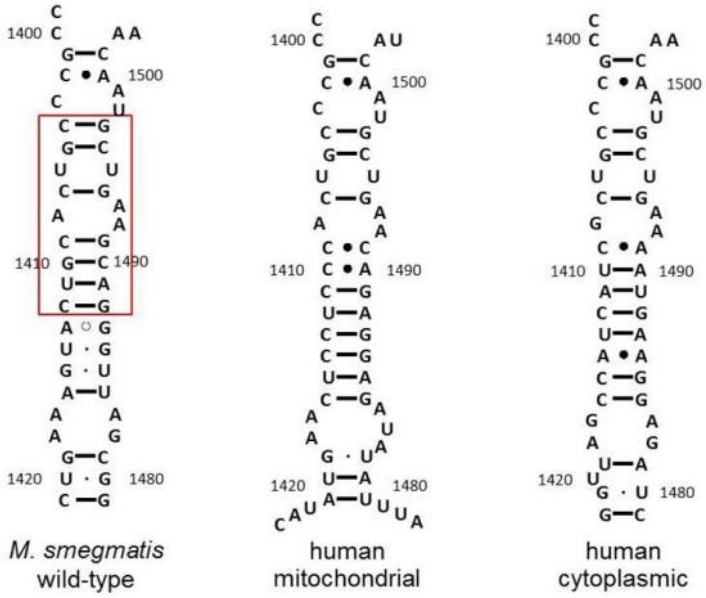

Fig. 9: Secondary Structure of the ribosomal A-site. The secondary structures of bacterial, mitochondrial and eukaryotic cytoplasmic helix 44 are shown. The bacterial A-site nucleotides are boxed in red.

pocket is stabilized by the G1405-C1496, C1407-G1494 and C1409-G1491 base pair interactions. As shown in Fig. 10A and B, ring I (shown in yellow) is located in the internal rRNA loop formed by A1408, A1492, A1493 and the C1409-G1491 base pair. In bacterial ribosomes, ring I forms a pseudo-base pair interaction by two direct hydrogen bonds with A1408. The oxygen of ring I accepts a hydrogen bond from the N6 of adenine and the amino or hydroxyl group donates a hydrogen bond to the N1 of the adenine (Fig. 11) (Vicens and Westhof 2003, Francois, Russell et al. 2005). In eukaryotic cytoplasmic ribosomes the G1408 nucleotide cannot form a hydrogen bond with the 6' amino group of ring I. In addition, the positive charge of the 6' amino group is repulsed by the N1 and N2 amino groups of guanine. If a 6' hydroxyl group of ring I is present, a hydrogen bond can be formed between the 6'OH and N1 or N2 of guanine (Pfister, Hobbie et al. 2003). Ring I also forms a stacking interaction with nucleotide G1491 and additional hydrogen bonds with hydroxyl groups at position O3' and O4' of the phosphate groups of flipped out adenines A1492 and A1493, which further stabilizes the pseudo base pair interaction of ring I with A1408 (Fig. 11) (Vicens and Westhof 2001, Vicens and Westhof 2002).

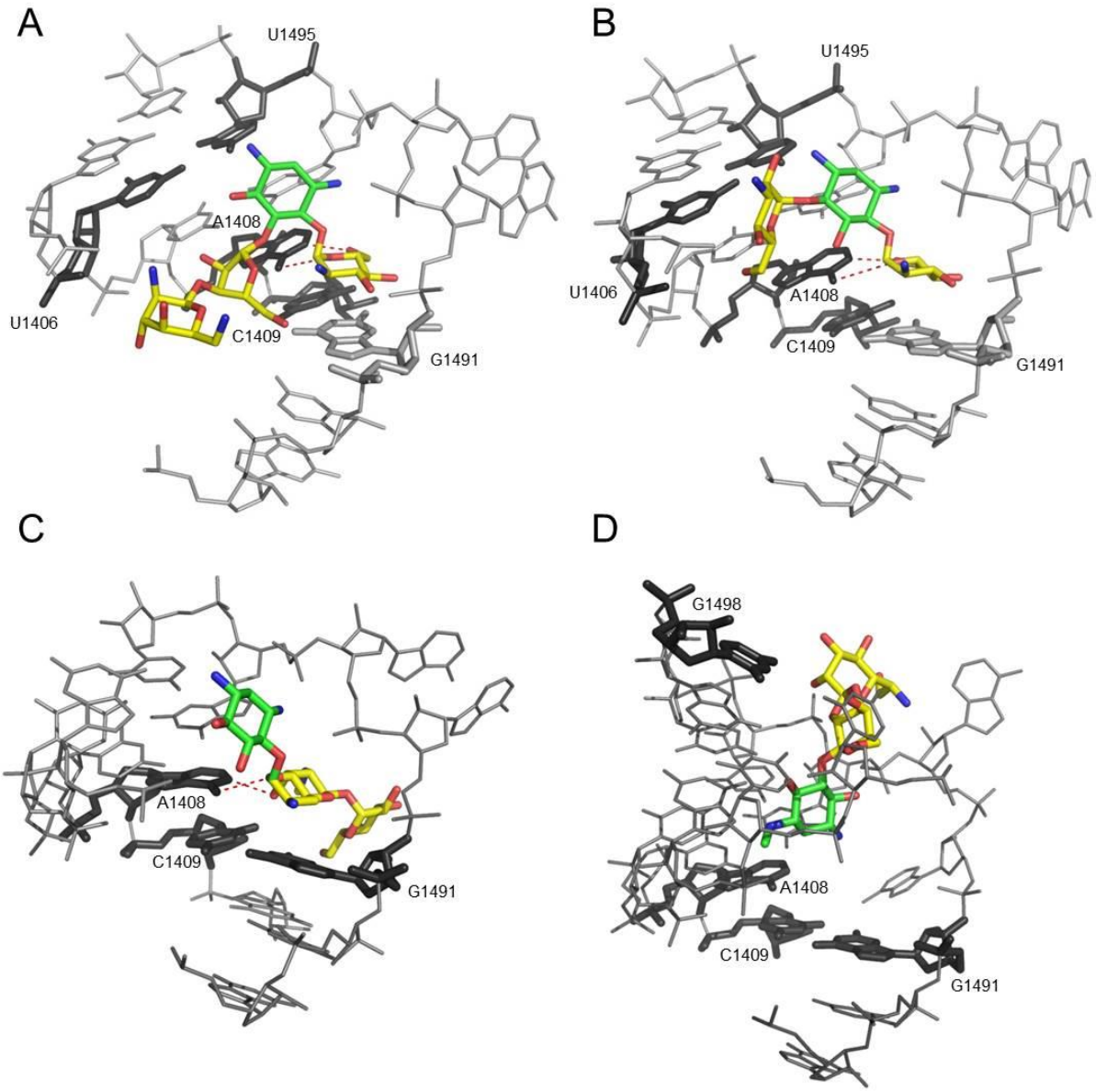

Fig. 10: Tertiary structures of the ribosomal A-site. (**A**) Tertiary structure of the bacterial A-site in complex with paromomycin. The ring I, III and IV are shown in yellow, the 2-DOS ring II in green, and the rRNA nucleotides are shown in grey. The two hydrogen bonds formed by ring I and A1408 are illustrated by red dashed lines. Adapted from (Vicens and Westhof 2001) (**B**) Tertiary structure of the bacterial A-site in complex with kanamycin A. The ring I and III are shown in yellow, the 2-DOS ring II in green, and the rRNA nucleotides are shown in grey. The two hydrogen bonds formed by ring I and A1408 are illustrated by red dashed lines. Adapted from (Francois, Russell et al. 2005). (**C**) Tertiary structure of the bacterial A-site in complex with apramycin. Helix 44 of 16S rRNA is shown in grey, apramycin in yellow, with the 2-DOS ring I highlighted in green. The two hydrogen bonds formed by A1408 and ring II are illustrated by red dashed lines. Adapted from (Matt, Ng et al. 2012). (**D**) Tertiary structure of the bacterial A-site in complex with hygromycin B. The helix 44 of 16S rRNA is shown in grey, hygromycin B in yellow, with the 2-DOS ring I highlighted in green. Adapted from (Borovinskaya, Shoji et al. 2008).

Ring II of the neamine core (shown in green) forms hydrogen bonds between its N1 and O4 of U1495 and between its N3 and N7 of G1494. In addition, the N3 makes two hydrogen bonds with the phosphate groups of A1493 and G1494 (Vicens and Westhof 2001, Vicens and Westhof 2002, Vicens and Westhof 2003, Francois, Russell et al. 2005). The sugars attached to position 5' or 6' to the neamine core results in additional interactions with the nucleotides of the A-site. As shown in Fig. 10A and B the orientation of the additional sugars differs significantly for 4,5- and 4,6-aminoglycosides. Ring III and IV of the 4,6-aminoglycosides reaches up towards U1406, while ring III of the 4,5-aminoglycosides reaches down to U1406 (Vicens and Westhof 2001, Vicens and Westhof 2002).

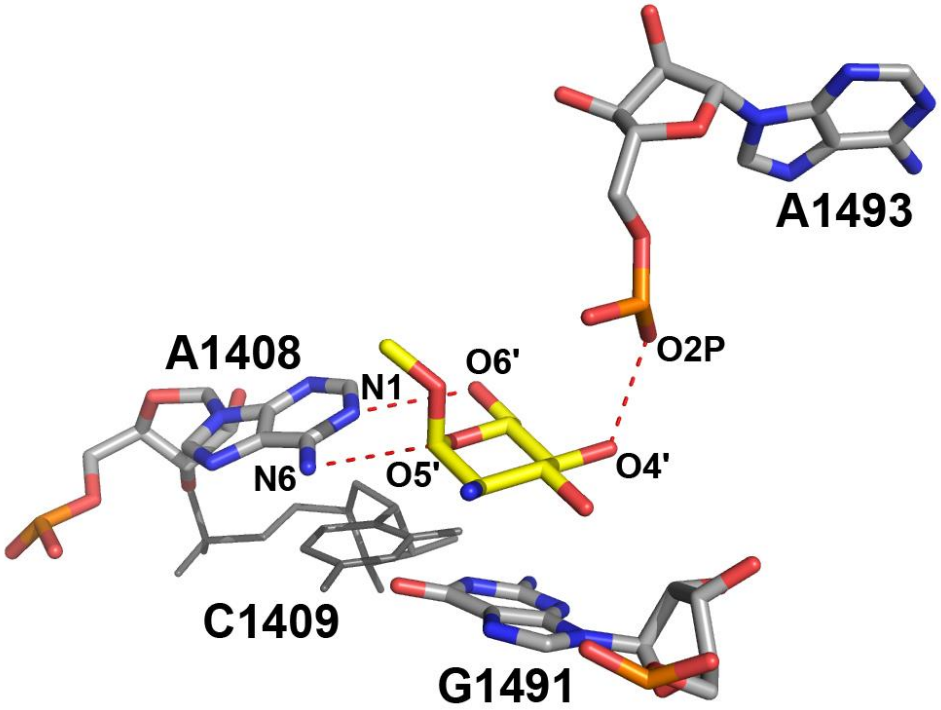

Fig. 11: Detailed view of interaction between paromomycin ring I and A-site nucleotides. Hydrogen bonding of ring I (shown in yellow) with A1408 and A1493 indicated by red dashed lines. For clarity only hydrogen bond between 4'OH and O2P of A1493 is shown. Interaction of 3'OH and phosphate group of A1492 is not illustrated. Stacking interaction between G1491 and ring I is shown. Adapted from (Perez-Fernandez, Shcherbakov et al. 2014).

The tertiary structures of apramycin and hygromycin B in complex with the bacterial A-site are shown in Fig. 10C and D. The hydrogen-bonding pattern and position of the 2-DOS moiety (ring I) of apramycin is similar to that of the 2-DOS moiety (ring II) of 4,5- and 4,6-aminoglycosides. Hydrogen bonds are formed between the N3 of apramycin and N7 of G1494 and the N1 of apramycin and O4 of U1495. The bicyclic ring II of apramycin is located above and parallel to the guanine of the C1409-G1491

base pair. The ring II oxygen and the 6' hydroxyl form hydrogen bonds to N6 and N1 of A1408, resulting in a pseudo base pair interaction with A1408. The ring III of apramycin directs into the solvent, with close proximity of its O6 to the N3 of A1491 and its 2-OH to the no bridging phosphate oxygen of A1493 (Matt, Ng et al. 2012).
The binding site of hygromycin B in helix 44 is a few angstroms away from the binding site of the other aminoglycosides. Due to the rigidity of the molecule, hygromycin B does not fit in the 2-DOS drug binding pocket. Ring I forms a network of hydrogen bonds that spans the major groove of nucleotides C1404, G1405, U1406 and G1494-C1496, to the phosphate of G1494. The ring II forms hydrogen bonds to C1403. The ring IV interacts with A1493 and the phosphate of U1495 by hydrogen bonds. Hygromycin B induces A1493 to flip out from helix44 and changes the conformation of A1492 (Borovinskaya, Shoji et al. 2008).

4.6 Aminoglycosides and mistranslation

The estimated error frequency of translation ranges from 10^{-3} to 10^{-4} per codon (Kramer and Farabaugh 2007). As a result of misreading, the amino acid carried by a near-cognate tRNA is incorporated into the growing polypeptide chain. Read-through is a special form of misreading: here, an amino acid is incorporated at a stop codon. Misreading and read-through can be enhanced by aminoglycosides in prokaryotes and eukaryotes. In the late 1970's, aminoglycoside-induced mistranslation was first described *in vivo* in *E. coli* (Edelmann and Gallant 1977). In subsequent publications aminoglycoside-induced read-through was also shown in lower and higher eukaryotes, demonstrating that aminoglycosides can impair eukaryotic translational fidelity (Palmer and Wilhelm 1978, Wilhelm, Jessop et al. 1978, Palmer, Wilhelm et al. 1979, Abraham and Pihl 1983, Stansfield, Jones et al. 1998)

Structural analyses revealed that upon binding of aminoglycosides the vacant A-site changes its conformation and both adenines 1492 and 1493 move from an intrahelical position to an extrahelical position. Normally, these two adenines monitor the cognate tRNA-mRNA complex by flipping out of the interior helix 44 into the minor groove of the codon-anticodon helix. By acting as a molecular ruler this mechanism is part of the tRNA selection pathway during translation. However, binding of aminoglycosides stabilizes the flipped-out position of the adenines similar to the conformation during correct codon-anticodon interaction. This conformational change makes it more likely for a near-cognate tRNA to accommodate in the A-site

leading to misincorporation of amino acids into the growing polypeptide chain (Ogle, Brodersen et al. 2001).

Aminoglycoside-induced stop-codon read-through is caused by the flip-out of A1493 sterically preventing the binding of the release factor (Laurberg, Asahara et al. 2008). Instead, a near-cognate tRNA can accommodate in the A-site and its amino acid can be incorporated into the growing polypeptide chain. As a result read-through leads to continuation of translation beyond the stop-codon. The suppressive effect of aminoglycosides on termination has been suggested to be useful for treatment of patients with genetic diseases caused by nonsense mutations (Finkel 2010, Nudelman, Glikin et al. 2010, Shulman, Belakhov et al. 2014). Here, a sense codon in the open reading frame is mutated into a premature stop codon resulting in synthesis of truncated and usually inactive proteins. For example, patients suffering from cystic fibrosis can carry a nonsense mutation in the cystic fibrosis transmembrane conductance regulator (CFTR) gene. A partial reconstitution of a functional CFTR in patients with a premature stop codon mutation after gentamicin treatment has been described (Wilschanski, Yahav et al. 2003).

4.7 Cellular stress responses to misfolded proteins

In higher eukaryotes there is no direct evidence that aminoglycosides induce misreading which would result in protein misfolding and cellular stress. In prokaryotes increasing the capacity of the folding machinery by chaperonine overexpression reduces the misfolded protein stress induced by aminoglycosides and improves the survival of cells (Goltermann, Good et al. 2013).

Corresponding mechanisms to cope with unfolded proteins also exist in eukaryotic cells. Unfolded proteins response pathways in eukaryotic cells include the cytoplasmic unfolded protein response (cytUPR), the endoplasmatic reticulum (ER) unfolded protein response (erUPR) and the mitochondrial unfolded protein response (mitUPR) (Fig. 12).

If chaperones, proteasome system and mitophagy fail to re-establish protein homeostasis during severe or persistent protein misfolding stress, cells will undergo apoptosis (Fig. 12). In particular, prolonged ER stress triggers CHOP-induced apoptosis (Matsumoto, Minami et al. 1996, McCullough, Martindale et al. 2001, Harding, Zhang et al. 2003, Ohoka, Yoshii et al. 2005).

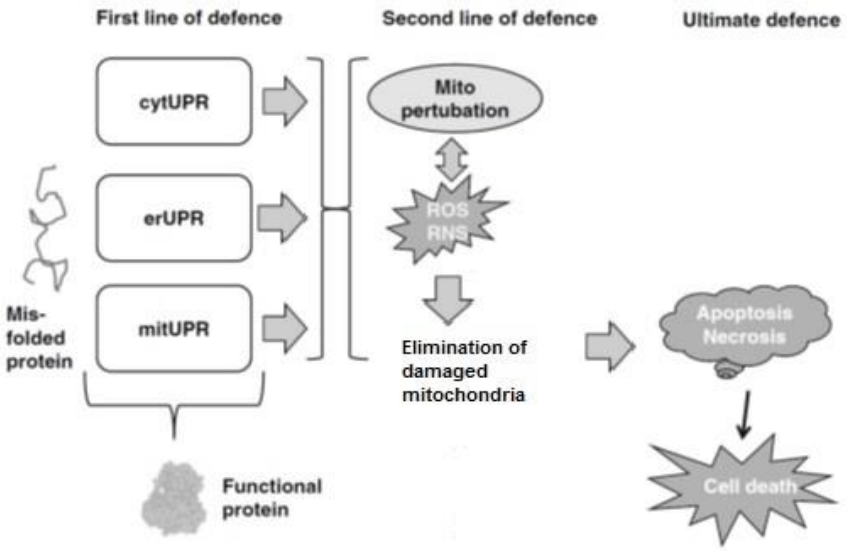

Fig. 12: Overview of mechanisms defending against unfolded protein stress. Misfolded proteins are substrate for the distinct unfolded protein responses. In case of severe or prolonged stress, dysfunctional mitochondria are eliminated to protect the cell. If the stress still persists cells undergo apoptosis or necrosis. Adapted from (Gregersen and Bross 2010).

4.8 The cytosolic unfolded protein response

In the cytosol two distinct chaperone networks are described (Albanese, Yam et al. 2006). The first cytosolic chaperone network interacts with nascent peptide chains and consists of a variety of chaperones and assistant factors, *i.e.* prefoldin (PFD), TCP-1 ring complex (TRiC), nascent-polypeptide-associated complex (NAC), heat shock proteins (Hsps) Hsp40 and Hsp70 (Hartl and Hayer-Hartl 2002). The majority of small peptides require no further folding assistance besides NAC activity to reach their native state, whereas some proteins need folding capacities of Hsp40 and Hsp70 chaperones to reach their native state. From these nascent proteins, some need to be transferred to Hsp90 for the final folding reaction (**Fig. 13**A). By another route of nascent peptide folding, prefoldin mediates the peptide-NAC-Hsp40-70 complex to chaperonine TRiC in co-or posttranslational fashion (**Fig. 13**B, C) (Hartl and Hayer-Hartl 2002). If the folding process is stuck or the interaction with TRiC is prolonged, the peptide is degraded by the ubiquitin proteasome system (McClellan, Scott et al. 2005).

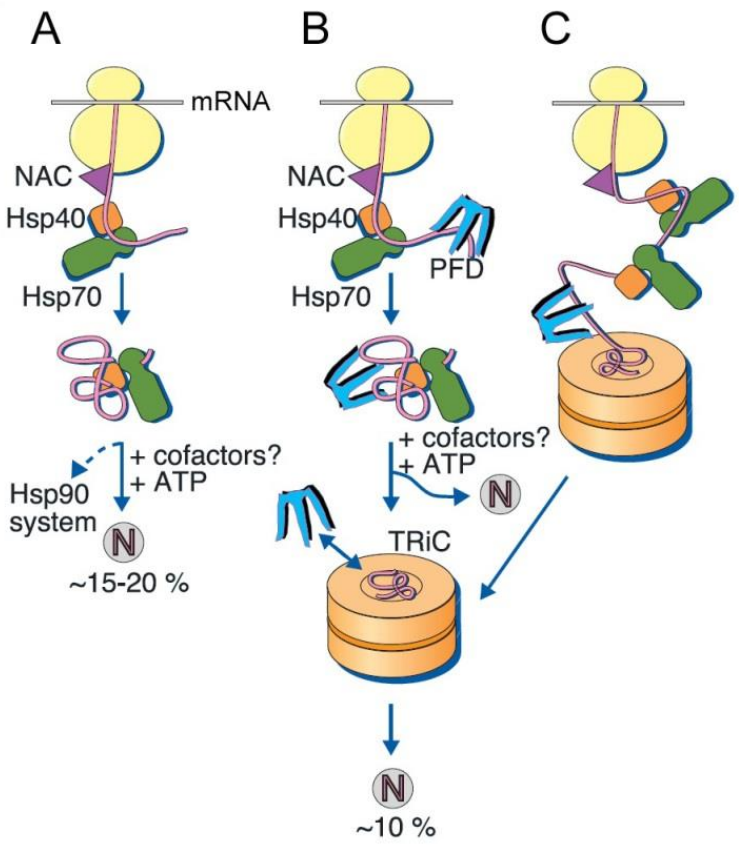

Fig. 13: Overview of chaperones associated with nascent peptide chains. The ribosome is shown in yellow, the nascent peptide chain in magenta; N, native protein. (A) Nascent peptide chains generally interact with the nascent-polypeptide-associated complex (NAC) and the majority folds without further assistance. About 15-20 % of proteins fold need help of Hsp70 and Hsp40 proteins and some need further assistance by Hsp90. Around 10% of peptides are posttranslationally (B) or cotranslationally (C) passed to chaperonine TCP-1 ring complex (TRiC) mediated by prefoldin (PFD). Adapted from (Hartl and Hayer-Hartl 2002).

The second cytosolic chaperone network is termed the cytosolic heat shock response or cytosolic UPR (cytUPR). Master regulator of the cytUPR is the heat-shock factor 1 (HSF1). Under non-stressed conditions HSF1 is bound as an inactive monomer to Hsp40, Hsp70 or Hsp90 proteins (Zou, Guo et al. 1998, Morimoto 2008). Upon accumulation of misfolded proteins Hsps are recruited to denaturated proteins and HSF1 is released (Fig. 14). The HSF1 monomers translocate into the nucleus, undergo a conformational change, form trimers, become phosphorylated and bind to heat-shock promotor elements (HSE) of various genes, including chaperones . When Hsp70 accumulates it interacts with HSF1 and inhibits the binding of HSF1 to the HSE promotor elements. This negative feedback from the Hsp70 expression levels, controls the transcriptional activity of HSF1 (Morimoto 2008).

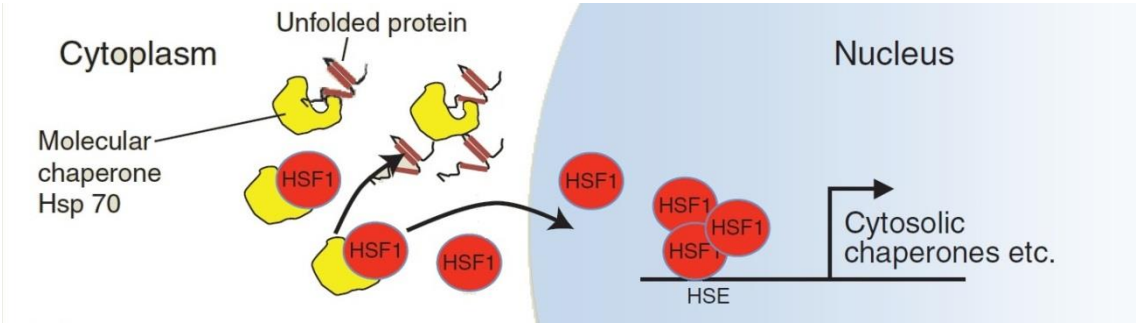

Fig. 14: The cytosolic heat shock response. HSF transcription factors are bound to Hsp proteins in the cytoplasm (here only Hsp70 and HSF1 are indicated). Upon accumulation of unfolded proteins Hsps preferentially interact with denatured proteins and HSF1 is released. HSF1 translocates into the nucleus, trimerizes and activates genes containing HSF1 binding sites or heat shock elements (HSE). Adapted from (Haynes and Ron 2010).

4.9 The unfolded protein response (UPR) in the ER

Folding in the ER is accomplished by a specialized set of chaperones, including BiP (GRP78) and GRP94, lectin chaperones like calnexin and calreticulin and protein disulfide isomerases (PDIs) (Malhotra and Kaufman 2007). The erUPR is regulated by three different pathways. Each pathway has a distinct sensor for misfolded proteins in the ER lumen. The three sensors are the membrane spanning proteins activating transcription factor 6 (ATF6), protein kinase RNA (PKR)-like ER kinase (PERK) and inositol-requiring enzyme 1 (IRE1), which are kept inactive in complex with BiP (Fig. 15) (Shi, Vattem et al. 1998, Tirasophon, Welihinda et al. 1998, Yoshida, Okada et al. 2000). Accumulation of misfolded proteins in the ER releases BiP from the transmembrane proteins and leads to the activation of the signaling cascade.

i) ATF6 translocates into the Golgi apparatus where S1P and S2P proteases cleave and activate ATF6, which is then trafficked to the nucleus and activates cytoprotective genes.

ii) PERK dimerizes, subsequently autophosphorylates and phosphorylates eukaryotic initiation factor 2 alpha (eIF2α), which leads to a general inhibition of translation.

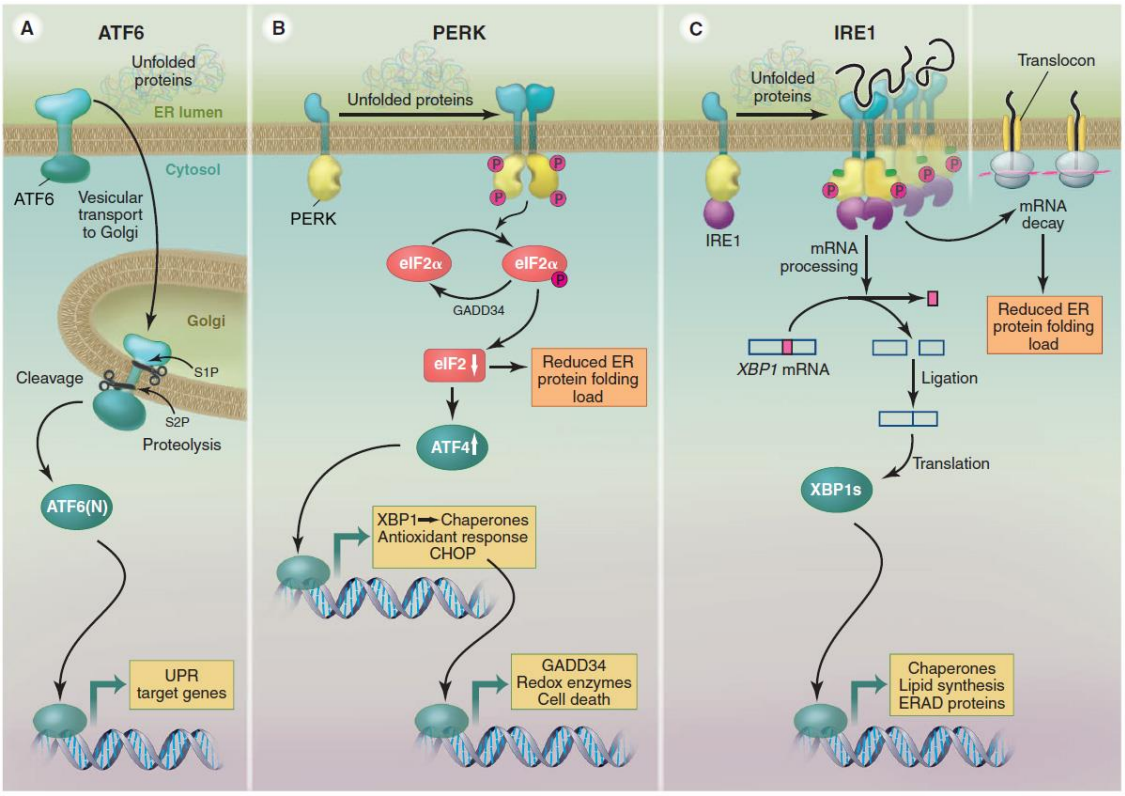

Fig. 15: Overview of the erUPR pathways. Unfolded proteins are sensed by BiP in the ER lumen and the three distinct UPR pathways are activated: (**A**) ATF6, (**B**) PERK, (**C**) IRE1. Upon mild ER stress cytoprotective genes are induced whereas severe or persisting ER stress leads to an apoptotic response, *e.g.* upregulation of CHOP. Adapted from (Walter and Ron 2011).

By decreasing the translation rate, the burden of newly synthesized polypeptides is reduced, enabling folding and degradation mechanisms to eliminate the misfolded proteins. At the same time p-eIF2α activates the translation of *Atf4* mRNA. ATF4 is a transcription factor that activates cytoprotective genes upon mild stress, but also can induce proapoptotic factors like C/EBP homology protein (CHOP) during permanent or severe ER stress.

iii) IRE1 dimerizes and forms an active endonuclease which removes a 26-nucleotide intron from the X-box binding protein 1 (XBP1) mRNA. Translation of spliced XBP1 mRNA results in a transcription factor, which activates transcription of cytoprotective genes (Schroder and Kaufman 2005, Hetz 2012). An additional mechanism to reduce the protein load in the ER during prolonged stress is the regulated IRE1-dependent decay (RIDD) of ER-bound mRNA (Hollien and Weissman 2006). As shown in Fig. 15C ribosomes connected with the ER membrane (rough ER) hold mRNA which is selectively degraded by RIDD to decrease the synthesis of new ER associated proteins.

4.10 The unfolded protein response in mitochondria

Mitochondria are composed of around 1000 different nuclear encoded proteins, which are synthesized by the cytosolic ribosome. In addition, 13 proteins are encoded by the mitochondrial DNA (mtDNA) and are translated by the mitochondrial ribosome. The mitochondrial proteins of cytosolic origin are kept in an unfolded state and shielded during synthesis by cytosolic chaperones. This nascent polypeptide chaperone complex is trafficked to the outer membrane of the organelle, where they interact with receptors and the peptides become imported. Depending on the import signal the proteins are placed into the outer membrane, the inner membrane (IM), the intermembrane space or the matrix of the mitochondria (Dudek, Rehling et al. 2013). Small proteins may fold to their functional conformation without further assistance, larger proteins are target for the mitochondrial chaperonines Hsp60 and Hsp10 (Ostermann, Horwich et al. 1989, Dubaquie, Looser et al. 1997).

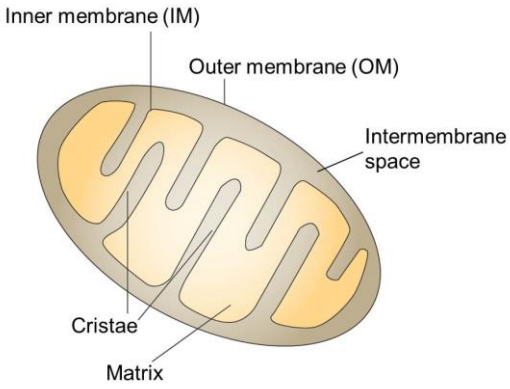

Fig. 16: The mitochondrial organelle. The structural components of the mitochondria are indicated. The organelle consists of one outer and one inner membrane, which enclose the intermembrane space. The inner membrane is compartmentalized into cristae to expand its surface and encompasses the mitochondrial matrix. Adapted from (Blanco, Rego et al. 2011).

Folding of cytosolic synthesized proteins destined for the mitochondrial matrix and IM is supported by mtHsp70. Proteins which cannot be properly folded are substrate for proteases, *i.e.* LON in the matrix and AAA-proteases of the IM (Ngo and Davies 2007, Tatsuta and Langer 2008). The detailed signaling pathway of the mtUPR is currently not known. It has been suggested that c-Jun N-terminal kinase 2 (JNK2) becomes phosphorylated by an unknown stress signal. Activated JNK2 and transcription factor Jun induce transcription of CHOP and C/EBPβ, by binding to their AP1 promotor element (Horibe and Hoogenraad 2007). In turn, CHOP and C/EBPβ activate mitochondrial chaperones like Hsp60 and Hsp10 and proteases. In addition

to the CHOP binding site there exist two other conserved promotor sequences, named mitochondrial UPR elements (MURE) (Fig. 17) (Aldridge, Horibe et al. 2007). Transcription factors interacting with the MURE are currently unknown and the presence of additional signaling pathways is likely.

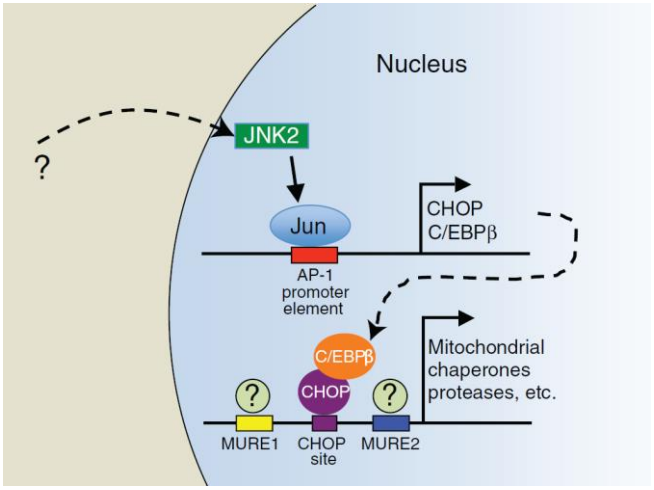

Fig. 17: Activation of the mitUPR: Upon an unknown stress signal the kinase JNK2 and transcription factor Jun activate CHOP and C/EBPβ, which in turn activate the mitochondrial chaperones and proteases. Besides CHOP, an unknown signaling pathway is proposed because of conserved regions MURE1 and 2. Adapted from (Haynes and Ron 2010).

4.11 Formation of ROS

In eukaryotes, oxidative phosphorylation is the main metabolic energy pathway. This pathway uses five multisubunit complexes of the mitochondrial respiratory chain to produce ATP (Fig. 18). Here, electrons are donated from NADH to complex I or from $FADH_2$ to complex II and are carried by coenzyme Q to complex III. Complex III passes the electrons to cytochrome C which finally transfers them to complex IV where hydrogen (H^+) ions and oxygen form water (H_2O). During the movement of the electrons through the complexes I, III and IV, H^+ ions are pumped across the inner membrane from the mitochondrial matrix into the intermembrane space. The resulting electrochemical gradient is used by complex V (ATP-synthase) to generate ATP from ADP and inorganic phosphate (West, Shadel et al. 2011). As a result of a leaky electron transport, electrons can be transferred to molecular oxygen, generating superoxide ($O2^{\cdot -}$). Under normal physiological conditions 1-2% of the consumed oxygen is transformed into $O2^{\cdot -}$ (Orrenius, Gogvadze et al. 2007). The electron leakage occurs at complexes I, II and III (Orrenius, Gogvadze et al. 2007,

Koopman, Nijtmans et al. 2010). At all three sites superoxide is released into the matrix, whereas complex III also can release it into the intermembrane space (Murphy 2009).

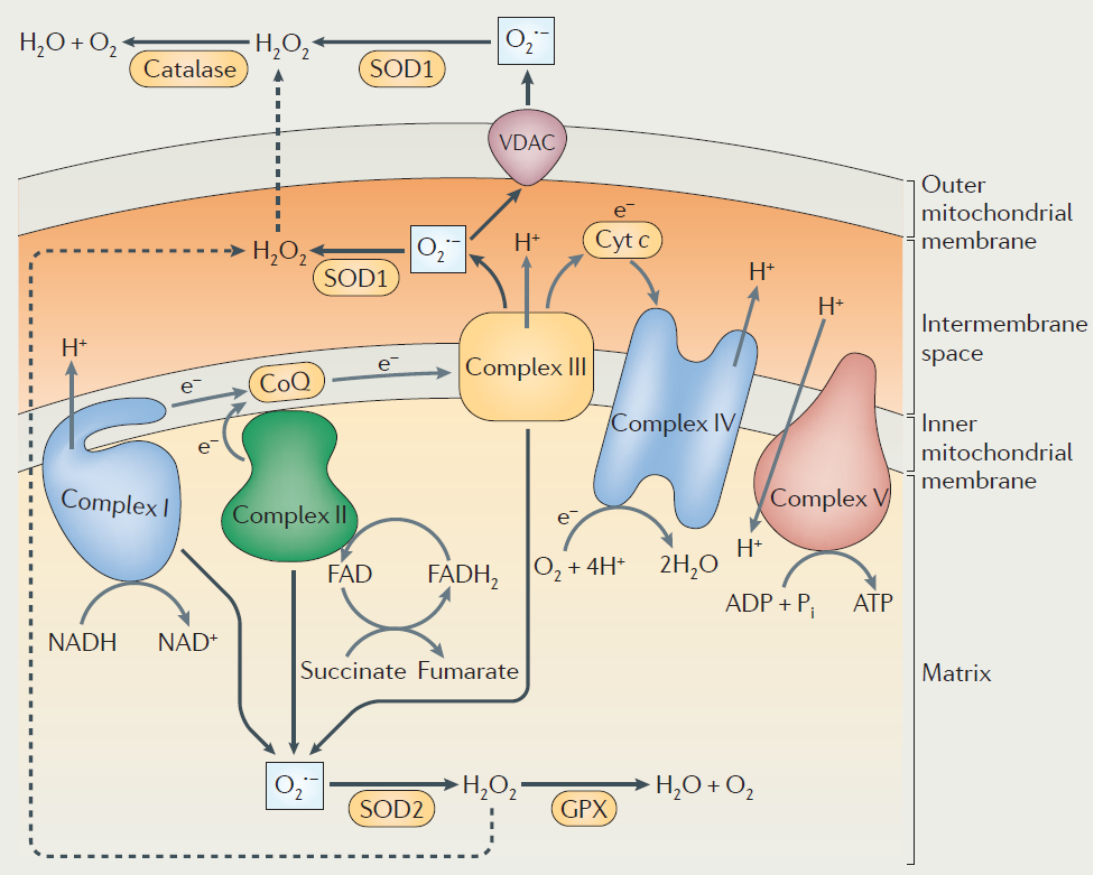

Fig. 18: Overview of the mitochondrial respiratory chain. Superoxide is formed by electron leakage from complexes I-III and can be aggravated under certain stress conditions. Antioxidant enzymes located in the mitochondrial matrix, intermembrane space and cytoplasm counteract against oxidative stress. Figure from (West, Shadel et al. 2011).

By a voltage-dependant anion selective channel (VDAC) superoxide can cross the outer membrane. Highly toxic superoxide can be converted by the matrix resident superoxide dismutase 2 (SOD2) or by the intermembrane space/cytoplasm located SOD1 to hydrogen peroxide (H_2O_2) (Han, Antunes et al. 2003). H_2O_2 can freely cross membranes and gets further converted and detoxified by antioxidant enzymes like catalase. Under certain stress conditions leakiness of the respiratory chain increases and mitochondrial superoxide production is aggravated. Mitochondrial oxidative stress occurs as a result of an imbalance between ROS production and ROS elimination if the antioxidant defence is overwhelmed or downregulated. Mitochondrial enzyme deficiencies and misfolded proteins may contribute to oxidative

stress due to loss of enzyme function and accumulation of toxic metabolites (Tonin, Ferreira et al. 2010, Schmidt, Corydon et al. 2011, Tonin, Amaral et al. 2013).
Cytosolic misfolded proteins can also induce mitochondrial ROS. Misfolded proteins may form fibril-like aggregates, which permeabilize membranes of intracellular compartments like the ER (Varadarajan, Yatin et al. 2000). The ER possesses Ca^{2+} at a concentration 100-fold higher than the cytoplasm. Release of ER-stored Ca^{2+} ions results in activation of mitochondrial metabolic processes and subsequently increases production of ROS (Zhang 2010).

Mitochondrial ROS formation can also be induced by impairment of the proteasome. Misfolded proteins may affect proteasome function. In neurodegenerative diseases like the prion, Alzheimer or Parkinson disease, accumulation of misfolded proteins is accompanied by increased levels of ubiquitin conjugates and decreased function of the proteasome (Rubinsztein 2006). The β-sheet-rich isoform of the cellular prion protein has been shown to directly impair the function of the proteasome (Deriziotis, Andre et al. 2011). Impairment of the proteasome in turn results in accumulation of polyubiquitinated proteins in the mitochondrial outer membrane, loss of mitochondrial membrane potential and increased generation of mitochondrial derived superoxide (Maharjan, Oku et al. 2014).

In the ER, ROS can be generated in presence of misfolded proteins by a process called oxidative protein folding. The ER has an oxidative milieu with distinct oxidoreductases like protein disulfide isomerases (PDIs). Together with ER oxidoreductin 1 (Ero1) PDIs form the mayor stress-induced oxidative folding pathway. These enzymes can create, disrupt and redistribute disulfide bonds. Ero1 catalyzes the generation of disulfide bonds by transferring electrons from dithiols to molecular oxygen. As a result, the activity of Ero1 produces one molecule H_2O_2 per *de novo* generated disulfide bond (Gross, Sevier et al. 2006). In the presence of an overload of misfolded proteins, hyperactivity of this enzyme results in elevated H_2O_2 production which contributes to the total ROS amount in a cell (Pagani, Fabbri et al. 2000, Araki, Iemura et al. 2013).

4.12 Aminoglycosides, ROS, and ototoxicity

Aminoglycosides have a higher affinity for bacterial ribosomes as compared to the cytoplasmic and mitochondrial ribosomes of eukaryotes. This is a result of the

phylogenetic sequence variability in positions 1408 and/or 1491 of the highly conserved helix 44 of the ribosomal A-site, the drug-binding pocket. However, aminoglycoside treatment is associated with severe side effects like ototoxicity (Keene and Hawke 1981).

Aminoglycoside-induced ototoxicity is irreversible and manifests in the cochlea and by aminoglycoside-induced hair cell loss (Ruedi, Furrer et al. 1952, Forge and Schacht 2000). Hair cells are the primary targets of aminoglycosides (Lautermann, Dehne et al. 2004, Schacht, Talaska et al. 2012). The exact mechanism of hair cell degradation is still unclear, but the formation of reactive oxygen species (ROS) presumably is an important factor. Addition of a ROS scavenger was able to protect hair cells from cell death after aminoglycoside treatment and overexpression of the superoxide dismutase rescued mice from kanamycin induced ototoxicity (Sha, Zajic et al. 2001). Since mitochondria are a major source of ROS (Brown and Borutaite 2012), aminoglycoside-induced ototoxicity is most likely mediated by these organelles. However, the exact mechanism of aminoglycoside-induced ROS formation is still speculative. Gentamicin may induce oxidative stress due to its chemical properties by forming a redox-active iron chelate (Sha and Schacht 1999).

Anecdotal evidence indicates that aminoglycosides induce mistranslation in eukaryotes *in vitro* and *in vivo* (Buchanan, Stevens et al. 1987). From an evolutionary point of view, the mitochondrial ribosome is more related to bacterial ribosomes than to the eukaryotic cytoplasmic ribosome. Structural similarity of the A-sites of the bacterial and the mitochondrial rRNAs allows aminoglycosides to bind to mitochondrial ribosomes inhibiting their translation (Hobbie, Akshay et al. 2008). The susceptibility of mitochondrial ribosomes to aminoglycosides correlates with their relative cochleotoxicity (Hobbie, Akshay et al. 2008). In addition, sequence alterations of the mitochondrial small ribosomal RNA, namely A1555G and C1494T, result in hyper-susceptibility to aminoglycosides and may lead to ototoxicity (Prezant, Agapian et al. 1993, Zhao, Li et al. 2004). Altogether these findings suggest that the mitochondrial ribosome is a key target for aminoglycosides.

5 Results

5.1 Dual luciferase read-through reporters

Dual luciferase constructs were used to investigate the efficacy of aminoglycosides to inhibit translation and to induce read-through of stop-codons. In these assays, N-terminal humanized renilla luciferase (hRluc) and C-terminal humanized firefly luciferase (hFluc) genes were fused together by a peptide linker (STCDQPFGF) using the PCR based overlap extension method. Two different reporter constructs were created for read-through assessment. The first construct was used for *in vitro* assays (Fig. 19A). Here, the peptide linker is used as a recoding site by mutating the CAA codon (encoding for glutamine) into a nonsense TGA stop codon (Salas-Marco and Bedwell 2005). The dual luciferase construct was cloned into a pT7 vector, where gene expression is driven by a T7 promotor, allowing *in vitro* transcription by the T7 polymerase. The resulting reporter mRNA was used for *in vitro* rabbit reticulocyte lysate (RRL) translation assays. The luminescence of hFluc is a direct measure of read-through events and the signal of hRluc permits for normalization to translation efficiency.

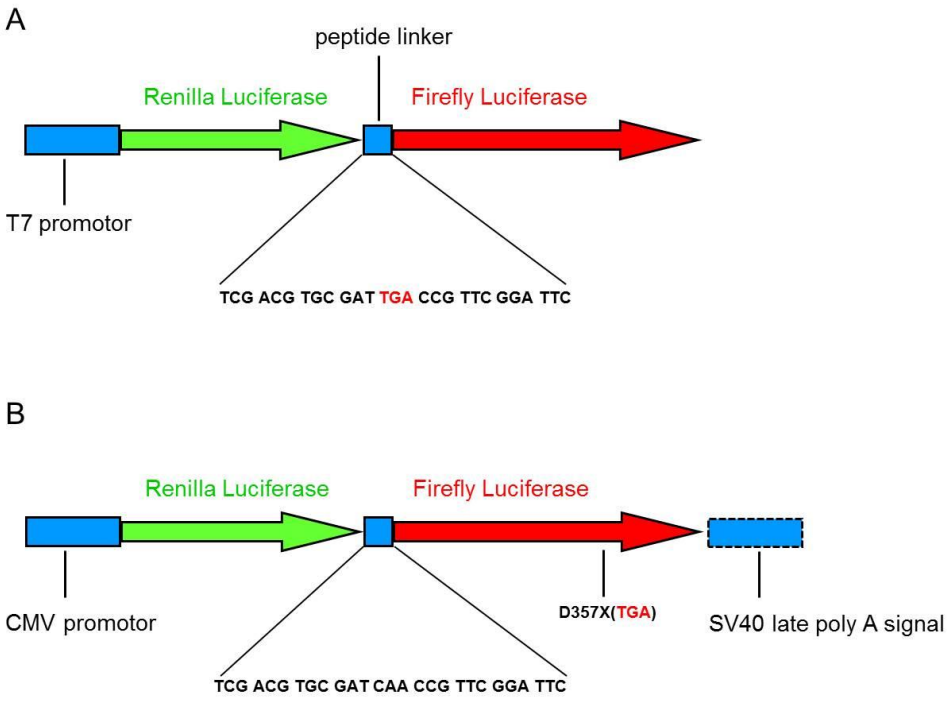

Fig. 19: Read-through reporter constructs. (**A**) *in vitro* read-through reporter construct used for RRL translation assays. (**B**) *in vivo* read-though reporter used in HEK cells. The nonsense stop codons are indicated in red.

The second read-through reporter construct shown in Fig. 19B was used for *in vivo* experiments. The dual luciferase construct was cloned into a pRM vector, where gene expression is driven by a cytomegalovirus (CMV) promotor. The SV40 late poly(A) signal is attached to the reporter gene, ensuring proper mRNA processing in eukaryotic cells. The nonsense stop codon mutation D357X_{TGA} is located at the 3' end of the hFluc gene. This codon position was chosen because structural analysis revealed that amino acid 357 is located in an unstructured and little conserved loop of hFluc providing high probability that any amino acid incorporated in this position will result in a functional protein.

To validate the read-through assay, autoradiography using S^{35}-labeled methionine was used to analyze the proteins translated in an *in vitro* RRL translation assay. Without drug treatment the N-terminal hRluc protein of the read-through reporter was exclusively translated. As shown in Fig. 20A, the hRluc-TGA-hFluc construct showed in the absence of paromomycin a pattern identical to the single hRluc reporter. Exposure to paromomycin, an efficient read-through inducer, resulted in increased synthesis of the hRluc-hFluc fusion protein. Drug titration demonstrated an increase in translation of a protein, which runs at the same position as the control hRluc-hFluc fusion protein without nonsense stop codon. This pattern indicated that the TGA stop codon of the linker was suppressed by paromomycin and a full-size fusion product was synthesized. No single hFluc bands were detected in the read-through reporter samples, revealing that hFluc was exclusively synthesized when a read-through event occurred. Densitometric analysis of the protein bands corresponding to the hRluc-hFluc fusion protein and hRluc demonstrated read-through induction (Fig. 20B) and translation inhibition (Fig. 20C) in a dose dependent manner. Beyond 20 µM paromomycin, the effect of translation inhibition exceeded the read-through effect and the intensities of the hRluc-hFluc fusion protein bands decreased.

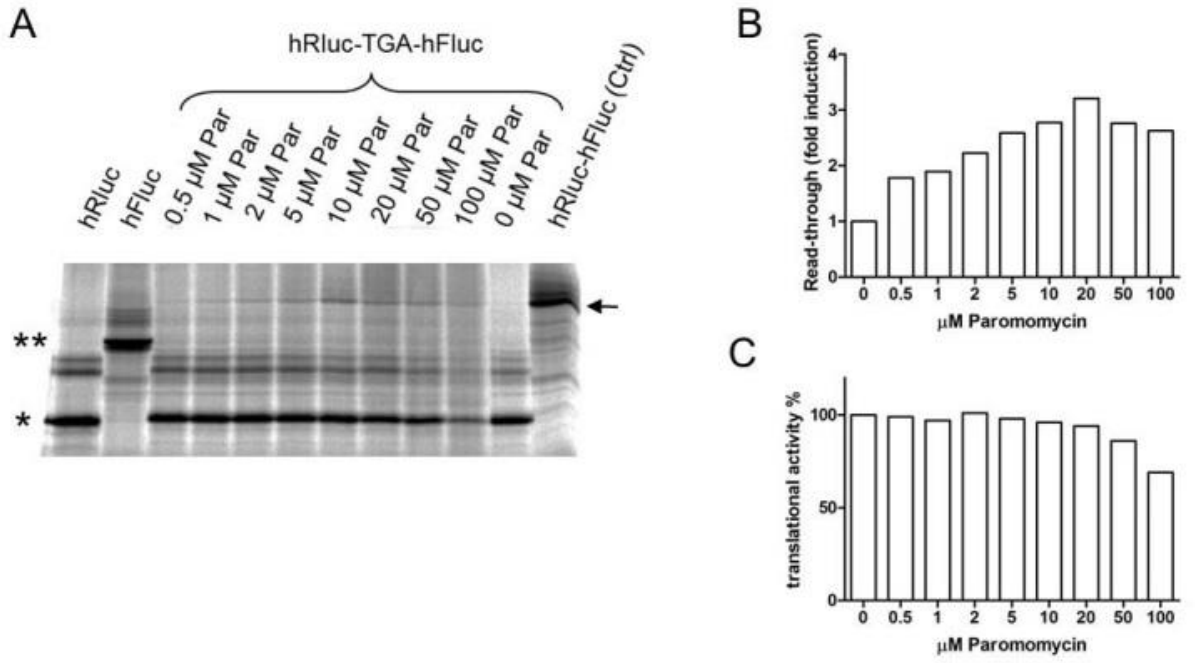

Fig. 20: Autoradiography of read-through reporter construct. (**A**) Autoradiography of RRL *in vitro* translation assay using S^{35}-labeled methionine. Paromomycin (Par) was used as *bona fide* inducer of read-through, the Par concentrations are indicated. The black arrow marks the position of the hRluc-hFluc fusion protein. Single hRluc, single hFluc and fusion hRluc-hFluc mRNAs were used as controls. The asterisk indicates the position of single hRluc protein, the double asterisk the position of single hFluc protein. (**B**) Densitometric analysis of the protein bands corresponding to the hRluc-hFluc protein, indicated by the black arrow in Fig. 20A. (**C**) Densitometric analysis of the protein bands corresponding to the single hRluc protein, indicated by the asterisk in Fig. 20A.

5.1.1 Aminoglycoside-induced read-through *in vitro*

Various aminoglycosides were tested in the *in vitro* RRL translation assay to determine their read-through activity. Geneticin, gentamicin and paromomycin were chosen as highly effective inducers of mistranslation (Buchanan, Stevens et al. 1987, Clancy, Bebok et al. 2001) and compared to tobramycin, neomycin, kanamycin A and its derivative amikacin. Apramycin, a structurally unique aminoglycoside was also included (O'Connor, Lam et al. 1976). As a control we used the translocation inhibitor hygromycin B (Manuvakhova, Keeling et al. 2000).

Among the aminoglycosides tested, hygromycin B and geneticin are the strongest translation inhibitors (IC_{50}: 0.04 µM and 0.43 µM, respectively) (See Table 1 and Fig. 21A). Apramycin, kanamycin A and amikacin showed modest translation inhibition with IC_{50} values of 93.5, 147.8 and 207.3 µM (Fig. 21A, B). Stop codon read-through

was 4 to 5-fold increased by geneticin, paromomycin and gentamicin compared to non-induced levels (Fig. 22A). Amikacin and neomycin showed minor effects on read-through (Fig. 22A,B), while apramycin, kanamycin A and hygromycin B had virtually no effect on read-through of stop codons (Fig. 22A, B). Relative read-through levels, *i.e.* the ratio of read-through induction and translation efficiency, revealed that geneticin, gentamicin and paromomycin effectively induced read-through. In contrast, apramycin, hygromycin B and kanamycin A do not induce any read-through (Fig. 23A, B).

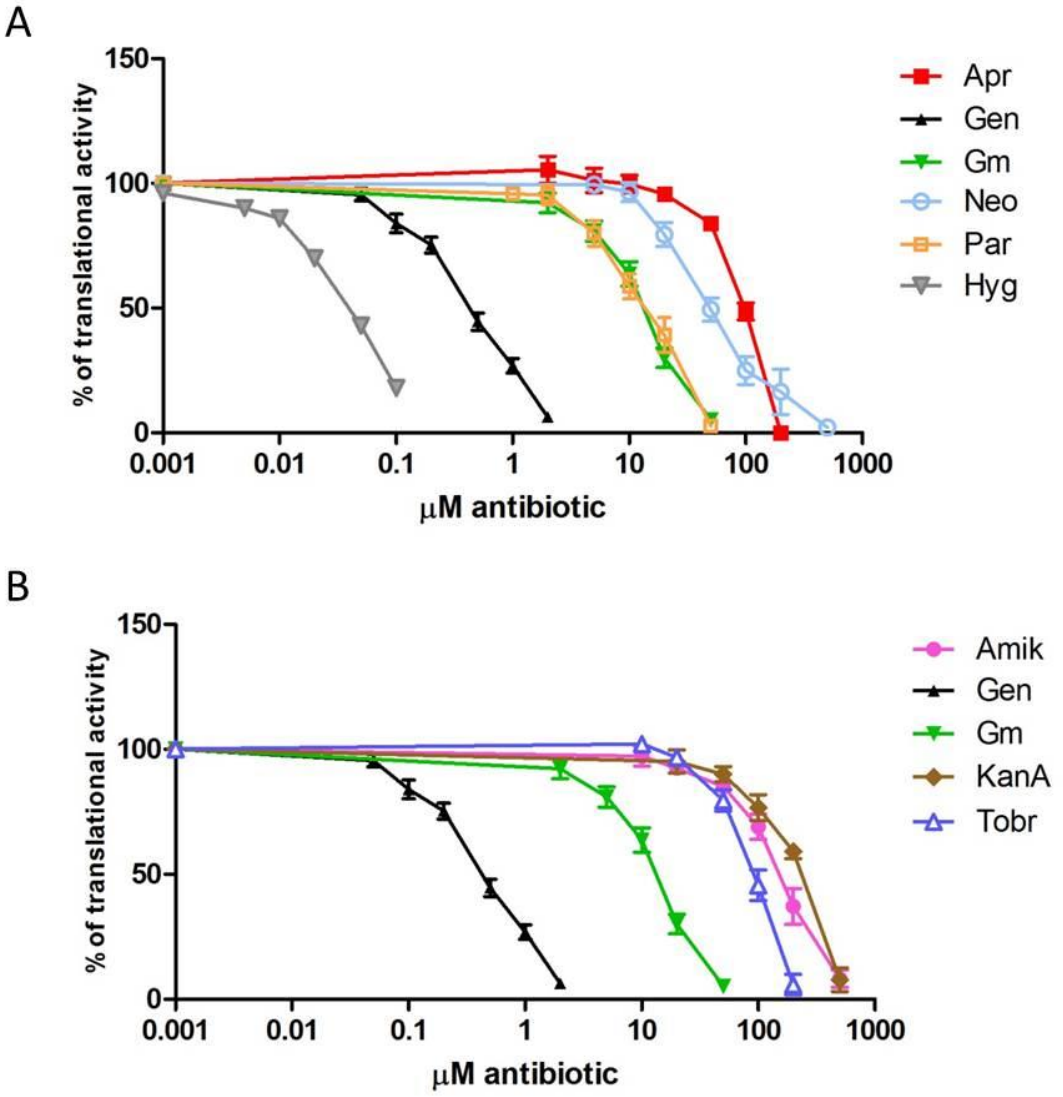

Fig. 21: Dual luciferase *in vitro* translation assay using RRL. Drug-induced translation inhibition measured by hRluc luminescence. (**A**) Apramycin (Apr), geneticin (Gen), gentamicin (Gm), neomycin (Neo), paromomycin (Par) and hygromycin B (Hyg). (**B**) Amikacin (Amik), kanamycin A (KanA) and tobramycin (Tobr), Gen and Gm are included for comparison (n=3, ±SEM).

Table 1: Inhibition of protein synthesis. *In vitro*-IC_{50} values of aminoglycoside antibiotics measured by *in vitro* dual luciferase assay using RRL ribosomes**.**

Antibiotic	IC_{50} values [µM]
Hyg	0.04
Gen	0.43
Gm	12.6
Par	12.9
Neo	51.2
Tobr	88.9
Apr	93.5
Amik	147.8
KanA	207.3

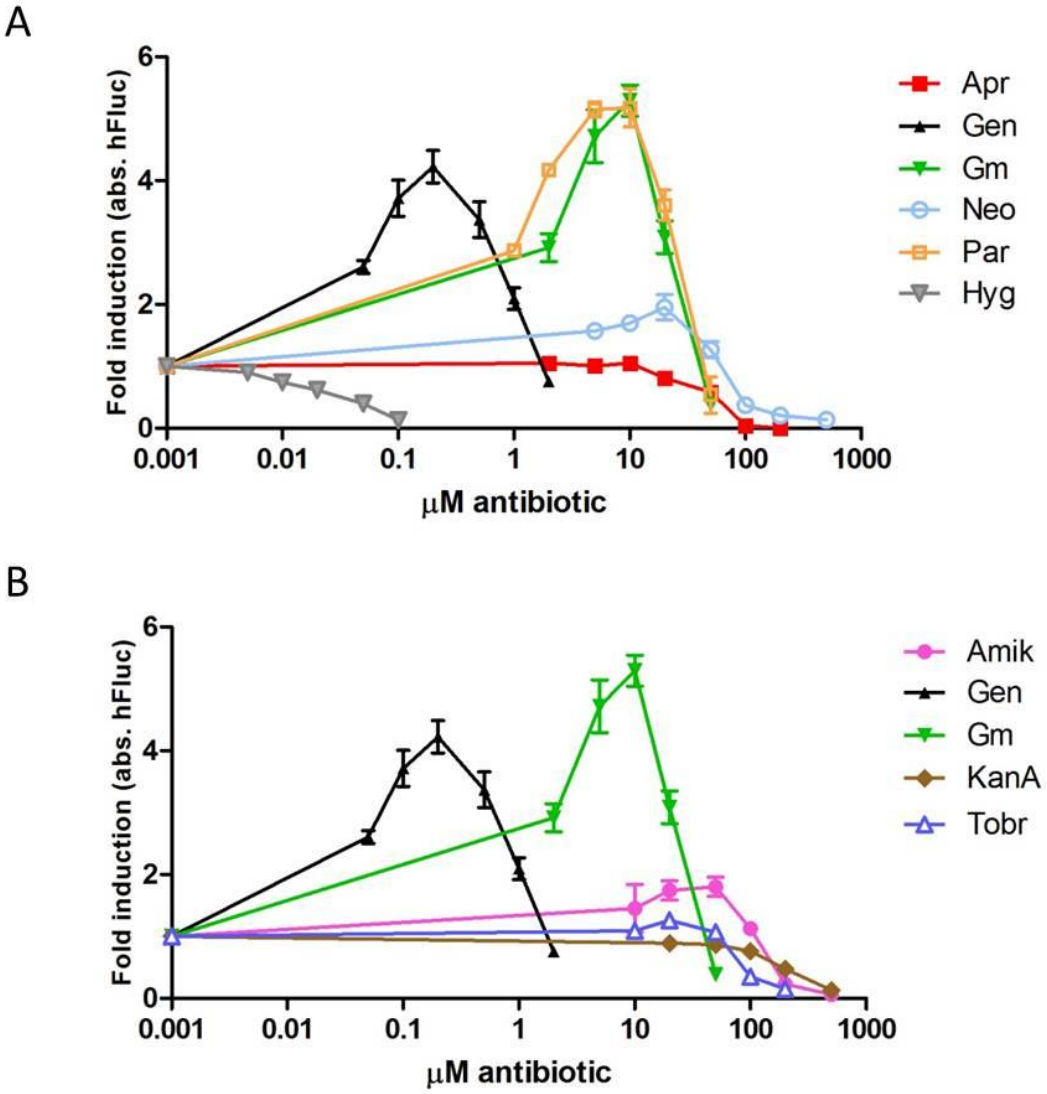

Fig. 22: Dual luciferase *in vitro* translation assay using RRL. Drug-induced read-through measured by hFluc luminescence. (**A**) Apramycin (Apr), geneticin (Gen), gentamicin (Gm), neomycin (Neo), paromomycin (Par) and hygromycin B (Hyg). (**B**) Amikacin (Amik), kanamycin A (KanA) and tobramycin (Tobr), Gen and Gm are included for comparison (n=3, ±SEM).

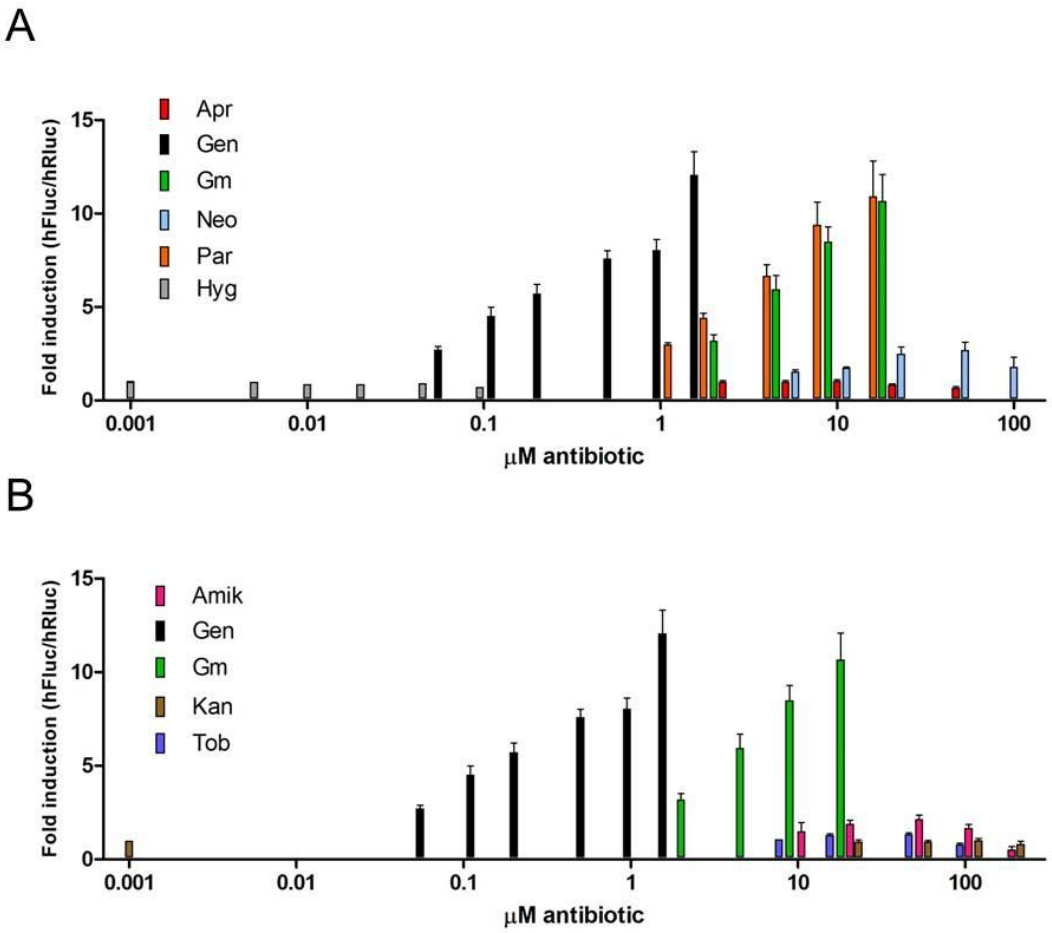

Fig. 23: *In vitro* read-through relative to translation efficiency. Relative read-through induction has been calculated by the ratio of hFluc/hRluc (n = 3, +SEM). The untreated samples were set as 1. (**A**) Apramycin (Apr), geneticin (Gen), gentamicin (Gm), neomycin (Neo), paromomycin (Par), hygromycin B (Hyg). (**B**) Amikacin (Amik), kanamycin A (KanA) and tobramycin (Tobr), Gen and Gm are included for comparison.

5.1.2 Aminoglycoside-induced read-through *in vivo*

The efficacy of aminoglycosides to induce read-through was studied *in vivo*. The dual luciferase reporter construct was cloned into the pRM vector, which is under the control of the CMV promotor. As host cell the HEK293 cell line was chosen. HEK cells are derived from human embryonic kidney cells, but do not have the megalin-mediated aminoglycoside endocytosis system in contrast to nephritic tubular cells. HEK cells rather show characteristics of neuronal than of endothelial, epithelial or fibroblast cells (Shaw, Morse et al. 2002). However, for our purposes it was important that HEK cells are easy to transfect and show a high translation rate (Geisse and Voedisch 2012), facilitating the use of reporter constructs to study drug-induced mistranslation. Following transfection with the pRM hRluc-hFluc D357X_{TGA} reporter

construct, the HEK293 cells were incubated in F10 media supplemented with saponin and serially diluted antibiotics. After 24 hours cells were lysed and luciferase activities were monitored.

In HEK293 cells hygromycin B was the most potent translation inhibitor (IC_{50} = 2.6 µM), followed by geneticin (IC_{50} = 9.0 µM) (See Table 2 and Fig. 24A). Paromomycin and gentamicin also inhibited translation but at a 30-fold higher concentration (IC_{50} = 376 and 337 µM, respectively). Apramycin, tobramycin, kanamycin A and neomycin had IC_{50} values higher than 450 µM (Fig. 24A, B).

Table 2: Inhibition of protein synthesis. *In vivo*-IC_{50} values of aminoglycoside antibiotics measured by *in vivo* dual luciferase assay in HEK293 cells.

Antibiotic	IC_{50} values [µM]
Hyg	2.6
Gen	9.0
Gm	337
Par	376
Apr	486
Amik	> 500
KanA	> 500
Neo	> 500
Tob	> 500

In agreement with the *in vitro* hFluc data, geneticin, gentamicin and paromomycin induced read-through (Fig. 25A), while amikacin and hygromycin B showed little effect on read-through (Fig. 25A. B). Apramycin had no impact on read-through in this assay (Fig. 25A).

Calculation of the relative read-through induction confirmed that geneticin, gentamicin and paromomycin are strong inducers of read-through. (Fig. 26A, B). Comparison of the IC_{50} values determined by the *in vivo* and *in vitro* assays demonstrated a good correlation with a squared Pearson product-moment correlation coefficient R^2 = 0.8749 (Fig. 27). The results demonstrate that the *in vitro* assays adequately reflect that of the whole cell in-vivo.

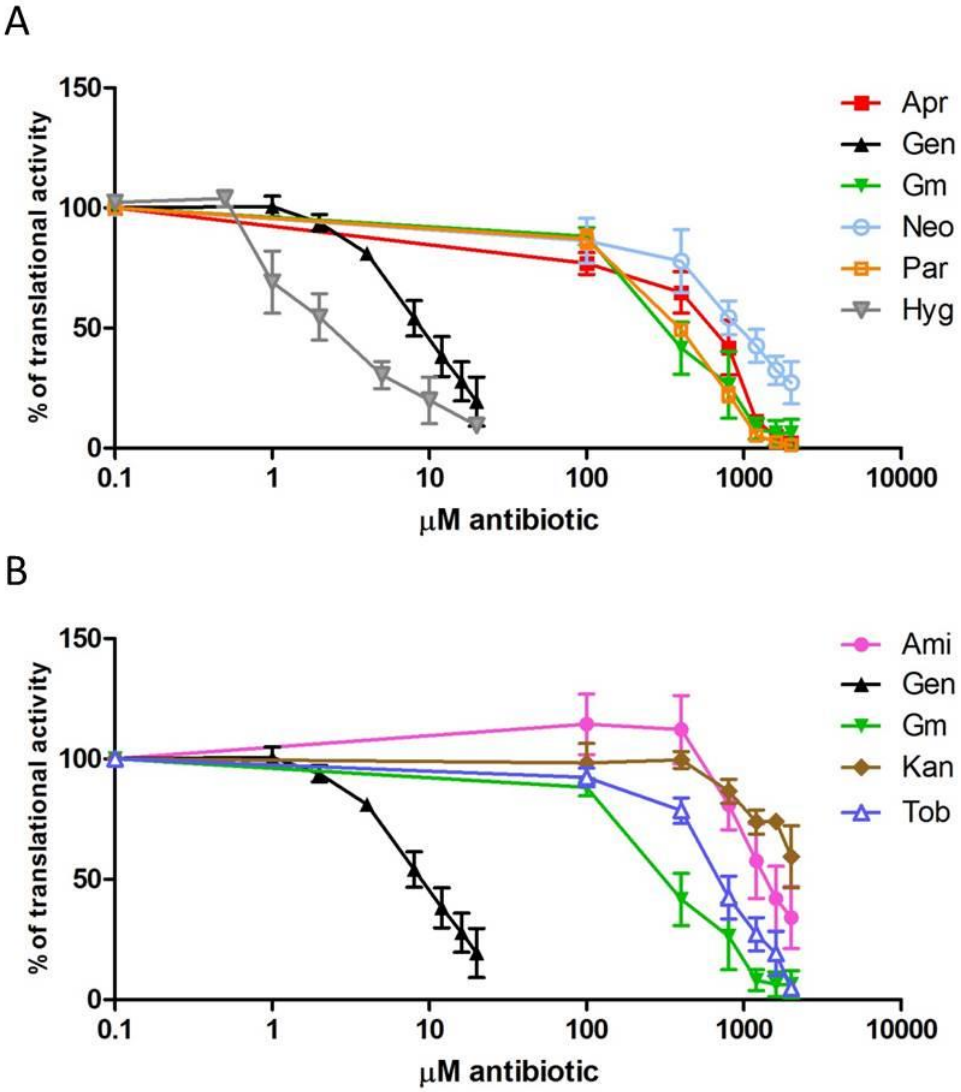

Fig. 24: Dual luciferase *in vivo* translation assay using HEK293 cells. Drug-induced translation inhibition measured by hRluc luminescence. (**A**) Apramycin (Apr), geneticin (Gen), gentamicin (Gm), neomycin (Neo), paromomycin (Par) and hygromycin B (Hyg). (**B**) Amikacin (Amik), kanamycin A (KanA) and tobramycin (Tobr), Gen and Gm are included for comparison (n=3, ±SEM).

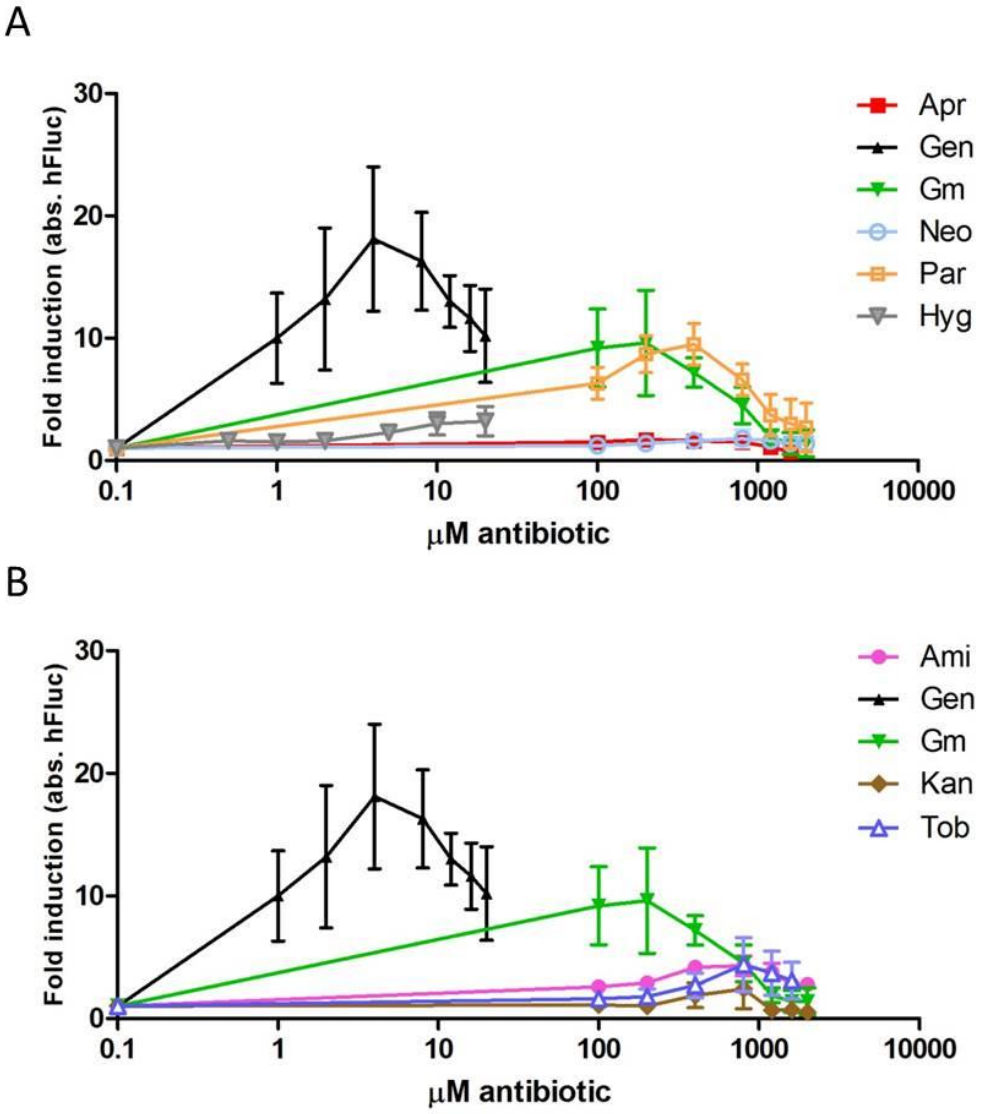

Fig. 25: Dual luciferase *in vivo* translation assay using HEK293 cells. Drug-induced read-through measured by hFluc luminescence. (**A**) Apramycin (Apr), geneticin (Gen), gentamicin (Gm), neomycin (Neo), paromomycin (Par) and hygromycin B (Hyg). (**B**) Amikacin (Amik), kanamycin A (KanA) and tobramycin (Tobr), Gen and Gm are included for comparison (n=3, ±SEM).

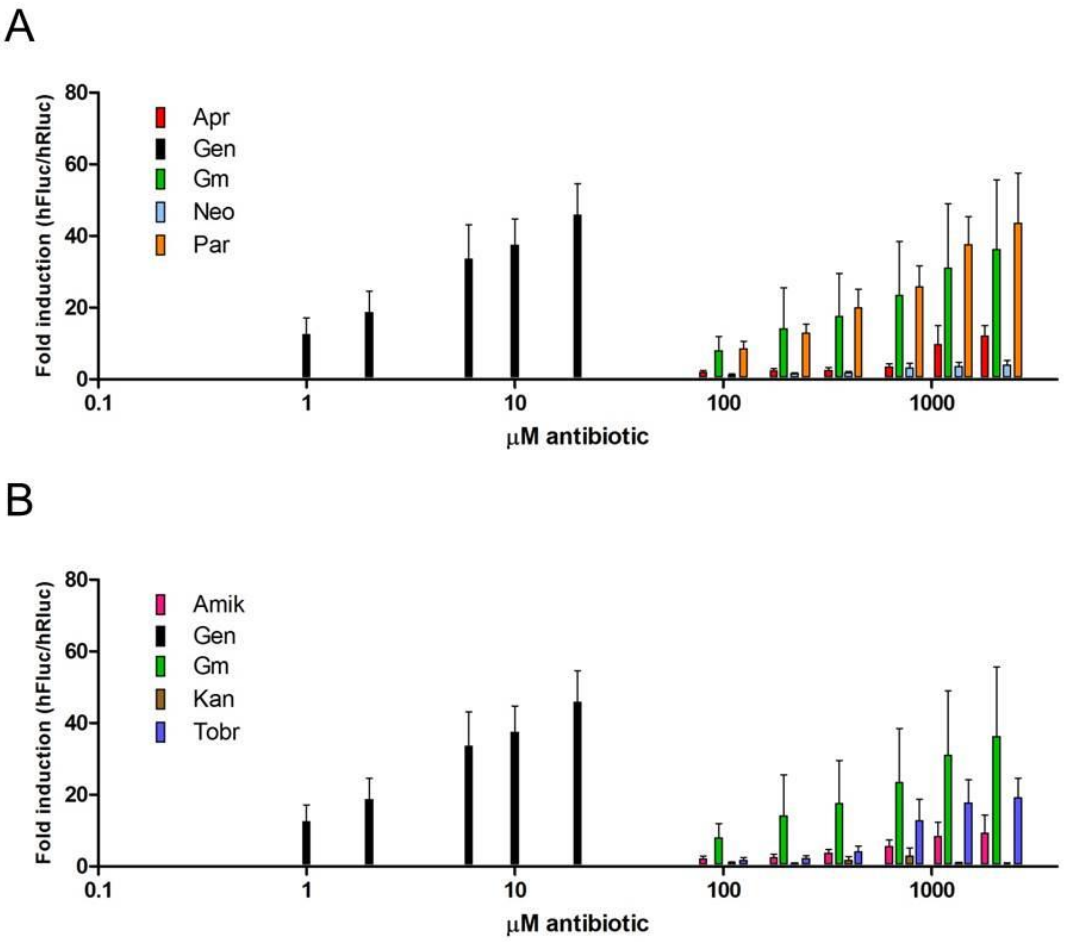

Fig. 26: *In vivo* read-through relative to translation efficiency. Relative read-through induction has been calculated by hFluc/hRluc (n = 3, +SEM). The untreated samples were set as 1. For simplicity, the drug concentrations 200, 400, 800, 1200 and 1600 µM are plotted beyond 100 µM. (**A**) apramycin (Apr), geneticin (Gen), gentamicin (Gm), neomycin (Neo), paromomycin (Par). (**B**) amikacin (Amik), kanamycin A (KanA) and tobramycin (Tobr), Gen and Gm are included for comparison.

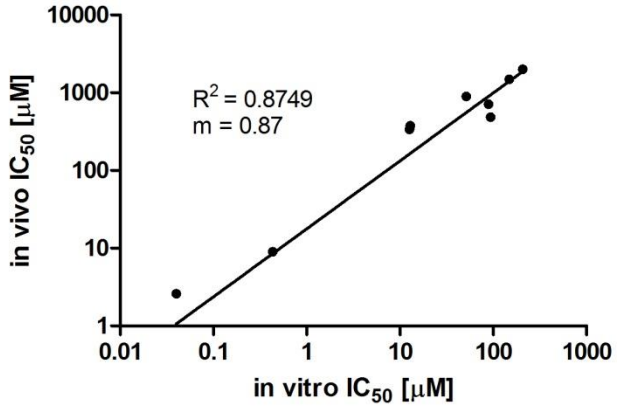

Fig. 27: Comparison of *in vivo* and *in vitro* IC_{50} values. Correlation of IC_{50} values determined *in vitro* and *in vivo* from the tested aminoglycosides. Squared Pearson product-moment correlation coefficient R^2 and the slope (m) of the regression line are indicated.

5.2 Aminoglycosides and ROS formation

Aminoglycosides were tested for their efficiency to induce reactive oxygen species (ROS), since increased ROS production is a hallmark of aminoglycoside-induced ototoxicity (Forge and Schacht 2000). For this purpose we used the MitoSOX dye which detects specifically mitochondrial superoxide. As a positive control, 20 µg/ml Antimycin A were used, which inhibit mitochondrial complex III and induce formation of superoxide (Ksenzenko, Konstantinov et al. 1983). HEK293 cells were incubated for 24 h and 48 h in F10 medium supplemented with saponin and serially diluted geneticin. HEK293 APH(3') cells served as a control. Geneticin can be modified by the 3' aminoglycoside-phosphotransferase APH(3'). As a result, geneticin loses its affinity towards the ribosome, which allows to test for ribosomal involvement of geneticin-induced ROS. Geneticin-treated cells incubated for 24 h showed minor elevated superoxide levels compared to the untreated control (Fig. 28A). Further incubation up to 48 h demonstrated in the HEK293 wt cell line an induction of MitoSOX fluorescence in a dose dependent manner (Fig. 28B). In contrast, the HEK293 APH(3') cells showed no induction of MitoSOX fluorescence, demonstrating that the action of geneticin on the ribosome is responsible for oxidative stress induction.

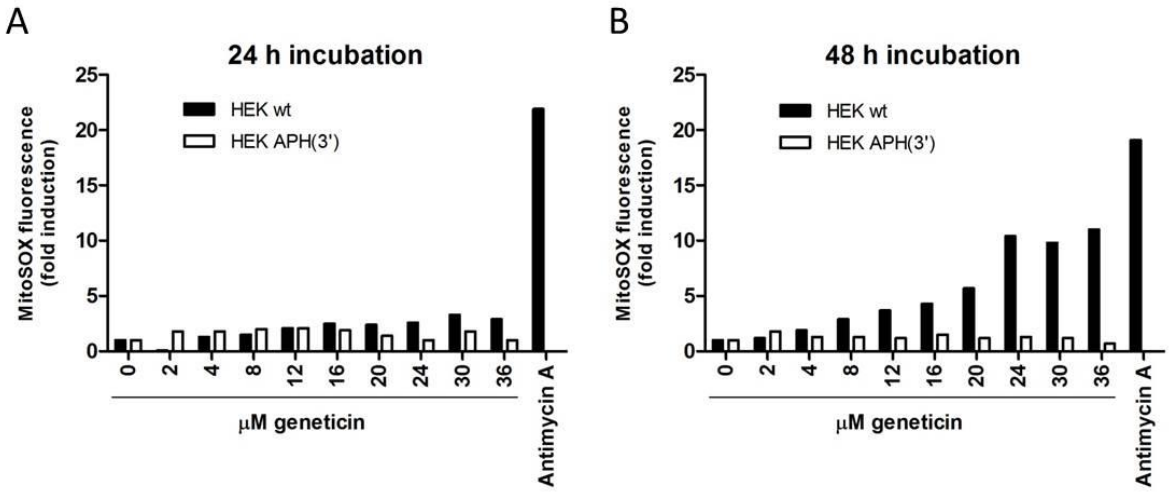

Fig. 28: Superoxide anion detection using MitoSOX dye. Cells were incubated for 24 h (**A**) or 48 h (**B**) with indicated geneticin concentrations and stained with MitoSOX. Fluorescence was measured by FACS, 10000 cells were gated. Antimycin A was used as a positive control.

To test for the specificity of mitochondrial superoxide detection by MitoSOX, osteosarcoma 143B wt and derived rho-0 cells were treated with geneticin. Rho-0

cells lack their mitochondrial DNA and as a result have no functional mitochondrial respiratory chain (King and Attardi 1989), which is the main source of mitochondrial ROS. Cells were incubated in DMEM, because F10 and saponin treatment was harmful for the osteosarcoma cells (data not shown). As a consequence higher geneticin concentrations were used. Antimycin A was used as a positive control. The 143B wild type cells showed an increase of MitoSOX fluorescence upon geneticin treatment in a dose dependent manner (Fig. 29). In contrast, the rho-0 cells did not show any induction of MitoSOX fluorescence in the geneticin and the Antimycin A treated sample, indicating that a functional respiratory chain is essential to increase superoxide levels upon geneticin or Antimycin A treatment.

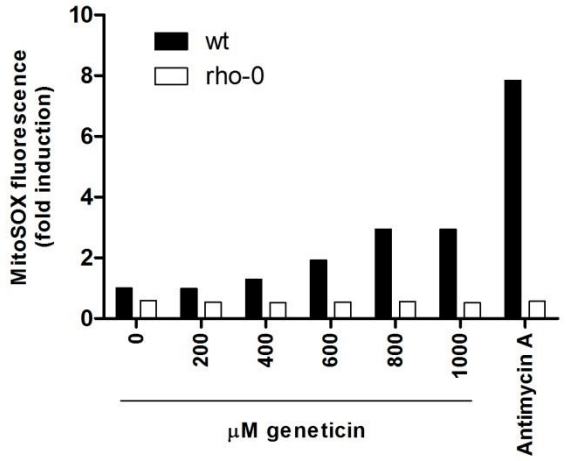

Fig. 29: Superoxide anion detection in osteosarcoma 143B cells. 143B wt and rho-0 cells were incubated for 48 h with indicated geneticin concentrations and stained with MitoSOX. Fluorescence was assessed by FACS, 10000 cells were gated. Antimycin A was used as a positive control.

In subsequent experiments, additional aminoglycosides were studied. Geneticin, hygromycin B, gentamicin and neomycin were tested. Hygromycin B was included to examine the influence of translocation inhibition on ROS generation. HEK293 cells were incubated for 48 h in F10 media supplemented with saponin. In addition to superoxide anions, total ROS levels were measured using the CM-H_2DCFDA dye. Mitochondria specific- and total ROS measurements revealed that hygromycin B induces the most intense oxidative stress at low drug concentrations. Geneticin is also a potent inducer of ROS, but 4-fold higher drug concentrations were needed to achieve similar ROS levels compared to hygromycin B treated cells. Gentamicin induced similar ROS levels at a 10-fold higher concentration compared to geneticin. Neomycin induced modest oxidative stress (Fig. 30A, B). In general, the ability to

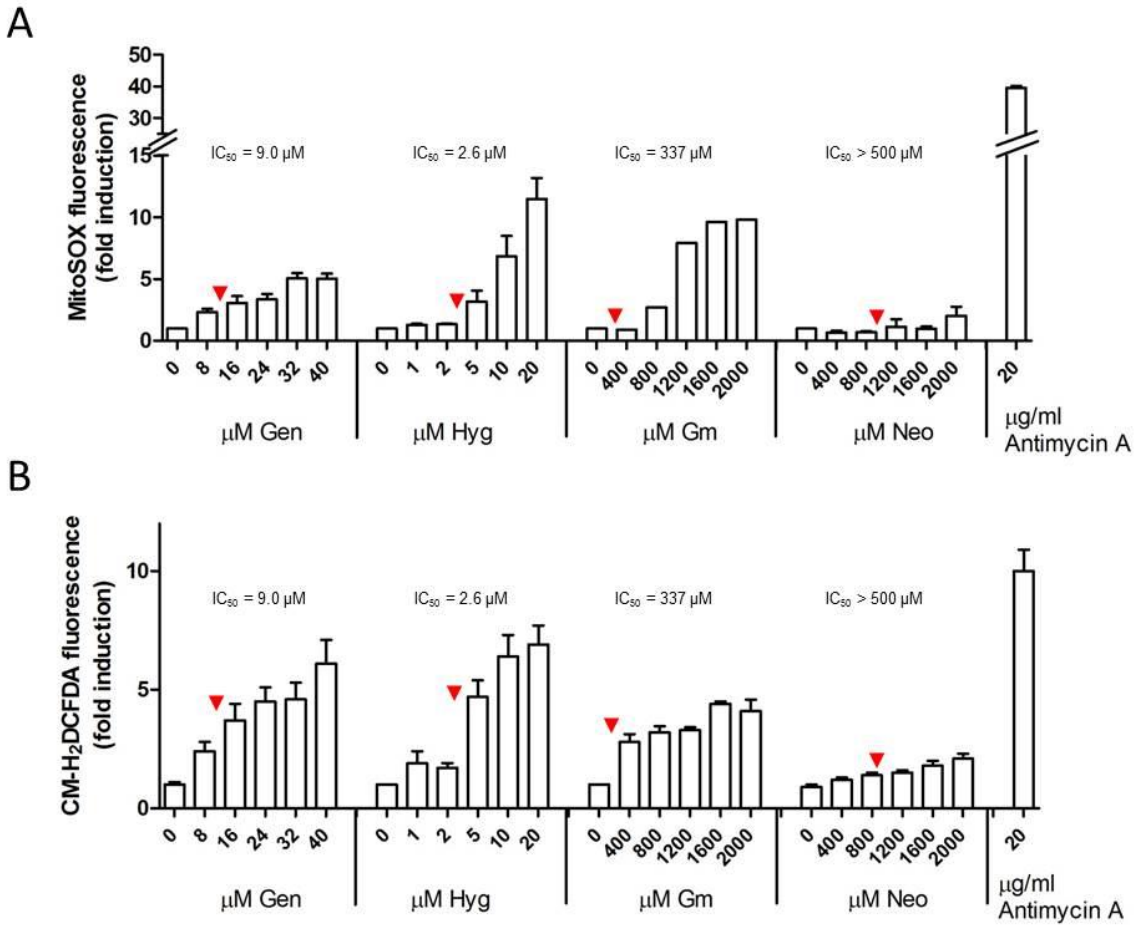

Fig. 30: Drug-induced mitochondrial superoxide and total ROS. HEK cells were incubated for 48 h with indicated drug concentrations. The induction of MitoSOX fluorescence (**A**) and the induction of CM-H_2DCFDA fluorescence (**B**) are shown. Antimycin A was used as a positive control. IC_{50} values are indicated by the red arrowheads (N > 3, except Gm MitoSOX, SEM is indicated).

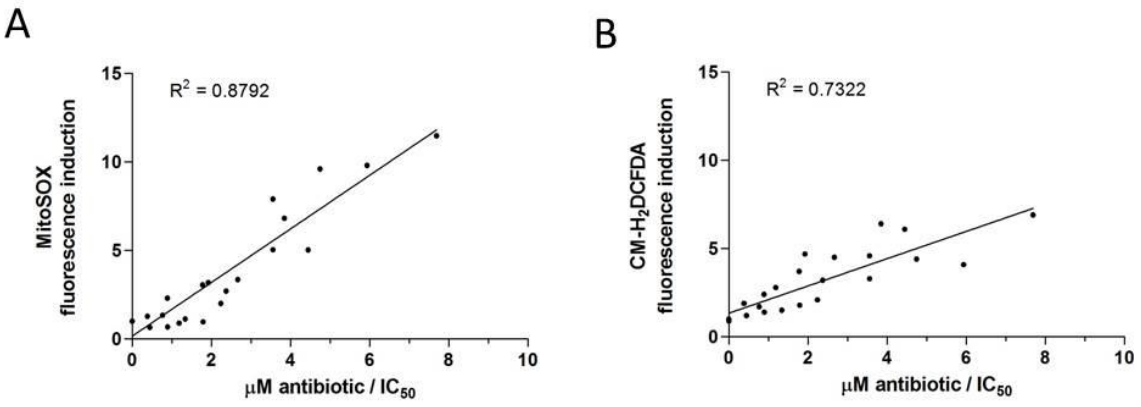

Fig. 31: Correlation of MitoSOX and CM-H_2DCFDA fluorescence induction and translation inhibition. Fold inductions of MitoSOX (**A**) and CM-H_2DCFDA (**B**) fluorescence were plotted against the corresponding drug concentration expressed by the ratio of tested drug concentration divided by the corresponding IC_{50} value. Squared Pearson product-moment correlation coefficient R^2 and the regression line are indicated.

induce oxidative stress correlates well with the IC_{50} values (Fig. 31), with hygromycin B as most potent ribosome inhibitor and ROS inducer, followed by geneticin, gentamicin and neomycin. Hygromycin B is a translocation inhibitor which interacts with both cytoplasmic and mitochondrial ribosomes (Gale 1981). To test for the involvement of either cytosolic or mitochondrial translation in ROS generation, the cytoplasmic translation inhibitor cycloheximide (Schneider-Poetsch, Ju et al. 2010) and the mitochondrial translation inhibitor linezolid were used. The IC_{50} concentration of CHX for cytosolic translation (IC_{50} = 1.2 µM) was determined using the dual luciferase assay. The IC_{50} concentration of linezolid for mitochondrial translation (IC_{50} ≈ 9 µg/ml) was assessed using a whole cell assay and autoradiography to determine S^{35} Methionine incorporation by the mitochondrial ribosome. Cycloheximide treatment induced significant MitoSOX and CM-H_2DCFDA fluorescence at a drug concentration < 50 µM. In contrast, linezolid did not show induction of oxidative stress at the maximum drug concentration (Fig. 32A, B).

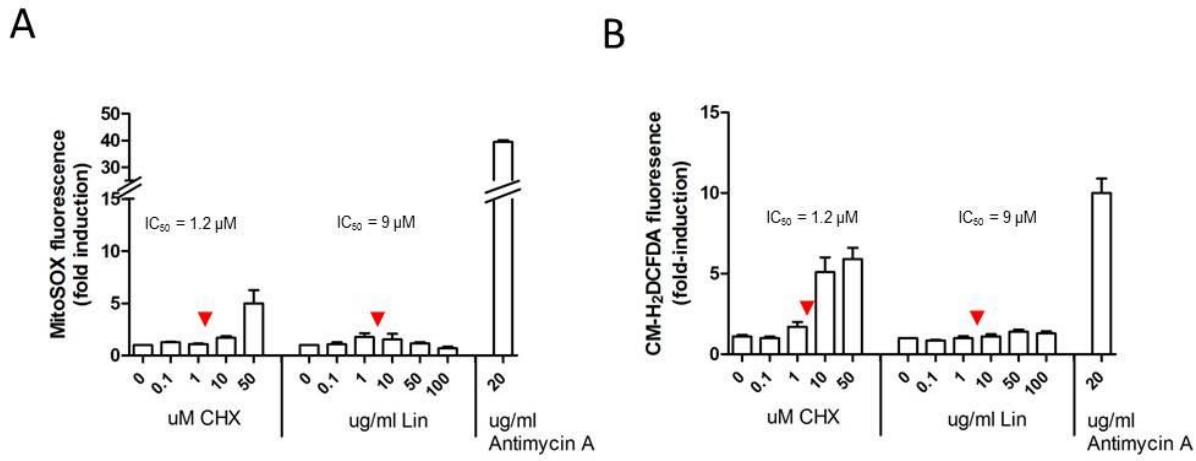

Fig. 32: Drug-induced mitochondrial superoxide and total ROS. HEK293 cells were incubated for 48 h with indicated drug concentrations. (**A**) MitoSOX fluorescence and (**B**) CM-H_2DCFDA fluorescence are shown for cycloheximide (CHX) and linezolid (Lin). Antimycin A was used as a positive control. The corresponding IC_{50} values are indicated by the red arrowheads (N > 3, SEM is indicated).

The data suggest that formation of ROS occurs as a result of translation inhibition of the cytoplasmic, but not of the mitochondrial ribosome. Simultaneous induction of fluorescence of CM-H_2DCFDA and MitoSOX dyes indicates that the main source of ROS is of mitochondrial origin (Fig. 33). ROS formation is dependent on time of incubation (Fig. 28) and a functional respiratory chain (Fig. 29), suggesting that the mitochondrial organelle is sensitive to cytoplasmic translation inhibition.

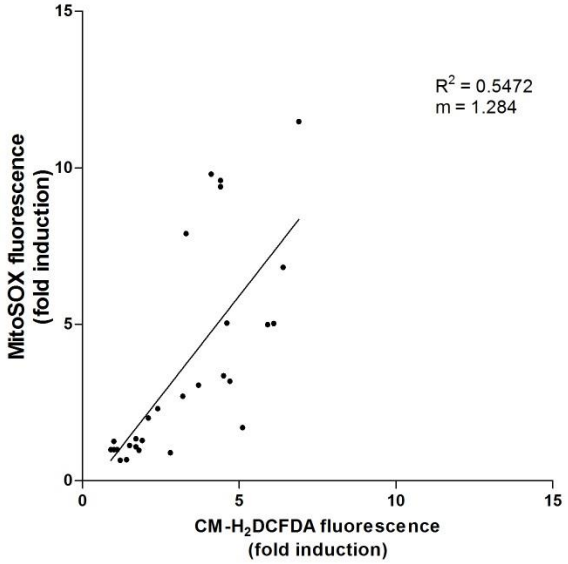

Fig. 33: Comparison of MitoSOX and CM-H_2DCFDA fluorescence. Correlation of MitoSOX and CM-H_2DCFDA fluorescence using tested aminoglycosides and cycloheximide. Squared Pearson product-moment correlation coefficient R^2 and the slope (m) of the regression line are indicated.

5.3 Alterations of the proteome after aminoglycoside treatment

By an unbiased mass spectrometry (MS) approach we wanted to study the effects of translocation inhibition and misreading on the proteome in higher eukaryotes. As shown in chapter 3.1, mistranslation is always accompanied by translation inhibition. To distinguish translation inhibition from mistranslation, two different aminoglycosides with comparable IC_{50} values were chosen. Hygromycin B was used to assess the cells' response to translocation inhibition. In addition, the effects of geneticin on the proteome were studied and were compared to those of hygromycin B to determine the pathways exclusively regulated in the geneticin-treated sample. These unique regulated pathways should give a good approximation on how higher eukaryotic cells react to mistranslation. Using the iTRAQ (isobaric tag for relative and absolute quantification) approach, whole cell protein extracts of geneticin and hygromycin B treated HEK293 cells were studied. In total two separate 4-plex iTRAQ-Mass spectrometry (MS) experiments were performed.

5.3.1 Effects of hygromycin B on the proteome

In the first experiment, two samples of untreated HEK293 cells and two samples of HEK293 cells treated with 7 µM hygromycin B for 32 h were analyzed. As a result,

1385 proteins were identified and quantified. However, the iTRAQ label 114 of one untreated sample was not detected in any spectrum, suggesting a manufacturer error of the reagent. Consequently, the hygromycin B data discussed here are result of one untreated (label 116) and two drug treated (labels 115 and 117) samples. Quantitative testing using permutation test and further correction by Bonferroni corrected p-value resulted in 90 significantly regulated proteins ($p<0.05$) (Fig. 34). Forty-six proteins were found up- and 44 were found downregulated. Table 3 shows the regulated proteins with their corresponding fold inductions and p-values.

Functional classification of the enriched proteins resulted in the main categories translation, mRNA metabolism, metabolism, cellular organization and protein folding. Proteins of the translation category are involved in translational initiation (EIF3D), elongation (EEF1A1, EEF2, and EEF1G), ribosome structure (RPLP0, RPL5) and aminoacyl tRNA synthesis (VARS). In addition, proteins involved in mRNA processing (CSDE1, YBX1, and DDX5) and nonsense mediated mRNA decay (NMD, PABPC1, GSPT1) are enriched, suggesting a general response towards a reduced translation rate and stalled ribosomes. The chaperones HSPH1, HSPA8 and FKBP4, which rescue stress denatured proteins are upregulated as are CCT4, a subunit of the nascent peptide folding complex TRiC, and PSMD6 and UBAP2L, two proteins of the protein degradation pathway. The category metabolism can be subgrouped in carbohydrate metabolism (LDHA, LDHB, GPI, GAPDH, and PGD), nucleic acid biosynthesis (CTPS1, ATIC, CAD, and PFAS) and fatty acid metabolism (FASN, ACAT2). Proteins involved in the structure of the cytoskeleton (TUBA1C, MYH9, FLNA and NEFM) are enriched. Other less represented functional categories comprised transport (TFRC, IPO5, and CAPRIN1), and DNA maintenance (IMPDH1, PFAS).

metabolism	biological function	short name	p-value (BF-corrected)	log_2
Isoform 3 of L-lactate dehydrogenase A chain	Carbonhydrate metabolism	LDHA	0.00017	0.5
L-lactate dehydrogenase B chain	Carbonhydrate metabolism	LDHB	0.0001	0.4
Phosphoribosylformylglycinamidine synthase	purine metabolism	PFAS	0.0023	0.4
Acetyl-CoA acetyltransferase, cytosolic	acyltransferase	ACAT2	0.0029	0.4
Glucose-6-phosphate isomerase	Carbonhydrate metabolism	GPI	0.0001	0.35
Fatty acid synthase	Fatty acid metabolism	FASN	0.0001	0.35
6-phosphogluconate dehydrogenase, decarboxylating	Carbonhydrate metabolism	PGD	0.05	0.3
Glyceraldehyde-3-phosphate dehydrogenase	Carbonhydrate metabolism	GAPDH	0.0001	0.3
Bifunctional purine biosynthesis protein PURH	purine biosynthesis	ATIC	0.0001	0.3
CTP synthase 1	nucleoside biosynthesis	CTPS1	0.0027	0.3
CAD protein	nucleoside biosynthesis	CAD	0.001	0.25
Trifunctional enzyme subunit alpha, mitochondrial	Fatty acid metabolism	HADHA	0.0058	-0.25
D-3-phosphoglycerate dehydrogenase	aminoacid biosynthesis	PHGDH	0.0032	-0.3
Isoform 2 of Triosephosphate isomerase	Carbonhydrate metabolism	TPI1	0.0001	-0.3
Adenylate kinase 2, mitochondrial	nucleoside biosynthesis	AK2	0.013	-0.45
Acetyl-CoA acetyltransferase, mitochondrial	Carbonhydrate metabolism	ACAT1	0.0001	-0.5
6-phosphogluconolactonase	Carbonhydrate metabolism	PGLS	0.0001	-0.55
Phosphoglycerate mutase 1	Carbonhydrate metabolism	PGAM1	0.0001	-0.55
Asparagine synthetase [glutamine-hydrolyzing]	aminoacid biosynthesis	ASNS	0.011	-0.7
DNA maintenance				
Nucleosome assembly protein 1-like 1	modulating chromatin formation	NAP1L1	0.0001	0.5
Isoform 2 of Inosine-5'-monophosphate dehydrogenase 1	de novo synthesis of guanine nucleotides	IMPDH1	0.023	0.45
Single-stranded DNA-binding protein, mitochondrial	mitochondrial DNA replication	SSBP1	0.0081	-0.2
Isoform 3 of Nuclear autoantigenic sperm protein	DNA replication	NASP	0.0068	-0.25
Structural maintenance of chromosomes protein 3	DNA replication / repair	SMC3	0.0001	-0.3
DNA mismatch repair protein Msh2	post-replicative DNA mismatch repair sytem	MSH2	0.0094	-0.35
Flap endonuclease 1	DNA replication / repair	FEN1	0.018	-0.4
DNA replication licensing factor MCM2	replication	MCM2	0.00042	-0.45
Proliferating cell nuclear antigen	DNA replication	PCNA	0.0001	-0.55
Histone acetyltransferase type B catalytic subunit	histone modifying enzyme	HAT1	0.0017	-0.55
Histone H2B type 3-B	histone	HIST3H2BB	0.044	-0.8
Histone H2A.Z	histone	H2AFZ	0.0043	-0.85
Replication protein A 14 kDa subunit	DNA replication	RPA3	0.0001	-1.2
Histone H4	histone	HIST1H4A	0.0001	-1.9
translation				
Elongation factor 1-alpha 1	elongation	EEF1A1	0.0001	0.7
Guanine nucleotide-binding protein subunit beta-2-like 1	translation (inhibition)	GNB2L1	0.0079	0.55
Valine--tRNA ligase	aminoacyl tRNA synthetase	VARS	0.0001	0.45
Elongation factor 1-gamma	elongation	EEF1G	0.0001	0.45
Elongation factor 2	elongation	EEF2	0.0001	0.3
60S acidic ribosomal protein P0	elongation	RPLP0	0.0001	0.3
Eukaryotic translation initiation factor 3 subunit D	initiation	EIF3D	0.0001	0.3
60S ribosomal protein L5	ribosome component	RPL5	0.011	0.2
Nucleolin	ribosome assembly	NCL	0.019	-0.2
40S ribosomal protein S5	ribosome component	RPS5	0.0001	-0.3
Glycine--tRNA ligase	aminoacyl tRNA synthetase	GARS	0.00085	-0.45
Ubiquitin-40S ribosomal protein S27a	ribosome component	RPS27A	0.012	-0.75
mRNA metabolism				
Polyadenylate-binding protein 1	component of autoregulatory ribonucleoprotein complex	PABPC1	0.0001	1.3
Isoform Short of Cold shock domain-containing protein E1	component of autoregulatory ribonucleoprotein complex	CSDE1	0.0001	0.8
Nuclease-sensitive element-binding protein 1	pre-mRNA alternative splicing regulation	YBX1	0.0001	0.75
Probable ATP-dependent RNA helicase DDX5	pre-mRNA alternative splicing regulation	DDX5	0.0037	0.35
Isoform 2 of Eukaryotic peptide chain release factor GTP-binding subunit ERF3A	recruits UPF1 to stalled ribosomes (NMD)+ stimulates termination	GSPT1	0.0056	0.25
Heterogeneous nuclear ribonucleoprotein M	mRNA splicing	HNRNPM	0.045	-0.15
Isoform 2 of Heterogeneous nuclear ribonucleoprotein A3	mRNA splicing	HNRNPA3	0.0014	-0.3
Exosome complex component MTR3	component of the RNA exosome complex	EXOSC6	0.019	-0.4
Isoform 2 of Heterogeneous nuclear ribonucleoprotein K	pre-mRNA-binding protein	HNRNPK	0.0033	-0.7
cellular organization				
Tubulin alpha-1C chain	cytoskeleton	TUBA1C	0.0001	0.4
Myosin-9	cytoskeleton	MYH9	0.0011	0.25
Neurofilament medium polypeptide	cytoskeleton	NEFM	0.0016	0.25
Isoform 2 of Filamin-A	cytoskeleton	FLNA	0.0001	0.15
Ras GTPase-activating-like protein IQGAP1	actin cytoskeleton reorganisation	IQGAP1	0.017	-0.2
Plastin-3	Actin-bundling protein	PLS3	0.0001	-0.4
Isoform 2 of Septin-2	organization of the actin cytoskeleton	SEPT2	0.0001	-0.4
Neuroblast differentiation-associated protein AHNAK	neuronal cell differentiation	AHNAK	0.0001	-0.5
protein degradation				
26S proteasome non-ATPase regulatory subunit 6	proteasome	PSMD6	0.041	0.5
Isoform 2 of Ubiquitin-associated protein 2-like	ubiquitination	UBAP2L	0.0003	0.4
Ubiquitin carboxyl-terminal hydrolase 7	ubiquitination	USP7	0.00075	-0.3
Lon protease homolog, mitochondrial	protease	LONP1	0.0018	-0.5
Palmitoyl-protein thioesterase 1	lysosomal degradation	PPT1	0.0001	-0.85
protein folding				
Heat shock cognate 71 kDa protein	folding of stress denatured protein	HSPA8	0.0001	0.45
Isoform Beta of Heat shock protein 105 kDa	folding of stress denatured protein	HSPH1	0.0001	0.4
Peptidyl-prolyl cis-trans isomerase FKBP4	folding of stress denatured protein	FKBP4	0.0019	0.3
T-complex protein 1 subunit delta	folding of nascent peptide chains	CCT4	0.00055	0.25
Stress-70 protein, mitochondrial	folding of stress denatured protein	HSPA9	0.015	-0.2
transport				
Transferrin receptor protein 1	iron uptake	TFRC	0.0001	0.95
Isoform 2 of Caprin-1	regulates transport and translation of mRNA	CAPRIN1	0.047	0.65
Isoform 3 of Importin-5	nuclear protein import receptor	IPO5	0.014	0.2
E3 SUMO-protein ligase RanBP2	nuclear protein export	RANBP2	0.0001	-0.4
signal transduction				
Acidic leucine-rich nuclear phosphoprotein 32 family member A	proliferation, differentiation, caspase-dependent apoptosis	ANP32A	0.00066	0.6
BolA-like protein 2	cell proliferation	BOLA2	0.0055	-0.35
14-3-3 protein epsilon	regulator protein	YWHAE	0.027	-0.35
Programmed cell death protein 4	apoptosis	PDCD4	0.0001	-1.4
others				
Nuclear migration protein nudC	cell proliferation (spindle apparatus)	NUDC	0.0001	0.65
Spermidine synthase	Spermidine biosynthesis	SRM	0.0001	0.6
Isoform 1 of Four and a half LIM domains protein 1	involved in hypertrophy and muscle development	FHL1	0.00034	0.55
Obg-like ATPase 1	ATPase	OLA1	0.037	0.3
Inorganic pyrophosphatase	hydrolase	PPA1	0.0027	0.25
Carbonic anhydrase 2	alpha-carbonic anhydrase	CA2	0.0096	0.25
Electron transfer flavoprotein subunit alpha, mitochondrial	electron transport	ETFA	0.0037	-0.3
Vacuolar protein sorting-associated protein 35	component of the retromer complex	VPS35	0.016	-0.35
Isoform 2 of Spectrin alpha chain, non-erythrocytic 1	secretion	SPTAN1	0.0001	-0.4
Annexin A5	anticoagulant protein	ANXA5	0.017	-0.45

Table 3: Significantly regulated proteins in HEK293 cells treated with hygromycin B. 90 regulated proteins with a significance level of $p < 0.05$ are shown. Proteins were grouped according to their function and sorted according to their log_2 change.

Downregulated proteins could be classified in the functional categories DNA maintenance, metabolism, RNA metabolism, cellular organization, protein degradation and translation. The proteins of the DNA maintenance group comprise histones and a histone modifying enzyme both involved in DNA organization (HIST1H4A, H2AFZ, HIST3H2BB, HAT1). Further proteins were involved in nuclear DNA replication (RPA3, MCM2, PCNA and NASP), mitochondrial DNA replication (SSBP1) and DNA damage repair (FEN1, MSH2, SMC3). Factors responsible for protein degradation (USP7, LONP1, PPT1), translation (RPS5, RPS27A, GARS, NCL), mRNA splicing (EXOSC6, HNRNPA3, HNRNPM, HNRNPK), cellular organization (SEPT2, PLS3, AHNAK, IQGAP1), and transport (RANBP2) were also identified. The category metabolism consisted of the 4 subgroups carbohydrate metabolism (PGAM1, PGLS, TPI1 and ACAT1), amino acid biosynthesis (ASNS, PHGDH), nucleic acid metabolism (AK2) and lipid metabolism (HADHA).

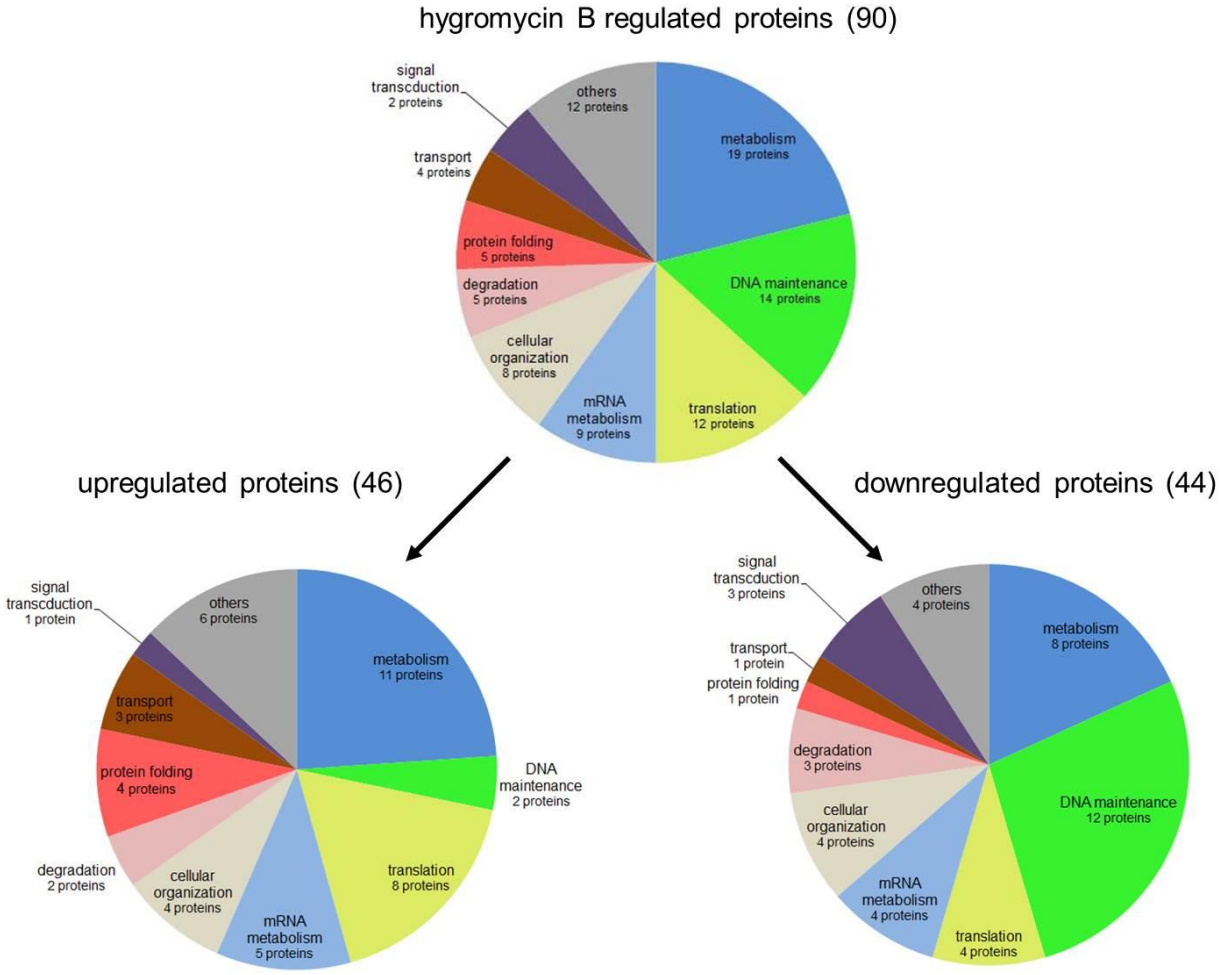

Fig. 34: Hygromycin B regulated proteins. 90 proteins were significantly regulated upon hygromycin B treatment (p-value<0.05). Of those, 46 proteins were upregulated, 44 were downregulated.

5.3.2 Effects of geneticin on the proteome

The second iTRAQ experiment consisted of two samples of untreated HEK293 cells and two samples of HEK293 cells treated with 16 µM geneticin for 32 h. As a result, 1785 proteins could be detected and quantified. The permutation test and further Bonferroni correction identified 74 proteins to be significantly regulated with a p-Value < 0.05 (Fig. 35). Table 4 contains these 74 proteins, their corresponding p-values and fold inductions.

40 of the 74 proteins were upregulated. Analysis of their biological function revealed that almost half of the upregulated proteins are involved in protein folding (Fig. 35). These seventeen proteins are part of the cytosolic and ER resident folding machinery. Proteins of the Hsp40 (DNAJA1), Hsp70 (BiP, HSPA1A, HSPA8), Hsp90 (Endoplasmin or GRP94) and Hsp110 (HSPH1) families were found enriched. Also, foldases and chaperones of the ER (PDIA3, PDIA4, PDIA6, P4HB, CALR, ERP44) and cytoplasm (FKBP4, ST13, STIP1) were induced upon geneticin treatment. Two chaperones linked to proteins synthesis (CLIPS) were upregulated (CCT2, PFDN5) as well. These chaperones participate in folding of nascent polypeptide chains, while the other chaperone network is responsible for folding of stress denatured proteins. Besides folding, the ubiquitin-conjugating enzyme E2 S (UBE2S), tagging proteins for proteasomal degradation, was induced.

Proteins involved in ribosomal translation were enriched. In addition to initiation factors (EIF1B, EIF3A, EIF4A1) and elongation factor eEF1G, structural ribosomal proteins were induced (RPLP2, RPL9, RPLP1). Other functional categories comprised proteins involved in transport, signal transduction and mRNA metabolism. The functional category transport included Importin subunit alpha (KPNA2) and nuceloporin NUP43, both involved in transport of *de novo* synthesized proteins. NACA and SRPRB which regulate targeting of nascent proteins to the ER were upregulated. The cell signaling group included the erUPR marker MANF (Apostolou, Shen et al. 2008). MANF regulates ER-stress mediated apoptosis and inhibition of cell proliferation and was highly enriched in geneticin treated samples. G3BP1, an effector of stress granule assembly is positively regulated as well. NUDC, which positively affects cell proliferation and CDKN2A, which negatively regulates cell proliferation were equally induced. ATXN-10, which promotes maintenance of

intracellular glycosylation levels, is found upregulated. Two proteins, which promote assembly of the mRNA spliceosome complex, are induced (CLNS1A, SMNDC1).

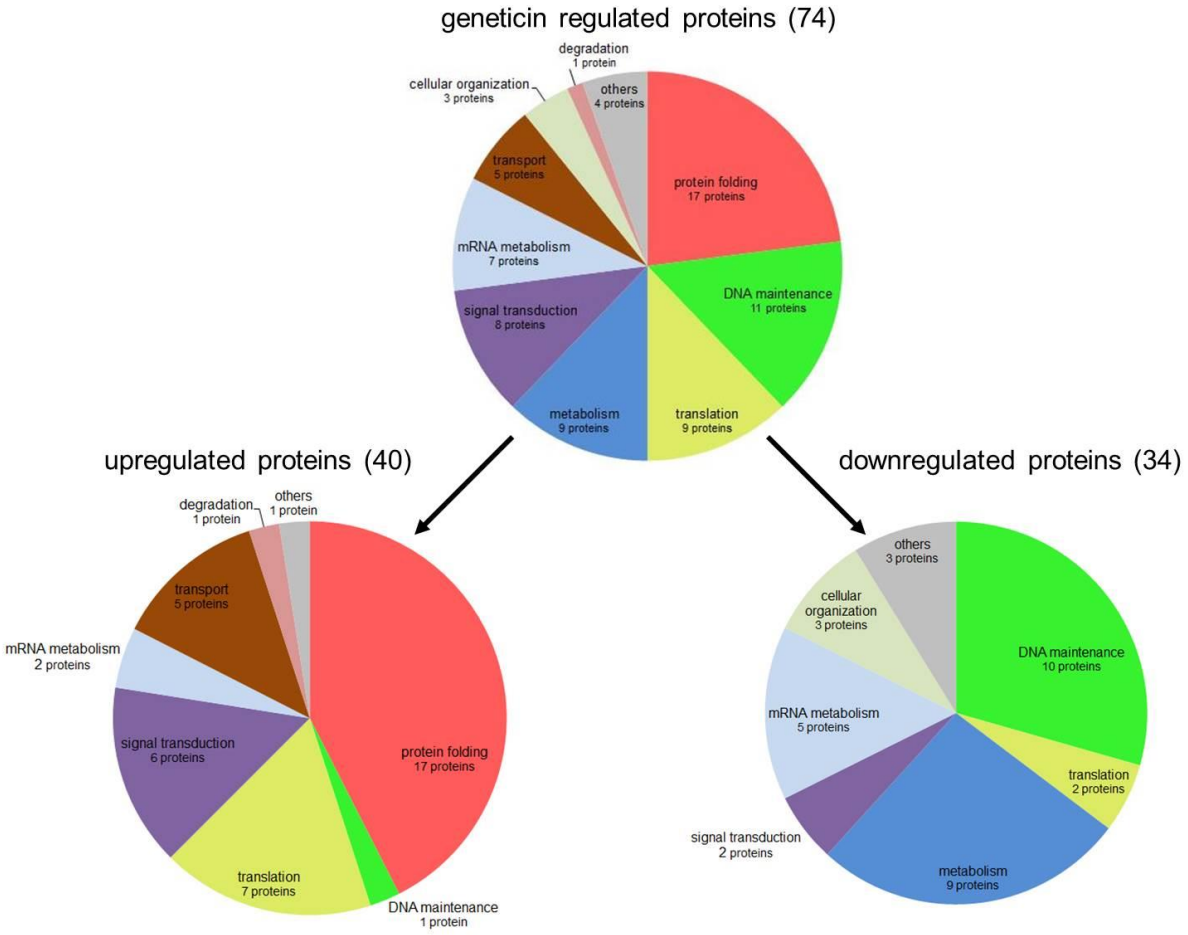

Fig. 35: Geneticin regulated proteins: 74 proteins were significantly regulated upon geneticin treatment (p-value<0.05). Of those, 40 proteins were upregulated, 34 were downregulated.

protein folding	biological function	short name	p-value (BF-corrected)	log_2
Heat shock 70 kDa protein 1A/1B	cytosolic HSP70	HSPA1A	0.0001	0.95
78 kDa glucose-regulated protein	ER HSP70	HSPA5	0.0001	0.75
DnaJ homolog subfamily A member 1	cytosolic Hsp40, import into mitochondria	DNAJA1	0.0001	0.65
Protein disulfide-isomerase A4	ER isomerase	PDIA4	0.0001	0.6
Isoform Beta of Heat shock protein 105 kDa	cytosolic Hsp110	HSPH1	0.0001	0.6
Prefoldin subunit 5	folding of nascent peptide chains	PFDN5	0.026	0.55
Heat shock cognate 71 kDa protein	cytosolic Hsp70	HSPA8	0.0001	0.4
Endoplasmin	ER Hsp90	HSP90B1	0.0001	0.4
Isoform 2 of Protein disulfide-isomerase A6	ER isomerase	PDIA6	0.0001	0.4
Protein disulfide-isomerase	ER isomerase	P4HB	0.00014	0.4
Endoplasmic reticulum resident protein 44	ER chaperone	ERP44	0.0092	0.4
Peptidyl-prolyl cis-trans isomerase FKBP4	cytosolic and mitochondrial isomerase	FKBP4	0.0001	0.3
Protein disulfide-isomerase A3	ER isomerase	PDIA3	0.00033	0.3
Hsc70-interacting protein	cytosolic chaperone	ST13	0.006	0.3
Stress-induced-phosphoprotein 1	cytosolic cochaperone	STIP1	0.00039	0.3
Calreticulin	ER lectin chaperone	CALR	0.0063	0.3
T-complex protein 1 subunit beta	folding of nascent peptide chains	CCT2	0.0001	0.2
DNA maintenance				
Isoform 3 of Histone-binding protein RBBP4	regulates chromatin metabolism	RBBP4	0.00024	0.2
RuvB-like 1	DNA replication / repair	RUVBL1	0.0001	-0.2
X-ray repair cross-complementing protein 5	DNA repair	XRCC5	0.0001	-0.25
Structural maintenance of chromosomes protein 1A	DNA repair	SMC1A	0.0001	-0.35
Poly [ADP-ribose] polymerase 1	DNA repair	PARP1	0.0001	-0.4
DNA replication licensing factor MCM6	replication	MCM6	0.0001	-0.4
DNA-dependent protein kinase catalytic subunit	DNA repair	PRKDC	0.0001	-0.45
DNA mismatch repair protein Msh2	DNA repair	MSH2	0.0001	-0.45
DNA damage-binding protein 1	DNA repair	DDB1	0.00032	-0.45
Isoform 2 of DNA (cytosine-5)-methyltransferase 1	methylation of DNA during replication	DNMT1	0.018	-0.5
DNA replication licensing factor MCM5	replication	MCM5	0.0001	-0.55
translation				
Eukaryotic translation initiation factor 1b	initiation	EIF1B	0.00099	0.7
60S acidic ribosomal protein P2	ribosome component	RPLP2	0.0001	0.5
60S acidic ribosomal protein P1	ribosome component	RPLP1	0.0012	0.45
Eukaryotic translation initiation factor 3 subunit A	initiation	EIF3A	0.0001	0.3
60S ribosomal protein L9	ribosome component	RPL9	0.013	0.25
Eukaryotic initiation factor 4A-I	initiation	EIF4A1	0.017	0.25
Elongation factor 1-gamma	elongation	EEF1G	0.014	0.15
Isoleucine--tRNA ligase, cytoplasmic	aminoacyl tRNA synthetase	IARS	0.0014	-0.35
Tyrosine--tRNA ligase, cytoplasmic	aminoacyl tRNA synthetase	YARS	0.048	-0.35
metabolism				
Isoform 2 of Triosephosphate isomerase	Carbohydrate metabolism	TPI1	0.046	-0.15
C-1-tetrahydrofolate synthase, cytoplasmic	methionine purine Synthesis	MTHFD1	0.028	-0.25
Acetyl-CoA acetyltransferase, mitochondrial	Carbohydrate metabolism	ACAT1	0.0001	-0.3
Transketolase	pentose phosphate pathway	TKT	0.0001	-0.3
Glycogen phosphorylase, liver form	Carbohydrate metabolism	PYGL	0.003	-0.3
Trifunctional enzyme subunit alpha, mitochondrial	fatty acid metabolism	HADHA	0.0001	-0.3
Dihydrolipoyllysine-residue acetyltransferase component of	Carbohydrate metabolism	DLAT	0.0039	-0.35
Enoyl-CoA delta isomerase 1, mitochondrial (Fragment)	fatty acid metabolism	ECI1	0.0001	-0.45
Phosphoserine aminotransferase	amino acid biosynthesis	PSAT1	0.00019	-0.5
signal transduction				
Mesencephalic astrocyte-derived neurotrophic factor	erUPR induced inhibitor of proliferation and cell death	MANF	0.0001	1.1
Growth factor receptor-bound protein 2	Ras signaling pathway, triggers active programmed cell death	GRB2	0.0043	0.6
Ras GTPase-activating protein-binding protein 1	effector of stress granule assembly	G3BP1	0.0001	0.45
Cyclin-dependent kinase inhibitor 2A, isoforms 1/2/3	negative regulator of the proliferation	CDKN2A	0.026	0.45
Isoform 2 of Serine/threonine-protein phosphatase 2A 55 kD	regulates substrate's selectivity and catalytic activity	PPP2R2A	0.0093	0.35
Ataxin-10	survival of cerebellar neurons, maintenance of intracellular glycosylation level	ATXN10	0.0031	0.35
Programmed cell death protein 4	apoptosis, inhibits translation initiation	PDCD4	0.0045	-0.3
Acidic leucine-rich nuclear phosphoprotein 32 family membe	apoptosis, proliferation, differentiation	ANP32A	0.0068	-0.3
mRNA metabolism				
Methylosome subunit pICln	chaperone regulating the spliceosome	CLNS1A	0.039	0.45
Survival of motor neuron-related-splicing factor 30	spliceosome assembly	SMNDC1	0.0001	0.35
Heterogeneous nuclear ribonucleoprotein M	mRNA splicing	HNRNPM	0.00031	-0.15
Heterogeneous nuclear ribonucleoprotein L	mRNA splicing	HNRNPL	0.0001	-0.25
Isoform 2 of Spliceosome RNA helicase DDX39B	spliceosome assembly and splicing	DDX39B	0.0001	-0.35
Isoform 2 of Heterogeneous nuclear ribonucleoprotein K	pre-mRNA-binding protein	HNRNPK	0.001	-0.5
Protein FAM98B	component of tRNA splicing ligase complex	FAM98B	0.0001	-0.6
transport				
Importin subunit alpha-2	nuclear protein import	KPNA2	0.0001	0.65
Nucleoporin Nup43	nuclear pore complex	NUP43	0.024	0.65
Isoform 2 of Caprin-1	transport and translation of mRNA	CAPRIN1	0.016	0.55
Signal recognition particle receptor subunit beta	targeting of the nascent secretory proteins to the ER	SRPRB	0.0003	0.3
Nascent polypeptide-associated complex subunit alpha	Prevents inappropriate targeting of non-secretory prot. to the ER	NACA	0.012	0.3
cellular organization				
Neuroblast differentiation-associated protein AHNAK	neuronal cell differentiation	AHNAK	0.0001	-0.35
Cytoplasmic dynein 1 heavy chain 1	motor for intracellular retrograde motility at microtubules	DYNC1H1	0.00085	-0.35
Profilin-1	binds actin and affects cytoskeleton structure	PFN1	0.0001	-0.55
degradation				
Ubiquitin-conjugating enzyme E2 S	ubiquitination	UBE2S	0.025	0.8
others				
Nuclear migration protein nudC	neurogenesis and cell proliferation	NUDC	0.0001	0.45
Nucleolar protein 58	60S subunit biogenesis	NOP58	0.018	-0.25
Succinate dehydrogenase [ubiquinone] flavoprotein subunit,	electron transport	SDHA	0.00046	-0.3
Nucleolin	ribosome assembly, chromatin condensation, transcriptional elongation	NCL	0.0015	-0.4

Table 4: Significantly regulated proteins in HEK293 cells treated with geneticin. Shown are 74 regulated proteins with a significance level of $p < 0.05$. Proteins were grouped according to their function and sorted according to their log_2 change.

Functional classification of the 34 significantly downregulated proteins showed that they can be grouped into four main families: DNA maintenance, metabolism, RNA metabolism, and cellular organization. The DNA maintenance group contained 10 proteins involved in DNA damage repair (DDB1, MSH2, XRCC5, RUVBL1, SMC1A, PARP1, PRKDC) and replication (MCM5, MCM6, DNMT1). The metabolism group can be divided into three subgroups, namely carbohydrate metabolism (TPI1, TKT, PYGL, ACAT1, DLAT), lipid metabolism (ECI1, HADHA) and amino acid metabolism (PSAT1, MTHFD1). This shows that geneticin treatment negatively influences main metabolic groups. Proteins of the RNA metabolism are involved in mRNA splicing (HNRNPM, HNRNPL, HNRNPK), assembly of the spliceosome (DDX39B) and tRNA splicing ligase complex (FAM98B). Interestingly, the aminoacyl tRNA synthetases for isoleucine (IARS) and tyrosine (YARS) were downregulated. Proteins involved in cellular organization include AHNAK, DYNC1H1 and PFN1, which are involved in neuronal cell differentiation, transport of vesicles and organelles along microtubules and regulation of cytoskeleton structure, respectively.

5.3.3 Comparison of functional categories

In each iTRAQ experiment, the total amount of upregulated proteins was set as 100% and the percentages of proteins belonging to the distinct functional categories were calculated and plotted side by side for geneticin and hygromycin B (Fig. 36A). Accordingly, the percentages of the downregulated proteins were calculated and plotted (Fig. 36B). Significant differences were found for upregulated proteins in the functional groups protein folding, signal transduction and metabolism (Fig. 36A). In contrast to hygromycin B, geneticin treatment resulted in an enrichment of chaperones (Fig. 36A). As shown by the mistranslation assay in chapter 5.1, geneticin but not hygromycin B induced mistranslation. As a result of mistranslation,

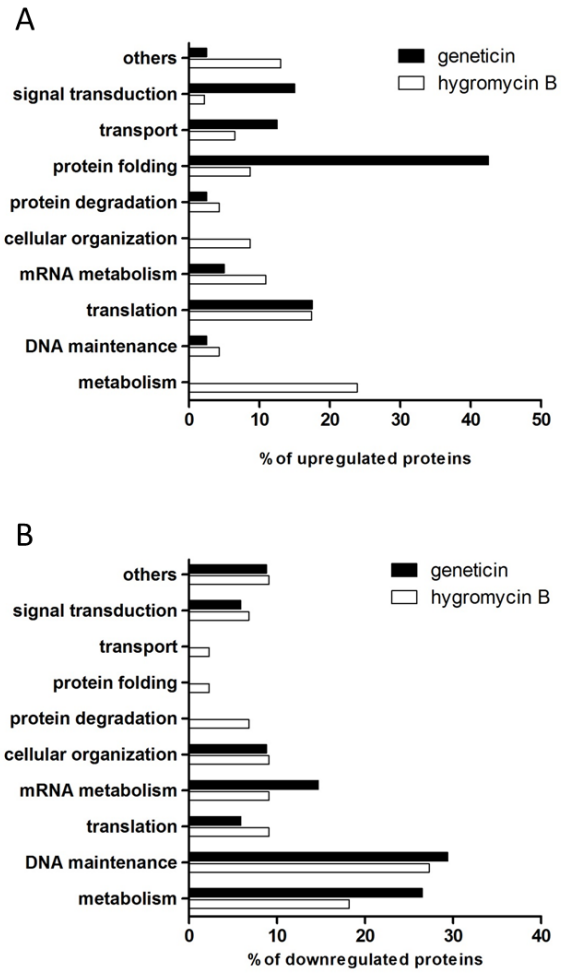

Fig. 36: Comparison of functional categories. Enrichment of proteins in their corresponding functional categories. For geneticin and hygromycin B the total amount of upregulated or downregulated proteins was set as 100% and the percentages of proteins belonging to the distinct categories was calculated. Distribution of (**A**) upregulated proteins and (**B**) downregulated proteins in their functional categories in geneticin and hygromycin B treated cells.

proteins can become misfolded and the cellular proteostasis becomes disturbed. Consequently, the unfolded protein responses of the cytosol and the ER are activated to restore homeostasis. As described in chapter 5.3.2, cytosolic chaperones of the HSP70, 90 and 110 families and erUPR markers BiP, GRP94 and PDIs are upregulated. In contrast, the translocation inhibitor hygromycin B does not induce UPRs and little accumulation of chaperones is found by MS.

Compared to hygromycin B treated cells, geneticin treatment results in a pronounced enrichment of proteins belonging to the functional category signal transduction. The geneticin group is composed of 6 proteins, including the erUPR marker MANF and the effector protein of stress granule assembly G3BP1. Both proteins are linked to misfolded protein stress responses, again pointing to geneticin as a mistranslator. In contrast, hygromycin B treatment resulted in upregulation of one regulatory protein involved in proliferation and caspase-dependent apoptosis (ANP32A), demonstrating distinct responses in signaling.

In hygromycin B treated cells, approximately 25 % of the upregulated proteins are involved in metabolism. As mentioned in chapter 5.3.1 the metabolic proteins of the hygromycin B treated samples can be subdivided in carbohydrate metabolism, nucleic acid biosynthesis and fatty acid metabolism. Notably, the geneticin treated samples lack an induction of metabolism-related proteins.

Hygromycin B and geneticin induced similar proteins involved in protein synthesis. Translation initiation factors, elongation factors, and ribosomal proteins were upregulated, revealing that the common translocation inhibition induces similar responses in geneticin and hygromycin B treated cells. Moreover, the response to hygromycin B mainly involves elongation factors (EEF1A1, EEF1G, EEF2) while geneticin treatment results in upregulation of initiation factors (EIF1B, EIF3A and EIF4A1).

Within the functional categories the distribution of downregulated proteins showed similar patterns for geneticin and hygromycin B. Minor exceptions exist in categories transport, protein folding and protein degradation. The main downregulated categories are DNA maintenance and metabolism. This seems to be a common response to the drugs, suggesting that translocation inhibition of aminoglycosides results in metabolic inactivity and reduced DNA repair and replication.

5.3.4 Proteins regulated by geneticin and hygromycin B

Comparison of proteins affected by geneticin and hygromycin B treatment identified 16 commonly regulated proteins (Fig. 37 A). The fold-changes and corresponding p-values of the proteins are shown in Table 5. Plotting the log_2 values of the proteins regulated by geneticin and hygromycin B revealed that 15 of 16 proteins were regulated similarly (Fig. 37 B). As an exception, the proapoptotic factor ANP32A (acidic leucine-rich nuclear phosphoprotein 32 family member A) is downregulated in geneticin but upregulated in hygromycin B treated samples.

Three chaperones (HSPH1, HSPA8, FKBP4), which are part of the cytosolic heat shock response in the cytoplasm, were consistently upregulated as were translation elongation factor EEF1G, and CAPRIN1, which regulates transport and translation of mRNA. HSPA8 is a chaperone involved in spliceosome assembly and is a repressor of transcriptional activation (Yahata, de Caestecker et al. 2000). In contrast, HSPH1 can inhibit HSPA8 and is a chaperone which prevents aggregation of proteins, activates HSP70 and suppresses oxidative stress (Yamagishi, Saito et al. 2008, Yamagishi, Goto et al. 2010).

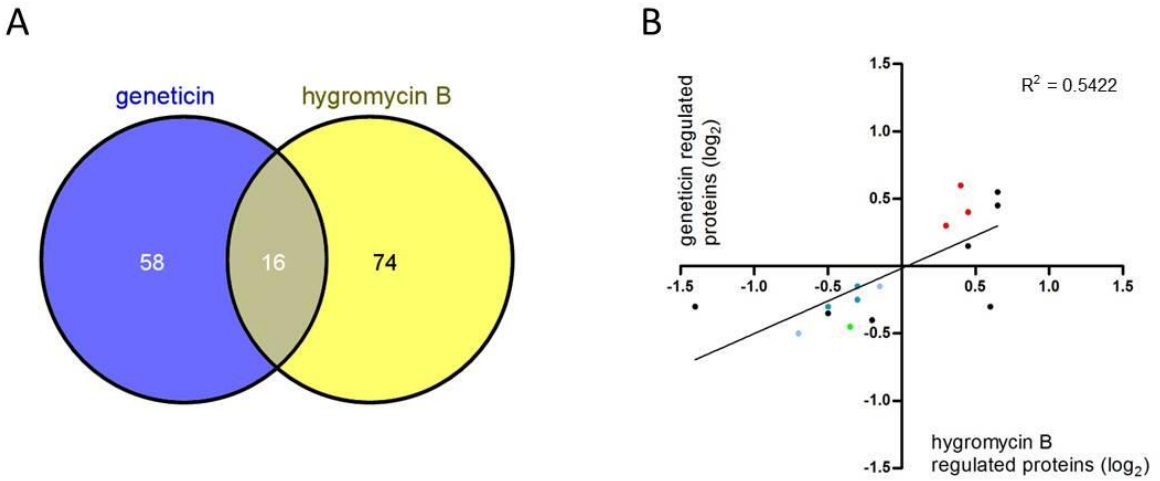

Fig. 37: Comparison of proteins regulated by geneticin and hygromycin B. (**A**) Venn diagram, (**B**) plotted log_2 values of the 16 common regulated proteins. Red dots indicate proteins involved in folding, green dots mark DNA maintenance, dark blue indicates proteins of metabolism, and light blue indicates proteins of mRNA metabolism. Squared Pearson product-moment correlation coefficient R^2 of the regression line is indicated.

FKBP4 has besides its chaperone function also a protective a role against oxidative stress in mitochondria (Gallo, Lagadari et al. 2011), suggesting the chaperones might be regulated upon oxidative stress during drug exposure. NUDC a protein necessary for correct formation of mitotic spindles and chromosome separation during mitosis is also upregulated in geneticin and hygromycin B treated cells.

Downregulated proteins can be grouped into metabolism, mRNA splicing, DNA repair and cell signaling. The proteins of the metabolic group are involved in glycolysis, ketone body metabolism and mitochondrial fatty acid β-oxidation (TPI, ACAT1, HADHA). Other downregulated proteins are involved in mRNA splicing (HNRNPM, HNRNPK), post replicative DNA mismatch repair (MSH2), neuronal cell differentiation(AHNAK) and ribosome assembly (NCL). Programmed cell death protein 4 (PDCD4), an apoptosis promoting factor, is also decreased in both drug treated samples. The pattern of the downregulated proteins suggests that part of the general energy metabolism is affected by translation inhibition.

Table 5: Fold-induction and p-values of proteins regulated by geneticin and hygromycin B.

	Hygromycin		Geneticin	
	log2 change	p-value	log2 change	p-value
HSPH1	0.4	0.0001	0.6	0.0001
CAPRIN1	0.65	0.047	0.55	0.016
NUDC	0.65	0.0001	0.45	0.0001
HSPA8	0.45	0.0001	0.4	0.0001
FKBP4	0.3	0.0019	0.3	0.0001
EEF1G	0.45	0.0001	0.15	0.014
HNRNPM	-0.15	0.045	-0.15	0.00031
TPI1	-0.3	0.0001	-0.15	0.046
ACAT1	-0.5	0.0001	-0.3	0.0001
PDCD4	-1.4	0.0001	-0.3	0.0045
ANP32A	0.6	0.00066	-0.3	0.0068
HADHA	-0.3	0.0058	-0.25	0.0001
AHNAK	-0.5	0.0001	-0.35	0.0001
NCL	-0.2	0.019	-0.4	0.0015
MSH2	-0.35	0.0094	-0.45	0.0001
HNRNPK	-0.7	0.0014	-0.5	0.001

5.3.5 Drug-regulated proteins and corresponding mRNAs

Significantly regulated proteins ($p < 0.05$) of the geneticin and the hygromycin B treated samples were compared with their corresponding mRNA levels. Data of two microarray experiments (geneticin and hygromycin B treated HEK293 cells) were

used to plot log_2 fold change of the mRNA against the respective log_2 fold-change of the protein levels measured by the iTRAQ experiment (Fig. 38).

Fig. 38A shows the comparison of transcriptome and proteome data of the geneticin treated samples. Components of the folding machinery (marked in red) reveal an upregulation at both the transcriptomic and the proteomic level. Proteins involved in DNA maintenance and metabolism are mostly downregulated at both levels. As indicated by the squared Pearson product-moment correlation coefficient of 0.4184 the scattering of the data follow a rather linear distribution, suggesting similar regulation at the mRNA and protein levels. A different distribution is present in the dot plot of hygromycin B treated HEK293 cells (Fig. 38C). Here, the regulation of the proteome is not accompanied by the mRNA fold change. The squared Pearson product-moment correlation coefficient of 0.0051, points to a random distribution. Chaperones, which were upregulated at the proteomic level, are not induced at the transcriptomic level. Proteins involved in metabolic pathways are found up- and downregulated on the proteomic level, however, their corresponding mRNA levels revealed a common negative regulation. The DNA maintenance promoting proteins were up and downregulated at the proteomic level, but induced or not regulated at the transcriptomic level. As shown in Fig. 38B, the distribution of dots in geneticin plot without the folding machinery proteins shows not an identical pattern to the hygromycin B plot in Fig. 38C. The squared Pearson product-moment correlation coefficient of 0.2380 is low, but shows rather a weak linear distribution than a random distribution.

The comparison of the transcriptome and the proteome data demonstrated a robust induction of cytUPR and erUPR in geneticin, but not in hygromycin B treated samples. This suggested that mistranslation mediated by geneticin results in misfolded proteins and in an upregulation of distinct chaperone networks. Translocation inhibition in both drug treatments leads to similar, but not identical patterns. In both conditions translation machinery components *i.e.* initiation factors, elongation factors and ribosomal proteins were upregulated. Another similar pattern is the downregulation of proteins involved in metabolism of the mitochondria, which suggests that the mitochondrial activity is reduced in order to minimize drug-induced oxidative stress.

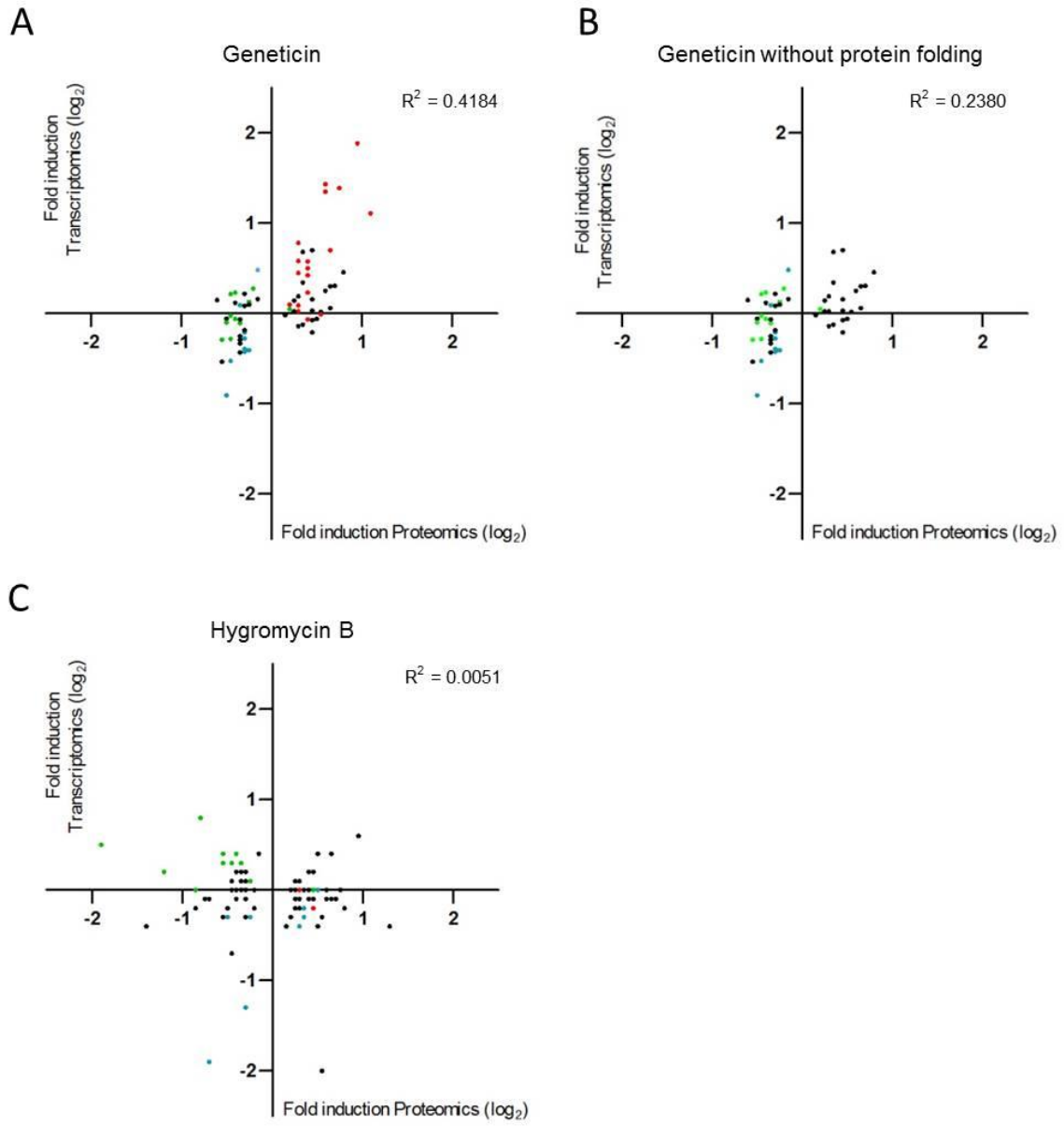

Fig. 38: Comparison of significantly regulated proteins and their corresponding mRNA levels. (**A**) geneticin treated HEK cells, (**B**) geneticin treated HEK cells without the proteins of the protein folding machinery (**C**) hygromycin B treated HEK cells. Red dots indicate proteins of the protein folding machinery, blue dots show proteins involved in metabolism and green dots highlight proteins responsible for DNA maintenance. Squared Pearson product-moment correlation coefficient R^2 of the linear regression line (not shown) is indicated.

6 Material and Methods

6.1 Cell lines and culture conditions

HEK293 wild-type (Innoprot) and HEK293 APH(3') cells (officially named 293FT, Life technologies) were cultured in DMEM medium (Life technologies) supplemented with 10% fetal bovine serum (Life technologies). Serum free F10 media (Life technologies) supplemented with 15 µg/ml saponin (Sigma) was used during drug treatment. The osteosarcoma cell lines 143B and its rho-0 derivative without mitochondrial DNA were kindly provided by Dr. Rafael Garesse Alarcón. Cells were kept with DMEM supplemented with 10% FBS or DMEM supplemented with 10% FBS and 50 µg/ml uridine, respectively (Chomyn, Lai et al. 1994). DMEM was used for 143B cells and DMEM with 50 µg/ml uridine was used for rho-0 cells during drug treatment.

6.2 Assessment of stop-codon read-through *in vitro*

For *in vitro* translation assays luciferase mRNA was produced *in vitro* using T7 polymerase (Thermo). The mammalian promotors of pGL4.14 (firefly luciferase, hFluc) and pGL4.75 (renilla luciferase, hRluc, both Promega) were replaced by T7 bacteriophage promotor resulting in pT7-hFluc and pT7-hRluc vectors, respectively. hRluc and hFluc were fused by a 27-nucleotide linker encoding the polypeptide STCDQPFGF (Salas-Marco and Bedwell 2005) using overlap PCR mutagenesis to result in the pT7 hRluc-hFluc vector. In addition, the first codon of the hFluc gene encoding for methionine (ATG) was replaced by CTC (Leucine) codon using site directed PCR mutagenesis to prevent internal ribosomal binding. To create the read-through construct a TGA nonsense codon was introduced instead of the glutamine residue (wild type CAA) in the linker sequence by site directed PCR mutagenesis. A standard 15 µl *in vitro* translation reaction contained 10 µl rabbit reticulocyte lysate (Promega), 2 µg reporter mRNA, amino acid mixture (final concentration of each amino acid 200 µM), 12 units RiboLock (Thermo), 1x Protease Inhibitor complete (Roche). Following addition of serially diluted aminoglycosides, the reaction mixture was incubated at 37°C for 35 min and stopped on ice. Firefly activities were determined using a luminometer FLx800 (BioTek Instruments). Luciferase activities of hRluc were always used to assess translation inhibition and relative read-through

induction was calculated by hFluc luminescence/hRluc luminescence. The basal error frequency rate of the eukaryotic cytoplasmic ribosome is 4 x 10^{-4} to 10^{-5}. For the untreated samples, the hFluc/hRluc ratio was set as 1, which reflects the basal error frequency.

6.3 Assessment of stop codon read-through *in vivo*

Read-through in HEK293 cells was determined using the pRM hRluc-hFluc D357X vector, where the Asp357 (GAC codon) of the firefly gene was replaced by a TGA nonsense codon in the pRM hRluc-hFluc vector (Matt, Ng et al. 2012). The construct was generated by site directed PCR mutagenesis. HEK293 wild-type cells were grown until 80% confluency in 6-well plates at 37°C, 5% CO_2 in DMEM supplemented with 10% FBS (vol/vol) (Life technologies) and subsequently transfected with 3 µg reporter plasmid using TurboFect transfection reagent (Thermo) according to manufacturer's protocol. Cells were incubated for 24 h and medium was replaced by F10 (Life technologies). Serially diluted antibiotics were added together with saponine (15 µg/ml final concentration) and cells were incubated for another 24 h. Cells were lysed using 1x passive lysis buffer (Promega) and luciferase activities were determined using the FLx800 luminometer (Bio-Tek Instruments).

6.4 Autoradiography

A standard 15 µl reaction contained 10 µl rabbit reticulocyte lysate (Promega), 2 µg reporter mRNA, amino-acid mixture without methionine (each 200 µM), 200 µM S^{35}-methionine (Hartmann Analytic), 12 units RiboLock (Thermo), 1x Protease Inhibitor complete (Roche). Following addition of serially diluted paromomycin the reaction mixture was incubated at 37°C for 35 min and stopped on ice. To analyze the translational products, 5 µl of each reaction was mixed with 5 µl of 2x SDS sample buffer (125 mM Tris-HCl pH 6.8, 4% SDS, 20% Glycerol, 0.02% Bromphenol Blue, 8 mM β-mercapto-ethanol), incubated at 95°C for 5 min and loaded on a 13.3% SDS-PAGE gel. After running the gel for 1 hour at 150 V, the SDS-PAGE was fixed using a buffer containing 40% methanol and 10% acetic acid. After drying, the gel was exposed to an IP-detection plate for at least 1h. The FLA-5100 imaging system was used to detect the resulting bands on the IP detection plate.

6.5 ROS detection

HEK293 cells were grown in DMEM supplemented with 10% FBS in 12-well plates until 80% confluency. For antibiotic treatment the growth medium was replaced by F10 (Life technologies) supplemented with 15 µg/ml saponin and serially diluted antibiotics were added. After 24 or 48 h of incubation the cells were stained for 30 min with 5 µM MitoSOX (Life technologies) in FACS buffer (1x PBS supplemented with 2% FBS) or 5 µM CM-H_2DCFDA (Life technologies) in FACS buffer. Cells were detached using accutase (Life technologies) and resuspended in FACS buffer. Prior to measurement the CM-H_2DCFDA- but not the MitoSOX-stained samples were washed three times using FACS buffer. The Fluorescence of both MitoSOX and CM-H_2DCFDA stained samples was measured using a FACS Canto II (BD). Data were analyzed using FlowJo software.

6.6 Isobaric Tag for relative and absolute quantitation (iTRAQ) assay

Cells were grown in DMEM supplemented with 10% FBS in 6-well plates until 70-80% of confluency were reached. Then media was replaced by F10 supplemented with saponin and 16 µM geneticin or 7 µM hygromycin. After 32 h, media was removed and cells were washed with 1x PBS. Subsequently, samples were incubated with lysis buffer (150 mM NaCl, 0,1% SDS, 0,5% Na-deoxycholat, 50 mM Tris, 1x complete protease inhibitor (Roche) for 10 min at room temperature and shaking. Subsequently, the lysate was ultrasonicated in a water bath for 10 min and centrifuged for 20 min at 13200 rpm at 4°C. The supernatant was used for further analysis. Protein quantification was performed using the Qubit kit (Invitrogen). 80 µg of total protein from each sample was used for iTRAQ labeling (AB SCIEX).

Two iTRAQ 4-plex experiments were performed. One 4-plex consisted of 2 biological replicates of untreated HEK293 cells (114 and 116 label) and 2 biological replicates of HEK293 cells treated with geneticin (16 µM) for 32 h (115 and 117 label). The other 4-plex experiment consisted of 2 untreated independent samples (114 and 116 label) and 2 independent samples treated with hygromycin (115 and 117 label) The cell lysates were first precipitated with 20% TCA and dried pellets were reconstituted in 50 mM triethyl ammonium bicarbonate buffer (TEAB), pH 8,5 supplemented with 0,1% SDS. Protein samples were reduced using tris-(2-carboxyethyl)phosphine (TCEP) and alkylated with methyl methane-thiosulfonate (MMTS). For digestion a ratio of trypsin to protein content of 1:50 was used and samples were incubated for 4

h at 37°C. For labeling the iTRAQ vials were reconstituted with 70 µl of ethanol and the tryptic digested peptides were added. Labeling reaction was performed for 2 h at room temperature. The labeling reaction was quenched for 10 min at room temperature using 10 mM of ethanolamine. iTRAQ samples were pooled, dried and reconstituted in 75% acetonitrile (ACN) with 8 mM KH_2PO_4, pH 4.5 and fractionated by HILIC-HPLC (Pack Polyamine II, 250 x 4mm, 120 Å S-5 µm, YMC) using a linear gradient with 5% ACN, 100 mM KH_2PO_4, pH 4.5. The eluted fractions were desalted using Zip Tip C18 cartridges (Millipore), dried and reconstituted in 15 µl 3% ACN and 0,1% formic acid for LC-MS/MS analysis. Samples were injected into an Eksigent-nano-HPLC system (Eksigent Technologies, Dublin (CA), USA) by an auto sampler and separated on a self-made reverse-phase column (75 µm x 150 mm) packed with C18 material (Magic C18, AQ, 3 µm, 200 Å, Bischoff GmbH, Leonberg, Germany). The column was equilibrated with 95% solvent A (0.1% formic acid (FA) in water) and 5% solvent B (0.1% FA in ACN). Peptides were eluted using the following gradient: 0-3 min; 1-5% B, 3-57 min; 5-35% B, 57-63 min; 35-50% B and 63-70 min; 50-99% B, at a flow rate of 0.3 µl/min. High accuracy mass spectra were acquired with an AB Sciex 5600 (AB Sciex, Concord, Canada) in the mass range of 385-1250 m/z. Up to 36 data dependent MS/MS were recorded in high sensitivity mode of the most intense ions with charge state 2+, 3+ and 4+ using collision induced dissociation. Target ions already selected for MS/MS were dynamically excluded for 90 s after three occurrences. After data collection the peak lists were generated using AB SCIEX MS Data Converter 1.3 (AB Sciex, Concord, Canada). All MS/MS data were analyzed using Mascot 2.4 (Matrix Science, London, UK). MS data were searched against a decoyed human database from Swissprot (release December 2012) concatenated with an in-house build contaminant database. Precursor ion mass tolerance was set to 20 ppm and the fragment ion mass tolerance was set to 0.05 Da. The following search parameters were used: Trypsin digestion (no missed cleavage allowed), fixed modifications of methyl methanethiosulfonate (MMTS) labelled cysteine, 4-plex-iTRAQ modifications of free amines at the N-termini and of lysine, and as variable modification 4-plex-iTRAQ of tyrosine. The peptides without any 4-plex-iTRAQ label at the N-terminus or at a lysine were excluded from the analysis. After the Mascot search the data were further evaluated by using Scaffold 4.3 software. In Scaffold the following parameters were used: protein threshold 95%,

minimum 2 peptides for identification of a protein, and a minimum Mascot Ionscore 40.

6.7 Microarray

HEK cells were treated with 16 µM geneticin in F10 medium with 15 µg/mL saponin at 37 °C for 32 h. RNA was extracted from four independent samples for each condition (geneticin-treated, untreated). Total RNA was processed and hybridized on GeneChip Human Gene 1.0 ST arrays (Affymetrix, Santa Clara, CA) by the IGBMC Microarray and Sequencing Platform as described (Ravens, Fournier et al. 2014). Significance of the difference in expression of each gene between geneticin-treated and untreated samples was tested using the TREAT method (McCarthy and Smyth 2009). Correction of Benjamini-Hochberg (Benjamini and Hochberg 1995) for multiple testing was applied in order to take into account the number of tests performed. Corrected p-values lower than 0.05 were considered as significant.

7 Discussion

In this thesis the link between mistranslation and cellular stress in eukaryotic cells was investigated using antibiotics of the aminoglycoside class. Besides induction of general mistranslation, aminoglycosides inhibit ribosomal translocation (Buchanan, Stevens et al. 1987). Thus far, it is not possible to manipulate ribosomal translation fidelity in higher eukaryotes without affecting translation efficiency. Previously, the accuracy of translation has been manipulated by mutating tRNAs or the editing domain of a tRNA aminoacyl transferase, which results in codon-specific mistranslation (Lee, Beebe et al. 2006, Paredes, Carreto et al. 2012).

7.1 Aminoglycoside mistranslation and translation inhibition

As a first step, the effect of various aminoglycosides on eukaryotic translation was assessed. For this purpose, we established dual luciferase assays using *in vitro* RRL ribosomes and *in vivo* HEK293 cells. Comparison of *in vitro* and *in vivo* IC_{50}-values showed a good correlation, suggesting that the *in vitro* assay is relevant and properly reflects the whole cell situation. Hygromycin B is a strong inhibitor of eukaryotic translation and is described as a drug with a subtle effect on decoding fidelity when using artificial polyU mRNA as a reporter (Eustice and Wilhelm 1984, Eustice and Wilhelm 1984). According to our dual luciferase assay, based on the gain of function principle, we could not detect hygromycin B mediated induction of read-through *in vitro* and only little induction *in vivo*. The relative read-through induction of hygromycin B *in vivo* has to be interpreted with caution. The experimentally determined hFluc luminescence showed little read-through induction. The ratio used to calculate the relative read-through (hFluc/hRluc), however, is a possible source of mathematical artefacts. Thus, little or no read-through induction which is accompanied by a strong translation inhibition will result in a prominent relative read-through induction. It follows that relative data should be always compared with the directly experimentally determined values to prevent misleading interpretations. The data presented here suggest that hygromycin B acts primarily as a translation inhibitor in higher eukaryotes, which is consistent with published data (Manuvakhova, Keeling et al. 2000).

The 4,6-disubstituted aminoglycoside geneticin is a strong translation inhibitor and a potent inducer of mistranslation. The 4,5-disubstituted aminoglycoside paromomycin

with a 6’ hydroxyl group and the 4,6-disubstituted aminoglycoside gentamicin with a 6’ amino group shows similar IC_{50} values and comparable efficacies to induce mistranslation. Both drugs can induce read-through in a comparable manner, which is in agreement with published data (Manuvakhova, Keeling et al. 2000, Kandasamy, Atia-Glikin et al. 2012).

The exchange of the 6’ OH group in ring I of the 4,5-disubstituted aminoglycoside paromomycin by an amino group (neomycin) results in an approximately three-fold less active compound with little, if any mistranslation efficacy, revealing the importance of the interaction of the 6’ group of ring I with the drug binding pocket. As described in the late 1970s, aminoglycosides with a 6’ hydroxyl group in ring I induce mistranslation of eukaryotic ribosomes (Wilhelm, Pettitt et al. 1978). Similar, the 6’ OH group of ring I in 4,6-disubstituted aminoglycosides gives rise to misreading in eukaryotic ribosomes, while a 6’ NH_3 group induces little if any mistranslation (Salian, Matt et al. 2012). Genetic manipulations of the ribosomal A-site and crystal structures of aminoglycosides bound to ribosomes gave further insights. Paromomycin’s hydroxyl group at the 6’ position of ring I can accept a hydrogen bond from N1 and/or N2 of G1408, which is located in the helix44 of the 18S rRNA. In contrast, the 6’ amino group of neomycin cannot interact with G1408 via hydrogen bonds and is furthermore sterically repulsed (Pfister, Hobbie et al. 2003, Kondo 2012).

The read-through data presented here were independently confirmed by studying ribosomal misreading (see thesis of Martin Meyer, Böttger group). Misreading was measured using a sensitive gain of function assay, *i.e.* the histidine (CAC) at amino acid position 245 in the active center of the firefly luciferase was replaced by an arginine, encoded by the near-cognate codon CGC. When arginine is incorporated in the active center the enzyme is non-functional. Histidine incorporated by a near-cognate tRNA at position 245 can restore the enzymatic function of hFluc, i.e. the signal of the firefly luciferase is a direct measure of mistranslation. Geneticin, paromomycin and gentamicin were the most potent inducer of misreading, whereas apramycin and amikacin showed little, if any misreading.

7.2 ROS formation by aminoglycosides

Formation of ROS is a hallmark of aminoglycoside-induced ototoxicity (Forge and Schacht 2000) which lead us to investigate a possible link between drug-mediated ribosomal malfunction and ROS formation.

The generation of a gentamicin-Fe^{2+} complex has been suggested to result in aminoglycoside-induced ROS formation. This iron-drug complex activates molecular oxygen and reduces it with electrons from a donor like arachidonic acid. Arachidonic acid is the main fatty acid in the 2' position of polyphosphoinositides. As a direct consequence, superoxide and lipid peroxides are formed, leading to cell damage. The correlation of the binding affinity of aminoglycosides to polyphosphoinositides and their ability to cause ototoxicity suggests this as a possible mechanism *in vivo* (Priuska and Schacht 1995, Sha and Schacht 1999, Sha and Schacht 1999). Supporting this idea, supplementation of iron in guinea pigs increases aminoglycoside ototoxicity (Conlon and Smith 1998). Vice versa, aminoglycoside ototoxicity is decreased by antioxidant exposure and iron chelation (Song, Anderson et al. 1997, Sha and Schacht 1999).

We wanted to address the question whether mistranslation or translation inhibition leads to increased ROS formation. In a first experiment, ROS generation during geneticin treatment was demonstrated and its dependence on the aminoglycosides' anti-ribosomal activity was shown. Inactivation of geneticin's antiribosomal activity by APH(3')-mediated phosphorylation prevented oxidative stress. Furthermore, ROS formation was dependent on a functional mitochondrial respiratory chain as it was shown by the 143B and the 143B derived rho-0 cell line. The rho-0 cell line was generated by using ethidiumbromide to remove the mtDNA. As a result, rho-0 cells possess rudimentary mitochondria, without a functional respiratory chain, due to the loss of the 13 mtDNA encoded proteins, which are involved in the respiratory complexes I, III, IV and V.

The HEK data suggest that geneticin-induced oxidative stress is not dependent on a proposed aminoglycoside-Fe^{2+} complex (Priuska and Schacht 1995). ROS in this experimental set-up is rather a result of a specific ribosomal impairment and its consecutive damages.

For further experiments hygromycin B was chosen as an inhibitor of translocation. Hygromycin B was found to be the most potent inducer of ROS at relatively low drug levels followed by geneticin, gentamicin and neomycin. This hierarchy correlated well the corresponding IC_{50} values, where hygromycin B is the strongest translational inhibitor followed by geneticin, gentamicin and neomycin. The data identifying hygromycin B as a ROS inducer are in agreement with a publication demonstrating that hygromycin B induced oxidative stress in the human retinal pigment epithelial cell line ARPE-19 in a dose dependent manner (Hoppe, Chai et al. 2003). As described in the literature, geneticin and gentamicin induced oxidative stress in mitochondrial and total ROS assays (Sha and Schacht 1999, Villalba, Gomez et al. 2007).

The correlation of total ROS levels (measured by CM-H_2DCFDA dye) and mitochondrial superoxide production (measured by MitoSOX dye) (Fig. 33) suggests that mitochondria are the main source of oxidative radical formation. In case of mistranslation and subsequent accumulation of misfolded proteins, the upregulation of oxidative folding in the ER might also contribute to ROS formation. As a stress response, the protein disulfide isomerases (PDIs) in the ER might be upregulated, increasing the organelles folding capacity and leading to increased formation of hydrogen peroxide.

Hygromycin B is a universal inhibitor of translation and impairs both the cytoplasmic and the mitochondrial ribosome. Incubation of cells using cycloheximide, a specific inhibitor of the cytoplasmic translation, resulted in elevated ROS formation. This finding indicates that cytosolic translation inhibition is sufficient to result in ROS formation and emphasizes that mistranslation is not necessary to induce oxidative stress. To test for the contribution of mitochondrial translation inhibition to oxidative stress the mitochondrial ribosome-specific inhibitor linezolid was investigated. Linezolid induced neither total ROS nor mitochondrial superoxide. Thus, inhibition of the mitochondrial ribosome does not induce formation of ROS *in vivo* under the conditions tested.

7.3 Mistranslation induces unfolded protein responses

Geneticin induces both mistranslation and translocation inhibition. In contrast, hygromycin B induces inhibition of translation. Hygromycin B allowed for the

identification of pathways and individual proteins involved in the response to translocation inhibition. In contrast, geneticin induced mechanisms which involve adaptation to both translation inhibition and misreading. Comparison to hygromycin B allowed for the identification of pathways induced by mistranslation.

A clear difference between geneticin and hygromycin B was found. In the geneticin treated samples a predominant upregulation of the folding machinery was detected. Thus, the erUPR markers BiP and GRP94 were induced upon geneticin treatment. In addition, a strong upregulation of heat shock response components like HSP70 and HSPH1 was detected in the cytoplasm and various ER-located isomerases were upregulated. These isomerases contribute to the free radical formation in the ER by oxidative folding (Araki, Iemura et al. 2013). In total, 17 proteins involved in protein folding were enriched in the geneticin treated samples, whereas in the hygromycin B treated cells only three chaperones were upregulated. Interestingly, these 3 chaperones are commonly induced in hygromycin B and geneticin treated samples. Upregulation of these three cytosolic chaperones suggests that translation inhibition results in a specific stress pattern by production of abnormal proteins, due to production of truncated polypeptides. In detail, HSPA8 and HSPH1 are both cytosolic chaperones and the latter can inhibit HSPA8. Furthermore, HSPH1 was suggested to be involved in protection of cells against oxidative stress. Together with FKBP4 a chaperone that can be translocated in mitochondria and protects cells from oxidative stress when overexpressed, a common stress response against elevated radical formation might be activated.

It has been suggested, that mistranslation leads to misfolded proteins in higher eukaryotes (Drummond and Wilke 2008); the data here demonstrate that mistranslation leads to an upregulation of the unfolded protein responses in the ER and cytoplasm. In agreement with the proteome data, in yeast paromomycin was shown to induce the cytosolic heat shock response marker Hsp70. In contrast, the translation inhibitor cycloheximide did not induce Hsp70 (Grant, Firoozan et al. 1989).

In mitochondria, neither geneticin nor hygromycin B induced chaperones (except FKBP4) or proteins of the antioxidant defense. This finding was surprising, because the drug concentrations used were shown to increase mitochondrial ROS formation. A possible explanation for this finding is the used growth media. Immortalized cell lines, as well as cancer cells change their energy metabolism from aerobic

respiration to aerobic glycolysis. This metabolic change is called the Warburg effect (Hanahan and Weinberg 2011). During the experiments cells were kept in growth media with a high glucose concentration. As a result, cells favor aerobic glycolysis instead of mitochondrial respiration. Consequently mitochondria are less active in respiration and the basal antioxidant defense and chaperone network might be capable to cope with the increased mitochondrial stress.

7.4 Aminoglycosides affect the metabolism of mitochondria

Mitochondrial metabolic enzymes were downregulated in both geneticin and hygromycin B treated cells. Geneticin treatment led to downregulation of enzymes involved in carbohydrate (ACAT1, DLAT) and fatty acid metabolism (HADHA, ECI1), hygromycin B treatment resulted in downregulation of enzymes involved in carbohydrate (ACAT1) and fatty acid metabolism (HADHA). (Carpenter, Pollitt et al. 1992). Acetyl-CoA acetyltransferase (ACAT1) is involved in both amino acid degradation and in fatty acid oxidation catalyzing the conversion of 2-methyl-acetoacetyl-CoA to propionyl-CoA and acetyl-CoA or the conversion of acetoacetyl-CoA to two molecules of acetyl-CoA (Huth, Jonas et al. 1975). HADHA is the central trifunctional enzyme of β-fatty acid oxidation in mitochondria (Carpenter, Pollitt et al. 1992). It catalyzes three out of four necessary steps of fatty acid oxidation to create acetyl-CoA. Acetyl-CoA is a substrate for the mitochondrial citric acid cycle, which delivers electrons to the mitochondrial respiratory chain via NADH (Fernie, Carrari et al. 2004). This suggests that mitochondrial metabolic activity is downregulated upon translation inhibition. As a result, less electrons are delivered to the respiratory chain and mitochondrial ATP production in reduced, resulting in reduced ROS formation. This decrease of mitochondrial activity helps the cell to reduce the demonstrated ROS increase and to resolve the stress condition. The reduced mitochondrial ATP production can be readily compensated by glycolysis, because cells were incubated in high glucose media.

7.5 Aminoglycosides upregulate the ubiquitin protease system

As a response to abnormal protein stress the ubiquitin protease system is upregulated (Grant, Firoozan et al. 1989). Both hygromycin B and geneticin treatment resulted in an induction of components of the ubiquitin protease system. In detail, geneticin treatment resulted in upregulation of the ubiquitin-conjugating

enzyme E2 and hygromycin B treatment induced the UBAP2l protein and proteasome subunit 6. In yeast, free ubiquitin polypeptides are critical for the survival during translation inhibition mediated by cycloheximide or hygromycin B. With a half-life of 2 h, ubiquitin is rapidly depleted upon translation inhibition. Low levels of free ubiquitin result in sensitivity to translation inhibition. In contrast, ubiquitin overexpression improves fitness during translocation inhibition (Hanna, Leggett et al. 2003). Geneticin and hygromycin B presumably promote formation of truncated and abnormal proteins, which need to be degraded by the ubiquitin-proteasome pathway to avoid cellular intoxication. The levels of free ubiquitin are reduced by binding of ubiquitin to abnormal proteins and by subsequent degradation by the proteasome. Because recycling of ubiquitin at the proteasome by substrate deubiquitination is not 100% efficient, the ubiquitin tagged to the substrate becomes expended. We hypothesize that in spite of translation inhibition, the translational machinery still can synthesize the small 8.5 kDa ubiquitin protein to replenish the decreasing level of free ubiquitin.

7.6 Translocation inhibition upregulates proteins of the translation machinery

Both hygromycin B and geneticin induced proteins involved in translation initiation, elongation factors as well as ribosomal proteins. This finding suggests that the cell compensates translation inhibition by increasing the capacity of protein synthesis. In order to react to cellular damage stress-related proteins must be synthesized. Thus, a residual functional protein synthesis is crucial for cellular survival (Ventoso, Kochetov et al. 2012). The upregulation of the translation machinery seems to be a specific adaptation to a prolonged translation inhibition.

Interestingly, proteins upregulated in hygromycin B-treated cells are mainly elongation factors, whereas in geneticin-treated cells, initiation factors were primarily upregulated. In the geneticin-treated samples the erUPR is activated and the EIF2A initiation factor is phosphorylated (p-EIF2A) by PERK (See Chapter 9, Fig.3). The phosphorylated EIF2A leads to a decrease in translation initiation by inhibiting EIF2B activity and subsequent loss of ternary complexes. In addition, the phosphorylation of EIF2A initiates the assembly of stress granules, which are discrete cytoplasmic foci where untranslated mRNAs are sequestered (Kedersha, Gupta et al. 1999). In geneticin treated cells, the initiation factors EIF1B and EIF3A, part of the 43S PIC and EIF4A, involved in mRNA recruitment to the ribosome, are upregulated,

suggesting a compensatory response to inhibition of translation initiation. In contrast, hygromycin B treated cells show an enrichment of the elongation factors subunits EEF1A1, EEF1G and EEF2. This upregulation might represent a compensatory response to drug-induced translocation inhibition, by increasing the efficacy of translocation by overexpressing elongation factors.

7.7 Conclusion

Taken together, aminoglycosides stress eukaryotic cells by impairing translation fidelity and efficiency. Inhibition of cytosolic translation leads to oxidative stress and changes in the metabolic activity of mitochondria; mistranslation results in activation of the cytosolic heat shock response and the erUPR. In case of geneticin more than 75% of upregulated proteins are involved in protein metabolism (folding, translation, degradation and signaling) indicating a strong response against mistranslation. Treatment with the translocation inhibitor hygromycin B did not result in a broad upregulation of the folding machinery; however, parts of the translational apparatus were upregulated. In detail, a distinct pattern is observed: geneticin treatment resulted in an upregulation of initiation factors possibly to compensate inhibition of translation initiation by erUPR mediated p-EIF2A and hygromycin B treatment resulted in upregulation of elongation factors to compensate translocation inhibition.

8 References

Abraham, A. K. and A. Pihl (1983). "Effect of protein synthesis inhibitors on the fidelity of translation in eukaryotic systems." Biochim Biophys Acta **741**(2): 197-203.

Albanese, V., A. Y. Yam, J. Baughman, C. Parnot and J. Frydman (2006). "Systems analyses reveal two chaperone networks with distinct functions in eukaryotic cells." Cell **124**(1): 75-88.

Aldridge, J. E., T. Horibe and N. J. Hoogenraad (2007). "Discovery of genes activated by the mitochondrial unfolded protein response (mtUPR) and cognate promoter elements." PLoS One **2**(9): e874.

Algire, M. A., D. Maag and J. R. Lorsch (2005). "Pi release from eIF2, not GTP hydrolysis, is the step controlled by start-site selection during eukaryotic translation initiation." Mol Cell **20**(2): 251-262.

Anger, A. M., J. P. Armache, O. Berninghausen, M. Habeck, M. Subklewe, D. N. Wilson and R. Beckmann (2013). "Structures of the human and Drosophila 80S ribosome." Nature **497**(7447): 80-85.

Apostolou, A., Y. Shen, Y. Liang, J. Luo and S. Fang (2008). "Armet, a UPR-upregulated protein, inhibits cell proliferation and ER stress-induced cell death." Exp Cell Res **314**(13): 2454-2467.

Araki, K., S. Iemura, Y. Kamiya, D. Ron, K. Kato, T. Natsume and K. Nagata (2013). "Ero1-alpha and PDIs constitute a hierarchical electron transfer network of endoplasmic reticulum oxidoreductases." J Cell Biol **202**(6): 861-874.

Ben-Shem, A., N. Garreau de Loubresse, S. Melnikov, L. Jenner, G. Yusupova and M. Yusupov (2011). "The structure of the eukaryotic ribosome at 3.0 A resolution." Science **334**(6062): 1524-1529.

Benjamini, Y. and Y. Hochberg (1995). "Controlling the False Discovery Rate: A Practical and Powerful Approach to Multiple Testing." J. R. Statist. Soc B **57**(1): 289-300.

Blanco, F. J., I. Rego and C. Ruiz-Romero (2011). "The role of mitochondria in osteoarthritis." Nat Rev Rheumatol **7**(3): 161-169.

Borovinskaya, M. A., S. Shoji, K. Fredrick and J. H. Cate (2008). "Structural basis for hygromycin B inhibition of protein biosynthesis." RNA **14**(8): 1590-1599.

Bouadloun, F., D. Donner and C. G. Kurland (1983). "Codon-specific missense errors in vivo." EMBO J **2**(8): 1351-1356.

Brown, G. C. and V. Borutaite (2012). "There is no evidence that mitochondria are the main source of reactive oxygen species in mammalian cells." Mitochondrion **12**(1): 1-4.

Buchanan, J. H., A. Stevens and J. Sidhu (1987). "Aminoglycoside antibiotic treatment of human fibroblasts: intracellular accumulation, molecular changes and the loss of ribosomal accuracy." Eur J Cell Biol **43**(1): 141-147.

Busscher, G. F., F. P. Rutjes and F. L. van Delft (2005). "2-Deoxystreptamine: central scaffold of aminoglycoside antibiotics." Chem Rev **105**(3): 775-791.

Carpenter, K., R. J. Pollitt and B. Middleton (1992). "Human liver long-chain 3-hydroxyacyl-coenzyme A dehydrogenase is a multifunctional membrane-bound beta-oxidation enzyme of mitochondria." Biochem Biophys Res Commun **183**(2): 443-448.

Chomyn, A., S. T. Lai, R. Shakeley, N. Bresolin, G. Scarlato and G. Attardi (1994). "Platelet-mediated transformation of mtDNA-less human cells: analysis of phenotypic variability among clones from normal individuals--and complementation behavior of the tRNALys mutation causing myoclonic epilepsy and ragged red fibers." Am J Hum Genet **54**(6): 966-974.

Clancy, J. P., Z. Bebok, F. Ruiz, C. King, J. Jones, L. Walker, H. Greer, J. Hong, L. Wing, M. Macaluso, R. Lyrene, E. J. Sorscher and D. M. Bedwell (2001). "Evidence that systemic gentamicin suppresses premature stop mutations in patients with cystic fibrosis." Am J Respir Crit Care Med **163**(7): 1683-1692.

Conlon, B. J. and D. W. Smith (1998). "Supplemental iron exacerbates aminoglycoside ototoxicity in vivo." Hear Res **115**(1-2): 1-5.

Davies, J., L. Gorini and B. D. Davis (1965). "Misreading of RNA codewords induced by aminoglycoside antibiotics." Mol Pharmacol **1**(1): 93-106.

Deriziotis, P., R. Andre, D. M. Smith, R. Goold, K. J. Kinghorn, M. Kristiansen, J. A. Nathan, R. Rosenzweig, D. Krutauz, M. H. Glickman, J. Collinge, A. L. Goldberg and S. J. Tabrizi (2011). "Misfolded PrP impairs the UPS by interaction with the 20S proteasome and inhibition of substrate entry." EMBO J **30**(15): 3065-3077.

Dever, T. E. and R. Green (2012). "The elongation, termination, and recycling phases of translation in eukaryotes." Cold Spring Harb Perspect Biol **4**(7): a013706.

Drummond, D. A. and C. O. Wilke (2008). "Mistranslation-induced protein misfolding as a dominant constraint on coding-sequence evolution." Cell **134**(2): 341-352.

Dubaquie, Y., R. Looser and S. Rospert (1997). "Significance of chaperonin 10-mediated inhibition of ATP hydrolysis by chaperonin 60." Proc Natl Acad Sci U S A **94**(17): 9011-9016.

Dudek, J., P. Rehling and M. van der Laan (2013). "Mitochondrial protein import: common principles and physiological networks." Biochim Biophys Acta **1833**(2): 274-285.

Edelmann, P. and J. Gallant (1977). "Mistranslation in E. coli." Cell **10**(1): 131-137.

Eustice, D. C. and J. M. Wilhelm (1984). "Fidelity of the eukaryotic codon-anticodon interaction: interference by aminoglycoside antibiotics." Biochemistry **23**(7): 1462-1467.

Eustice, D. C. and J. M. Wilhelm (1984). "Mechanisms of action of aminoglycoside antibiotics in eucaryotic protein synthesis." Antimicrob Agents Chemother **26**(1): 53-60.

Fernie, A. R., F. Carrari and L. J. Sweetlove (2004). "Respiratory metabolism: glycolysis, the TCA cycle and mitochondrial electron transport." Curr Opin Plant Biol **7**(3): 254-261.

Finkel, R. S. (2010). "Read-through strategies for suppression of nonsense mutations in Duchenne/ Becker muscular dystrophy: aminoglycosides and ataluren (PTC124)." J Child Neurol **25**(9): 1158-1164.

Forge, A. and J. Schacht (2000). "Aminoglycoside antibiotics." Audiol Neurootol **5**(1): 3-22.

Francois, B., R. J. Russell, J. B. Murray, F. Aboul-ela, B. Masquida, Q. Vicens and E. Westhof (2005). "Crystal structures of complexes between aminoglycosides and decoding A site oligonucleotides: role of the number of rings and positive charges in the specific binding leading to miscoding." Nucleic Acids Res **33**(17): 5677-5690.

Frolova, L., X. Le Goff, G. Zhouravleva, E. Davydova, M. Philippe and L. Kisselev (1996). "Eukaryotic polypeptide chain release factor eRF3 is an eRF1- and ribosome-dependent guanosine triphosphatase." RNA **2**(4): 334-341.

Gale, E. F. C., E.; Reynolds, P.E.; Richmond, M.H.; Waring, M.J. (1981). The Molecular Basis of Antibiotic Action, John Wiley & Sons, London.

Gallo, L. I., M. Lagadari, G. Piwien-Pilipuk and M. D. Galigniana (2011). "The 90-kDa heat-shock protein (Hsp90)-binding immunophilin FKBP51 is a mitochondrial protein that translocates to the nucleus to protect cells against oxidative stress." J Biol Chem **286**(34): 30152-30160.

Gao, Y. G., M. Selmer, C. M. Dunham, A. Weixlbaumer, A. C. Kelley and V. Ramakrishnan (2009). "The structure of the ribosome with elongation factor G trapped in the posttranslocational state." Science **326**(5953): 694-699.

Garreau de Loubresse, N., I. Prokhorova, W. Holtkamp, M. V. Rodnina, G. Yusupova and M. Yusupov (2014). "Structural basis for the inhibition of the eukaryotic ribosome." Nature **513**(7519): 517-522.

Geisse, S. and B. Voedisch (2012). "Transient expression technologies: past, present, and future." Methods Mol Biol **899**: 203-219.

Goltermann, L., L. Good and T. Bentin (2013). "Chaperonins fight aminoglycoside-induced protein misfolding and promote short-term tolerance in Escherichia coli." J Biol Chem **288**(15): 10483-10489.

Grant, C. M., M. Firoozan and M. F. Tuite (1989). "Mistranslation induces the heat-shock response in the yeast Saccharomyces cerevisiae." Mol Microbiol **3**(2): 215-220.

Gregersen, N. and P. Bross (2010). "Protein misfolding and cellular stress: an overview." Methods Mol Biol **648**: 3-23.

Gromadski, K. B. and M. V. Rodnina (2004). "Kinetic determinants of high-fidelity tRNA discrimination on the ribosome." Mol Cell **13**(2): 191-200.

Gross, E., C. S. Sevier, N. Heldman, E. Vitu, M. Bentzur, C. A. Kaiser, C. Thorpe and D. Fass (2006). "Generating disulfides enzymatically: reaction products and electron acceptors of the endoplasmic reticulum thiol oxidase Ero1p." Proc Natl Acad Sci U S A **103**(2): 299-304.

Han, D., F. Antunes, R. Canali, D. Rettori and E. Cadenas (2003). "Voltage-dependent anion channels control the release of the superoxide anion from mitochondria to cytosol." J Biol Chem **278**(8): 5557-5563.

Hanahan, D. and R. A. Weinberg (2011). "Hallmarks of cancer: the next generation." Cell **144**(5): 646-674.

Hanna, J., D. S. Leggett and D. Finley (2003). "Ubiquitin depletion as a key mediator of toxicity by translational inhibitors." Mol Cell Biol **23**(24): 9251-9261.

Harding, H. P., Y. Zhang, H. Zeng, I. Novoa, P. D. Lu, M. Calfon, N. Sadri, C. Yun, B. Popko, R. Paules, D. F. Stojdl, J. C. Bell, T. Hettmann, J. M. Leiden and D. Ron (2003). "An integrated stress response regulates amino acid metabolism and resistance to oxidative stress." Mol Cell **11**(3): 619-633.

Hartl, F. U. and M. Hayer-Hartl (2002). "Molecular chaperones in the cytosol: from nascent chain to folded protein." Science **295**(5561): 1852-1858.

Haynes, C. M. and D. Ron (2010). "The mitochondrial UPR - protecting organelle protein homeostasis." J Cell Sci **123**(Pt 22): 3849-3855.

Hetz, C. (2012). "The unfolded protein response: controlling cell fate decisions under ER stress and beyond." Nat Rev Mol Cell Biol **13**(2): 89-102.

Hinnebusch, A. G. (2011). "Molecular mechanism of scanning and start codon selection in eukaryotes." Microbiol Mol Biol Rev **75**(3): 434-467, first page of table of contents.

Hobbie, S. N., S. Akshay, S. K. Kalapala, C. M. Bruell, D. Shcherbakov and E. C. Bottger (2008). "Genetic analysis of interactions with eukaryotic rRNA identify the mitoribosome as target in aminoglycoside ototoxicity." Proc Natl Acad Sci U S A **105**(52): 20888-20893.

Hollien, J. and J. S. Weissman (2006). "Decay of endoplasmic reticulum-localized mRNAs during the unfolded protein response." Science **313**(5783): 104-107.

Hoppe, G., Y. C. Chai and J. Sears (2003). "Endogenous oxidoreductase expression is induced by aminoglycosides." Arch Biochem Biophys **414**(1): 19-23.

Horibe, T. and N. J. Hoogenraad (2007). "The chop gene contains an element for the positive regulation of the mitochondrial unfolded protein response." PLoS One **2**(9): e835.

Huth, W., R. Jonas, I. Wunderlich and W. Seubert (1975). "On the mechanism of ketogenesis and its control. Purification, kinetic mechanism and regulation of different forms of mitochondrial acetoacetyl-CoA thiolases from ox liver." Eur J Biochem **59**(2): 475-489.

Jackson, R. J., C. U. Hellen and T. V. Pestova (2010). "The mechanism of eukaryotic translation initiation and principles of its regulation." Nat Rev Mol Cell Biol **11**(2): 113-127.

Jenner, L., N. Demeshkina, G. Yusupova and M. Yusupov (2010). "Structural rearrangements of the ribosome at the tRNA proofreading step." Nat Struct Mol Biol **17**(9): 1072-1078.

Kandasamy, J., D. Atia-Glikin, E. Shulman, K. Shapira, M. Shavit, V. Belakhov and T. Baasov (2012). "Increased selectivity toward cytoplasmic versus mitochondrial ribosome confers improved efficiency of synthetic aminoglycosides in fixing damaged genes: a strategy for treatment of genetic diseases caused by nonsense mutations." J Med Chem **55**(23): 10630-10643.

Kedersha, N. L., M. Gupta, W. Li, I. Miller and P. Anderson (1999). "RNA-binding proteins TIA-1 and TIAR link the phosphorylation of eIF-2 alpha to the assembly of mammalian stress granules." J Cell Biol **147**(7): 1431-1442.

Keene, M. and M. Hawke (1981). "Pathogenesis and detection of aminoglycoside ototoxicity." J Otolaryngol **10**(3): 228-236.

King, M. P. and G. Attardi (1989). "Human cells lacking mtDNA: repopulation with exogenous mitochondria by complementation." Science **246**(4929): 500-503.

Klinge, S., F. Voigts-Hoffmann, M. Leibundgut, S. Arpagaus and N. Ban (2011). "Crystal structure of the eukaryotic 60S ribosomal subunit in complex with initiation factor 6." Science **334**(6058): 941-948.

Kondo, J. (2012). "A structural basis for the antibiotic resistance conferred by an A1408G mutation in 16S rRNA and for the antiprotozoal activity of aminoglycosides." Angew Chem Int Ed Engl **51**(2): 465-468.

Koopman, W. J., L. G. Nijtmans, C. E. Dieteren, P. Roestenberg, F. Valsecchi, J. A. Smeitink and P. H. Willems (2010). "Mammalian mitochondrial complex I: biogenesis, regulation, and reactive oxygen species generation." Antioxid Redox Signal **12**(12): 1431-1470.

Kotra, L. P., J. Haddad and S. Mobashery (2000). "Aminoglycosides: perspectives on mechanisms of action and resistance and strategies to counter resistance." Antimicrob Agents Chemother **44**(12): 3249-3256.

Kramer, E. B. and P. J. Farabaugh (2007). "The frequency of translational misreading errors in E. coli is largely determined by tRNA competition." RNA **13**(1): 87-96.

Ksenzenko, M., A. A. Konstantinov, G. B. Khomutov, A. N. Tikhonov and E. K. Ruuge (1983). "Effect of electron transfer inhibitors on superoxide generation in the cytochrome bc1 site of the mitochondrial respiratory chain." FEBS Lett **155**(1): 19-24.

Laurberg, M., H. Asahara, A. Korostelev, J. Zhu, S. Trakhanov and H. F. Noller (2008). "Structural basis for translation termination on the 70S ribosome." Nature **454**(7206): 852-857.

Lautermann, J., N. Dehne, J. Schacht and K. Jahnke (2004). "[Aminoglycoside- and cisplatin-ototoxicity: from basic science to clinics]." Laryngorhinootologie **83**(5): 317-323.

Lecompte, O., R. Ripp, J. C. Thierry, D. Moras and O. Poch (2002). "Comparative analysis of ribosomal proteins in complete genomes: an example of reductive evolution at the domain scale." Nucleic Acids Res **30**(24): 5382-5390.

Lee, J. W., K. Beebe, L. A. Nangle, J. Jang, C. M. Longo-Guess, S. A. Cook, M. T. Davisson, J. P. Sundberg, P. Schimmel and S. L. Ackerman (2006). "Editing-defective tRNA synthetase causes protein misfolding and neurodegeneration." Nature **443**(7107): 50-55.

Maharjan, S., M. Oku, M. Tsuda, J. Hoseki and Y. Sakai (2014). "Mitochondrial impairment triggers cytosolic oxidative stress and cell death following proteasome inhibition." Sci Rep **4**: 5896.

Malhotra, J. D. and R. J. Kaufman (2007). "Endoplasmic reticulum stress and oxidative stress: a vicious cycle or a double-edged sword?" Antioxid Redox Signal **9**(12): 2277-2293.

Manuvakhova, M., K. Keeling and D. M. Bedwell (2000). "Aminoglycoside antibiotics mediate context-dependent suppression of termination codons in a mammalian translation system." RNA **6**(7): 1044-1055.

Martemyanov, K. A. and A. T. Gudkov (1999). "Domain IV of elongation factor G from Thermus thermophilus is strictly required for translocation." FEBS Lett **452**(3): 155-159.

Matsumoto, M., M. Minami, K. Takeda, Y. Sakao and S. Akira (1996). "Ectopic expression of CHOP (GADD153) induces apoptosis in M1 myeloblastic leukemia cells." FEBS Lett **395**(2-3): 143-147.

Matt, T., C. L. Ng, K. Lang, S. H. Sha, R. Akbergenov, D. Shcherbakov, M. Meyer, S. Duscha, J. Xie, S. R. Dubbaka, D. Perez-Fernandez, A. Vasella, V. Ramakrishnan, J. Schacht and E. C. Bottger (2012). "Dissociation of antibacterial activity and

aminoglycoside ototoxicity in the 4-monosubstituted 2-deoxystreptamine apramycin." Proc Natl Acad Sci U S A **109**(27): 10984-10989.

McCarthy, D. J. and G. K. Smyth (2009). "Testing significance relative to a fold-change threshold is a TREAT." Bioinformatics **25**(6): 765-771.

McClellan, A. J., M. D. Scott and J. Frydman (2005). "Folding and quality control of the VHL tumor suppressor proceed through distinct chaperone pathways." Cell **121**(5): 739-748.

McCullough, K. D., J. L. Martindale, L. O. Klotz, T. Y. Aw and N. J. Holbrook (2001). "Gadd153 sensitizes cells to endoplasmic reticulum stress by down-regulating Bcl2 and perturbing the cellular redox state." Mol Cell Biol **21**(4): 1249-1259.

Melnikov, S., A. Ben-Shem, N. Garreau de Loubresse, L. Jenner, G. Yusupova and M. Yusupov (2012). "One core, two shells: bacterial and eukaryotic ribosomes." Nat Struct Mol Biol **19**(6): 560-567.

Morimoto, R. I. (2008). "Proteotoxic stress and inducible chaperone networks in neurodegenerative disease and aging." Genes Dev **22**(11): 1427-1438.

Murphy, M. P. (2009). "How mitochondria produce reactive oxygen species." Biochem J **417**(1): 1-13.

Ngo, J. K. and K. J. Davies (2007). "Importance of the lon protease in mitochondrial maintenance and the significance of declining lon in aging." Ann N Y Acad Sci **1119**: 78-87.

Noller, H. F. (1991). "Ribosomal RNA and translation." Annu Rev Biochem **60**: 191-227.

Nudelman, I., D. Glikin, B. Smolkin, M. Hainrichson, V. Belakhov and T. Baasov (2010). "Repairing faulty genes by aminoglycosides: development of new derivatives of geneticin (G418) with enhanced suppression of diseases-causing nonsense mutations." Bioorg Med Chem **18**(11): 3735-3746.

O'Connor, S., L. K. Lam, N. D. Jones and M. O. Chaney (1976). "Apramycin, a unique aminocyclitol antibiotic." J Org Chem **41**(12): 2087-2092.

Ogle, J. M., D. E. Brodersen, W. M. Clemons, Jr., M. J. Tarry, A. P. Carter and V. Ramakrishnan (2001). "Recognition of cognate transfer RNA by the 30S ribosomal subunit." Science **292**(5518): 897-902.

Ohoka, N., S. Yoshii, T. Hattori, K. Onozaki and H. Hayashi (2005). "TRB3, a novel ER stress-inducible gene, is induced via ATF4-CHOP pathway and is involved in cell death." EMBO J **24**(6): 1243-1255.

Orrenius, S., V. Gogvadze and B. Zhivotovsky (2007). "Mitochondrial oxidative stress: implications for cell death." Annu Rev Pharmacol Toxicol **47**: 143-183.

Ostermann, J., A. L. Horwich, W. Neupert and F. U. Hartl (1989). "Protein folding in mitochondria requires complex formation with hsp60 and ATP hydrolysis." Nature **341**(6238): 125-130.

Pagani, M., M. Fabbri, C. Benedetti, A. Fassio, S. Pilati, N. J. Bulleid, A. Cabibbo and R. Sitia (2000). "Endoplasmic reticulum oxidoreductin 1-lbeta (ERO1-Lbeta), a human gene induced in the course of the unfolded protein response." J Biol Chem **275**(31): 23685-23692.

Palmer, E. and J. M. Wilhelm (1978). "Mistranslation in a eucaryotic organism." Cell **13**(2): 329-334.

Palmer, E., J. M. Wilhelm and F. Sherman (1979). "Phenotypic suppression of nonsense mutants in yeast by aminoglycoside antibiotics." Nature **277**(5692): 148-150.

Pape, T., W. Wintermeyer and M. Rodnina (1999). "Induced fit in initial selection and proofreading of aminoacyl-tRNA on the ribosome." EMBO J **18**(13): 3800-3807.

Pape, T., W. Wintermeyer and M. V. Rodnina (1998). "Complete kinetic mechanism of elongation factor Tu-dependent binding of aminoacyl-tRNA to the A site of the E. coli ribosome." EMBO J **17**(24): 7490-7497.

Paredes, J. A., L. Carreto, J. Simoes, A. R. Bezerra, A. C. Gomes, R. Santamaria, M. Kapushesky, G. R. Moura and M. A. Santos (2012). "Low level genome mistranslations deregulate the transcriptome and translatome and generate proteotoxic stress in yeast." BMC Biol **10**: 55.

Perez-Fernandez, D., D. Shcherbakov, T. Matt, N. C. Leong, I. Kudyba, S. Duscha, H. Boukari, R. Patak, S. R. Dubbaka, K. Lang, M. Meyer, R. Akbergenov, P. Freihofer, S. Vaddi, P. Thommes, V. Ramakrishnan, A. Vasella and E. C. Bottger (2014). "4'-O-substitutions determine selectivity of aminoglycoside antibiotics." Nat Commun **5**: 3112.

Pfister, P., S. Hobbie, Q. Vicens, E. C. Bottger and E. Westhof (2003). "The molecular basis for A-site mutations conferring aminoglycoside resistance:

relationship between ribosomal susceptibility and X-ray crystal structures." Chembiochem **4**(10): 1078-1088.

Prezant, T. R., J. V. Agapian, M. C. Bohlman, X. Bu, S. Oztas, W. Q. Qiu, K. S. Arnos, G. A. Cortopassi, L. Jaber, J. I. Rotter and et al. (1993). "Mitochondrial ribosomal RNA mutation associated with both antibiotic-induced and non-syndromic deafness." Nat Genet **4**(3): 289-294.

Priuska, E. M. and J. Schacht (1995). "Formation of free radicals by gentamicin and iron and evidence for an iron/gentamicin complex." Biochem Pharmacol **50**(11): 1749-1752.

Rasmussen, B. A., K. Bush and F. P. Tally (1997). "Antimicrobial resistance in anaerobes." Clin Infect Dis **24 Suppl 1**: S110-120.

Ravens, S., M. Fournier, T. Ye, M. Stierle, D. Dembele, V. Chavant and L. Tora (2014). "MOF-associated complexes have overlapping and unique roles in regulating pluripotency in embryonic stem cells and during differentiation." Elife: e02104.

Rodnina, M. V., R. Fricke, L. Kuhn and W. Wintermeyer (1995). "Codon-dependent conformational change of elongation factor Tu preceding GTP hydrolysis on the ribosome." EMBO J **14**(11): 2613-2619.

Rodnina, M. V., R. Fricke and W. Wintermeyer (1994). "Transient conformational states of aminoacyl-tRNA during ribosome binding catalyzed by elongation factor Tu." Biochemistry **33**(40): 12267-12275.

Rodnina, M. V., A. Savelsbergh, V. I. Katunin and W. Wintermeyer (1997). "Hydrolysis of GTP by elongation factor G drives tRNA movement on the ribosome." Nature **385**(6611): 37-41.

Rubinsztein, D. C. (2006). "The roles of intracellular protein-degradation pathways in neurodegeneration." Nature **443**(7113): 780-786.

Ruedi, L., W. Furrer, F. Luthy, G. Nager and B. Tschirren (1952). "Further observations concerning the toxic effects of streptomycin and quinine on the auditory organ of guinea pigs." Laryngoscope **62**(4): 333-351.

Salas-Marco, J. and D. M. Bedwell (2005). "Discrimination between defects in elongation fidelity and termination efficiency provides mechanistic insights into translational readthrough." J Mol Biol **348**(4): 801-815.

Salian, S., T. Matt, R. Akbergenov, S. Harish, M. Meyer, S. Duscha, D. Shcherbakov, B. B. Bernet, A. Vasella, E. Westhof and E. C. Bottger (2012). "Structure-activity relationships among the kanamycin aminoglycosides: role of ring I hydroxyl and amino groups." Antimicrob Agents Chemother **56**(12): 6104-6108.

Schacht, J., A. E. Talaska and L. P. Rybak (2012). "Cisplatin and aminoglycoside antibiotics: hearing loss and its prevention." Anat Rec (Hoboken) **295**(11): 1837-1850.

Schmeing, T. M. and V. Ramakrishnan (2009). "What recent ribosome structures have revealed about the mechanism of translation." Nature **461**(7268): 1234-1242.

Schmeing, T. M., R. M. Voorhees, A. C. Kelley, Y. G. Gao, F. V. t. Murphy, J. R. Weir and V. Ramakrishnan (2009). "The crystal structure of the ribosome bound to EF-Tu and aminoacyl-tRNA." Science **326**(5953): 688-694.

Schmeing, T. M., R. M. Voorhees, A. C. Kelley and V. Ramakrishnan (2011). "How mutations in tRNA distant from the anticodon affect the fidelity of decoding." Nat Struct Mol Biol **18**(4): 432-436.

Schmidt, S. P., T. J. Corydon, C. B. Pedersen, S. Vang, J. Palmfeldt, V. Stenbroen, R. J. Wanders, J. P. Ruiter and N. Gregersen (2011). "Toxic response caused by a misfolding variant of the mitochondrial protein short-chain acyl-CoA dehydrogenase." J Inherit Metab Dis **34**(2): 465-475.

Schneider-Poetsch, T., J. Ju, D. E. Eyler, Y. Dang, S. Bhat, W. C. Merrick, R. Green, B. Shen and J. O. Liu (2010). "Inhibition of eukaryotic translation elongation by cycloheximide and lactimidomycin." Nat Chem Biol **6**(3): 209-217.

Schroder, M. and R. J. Kaufman (2005). "The mammalian unfolded protein response." Annu Rev Biochem **74**: 739-789.

Sha, S. H. and J. Schacht (1999). "Formation of reactive oxygen species following bioactivation of gentamicin." Free Radic Biol Med **26**(3-4): 341-347.

Sha, S. H. and J. Schacht (1999). "Salicylate attenuates gentamicin-induced ototoxicity." Lab Invest **79**(7): 807-813.

Sha, S. H. and J. Schacht (1999). "Stimulation of free radical formation by aminoglycoside antibiotics." Hear Res **128**(1-2): 112-118.

Sha, S. H., G. Zajic, C. J. Epstein and J. Schacht (2001). "Overexpression of copper/zinc-superoxide dismutase protects from kanamycin-induced hearing loss." Audiol Neurootol **6**(3): 117-123.

Shaw, G., S. Morse, M. Ararat and F. L. Graham (2002). "Preferential transformation of human neuronal cells by human adenoviruses and the origin of HEK 293 cells." FASEB J **16**(8): 869-871.

Shi, Y., K. M. Vattem, R. Sood, J. An, J. Liang, L. Stramm and R. C. Wek (1998). "Identification and characterization of pancreatic eukaryotic initiation factor 2 alpha-subunit kinase, PEK, involved in translational control." Mol Cell Biol **18**(12): 7499-7509.

Shulman, E., V. Belakhov, G. Wei, A. Kendall, E. G. Meyron-Holtz, D. Ben-Shachar, J. Schacht and T. Baasov (2014). "Designer aminoglycosides that selectively inhibit cytoplasmic rather than mitochondrial ribosomes show decreased ototoxicity: a strategy for the treatment of genetic diseases." J Biol Chem **289**(4): 2318-2330.

Singh, C. R., B. Lee, T. Udagawa, S. S. Mohammad-Qureshi, Y. Yamamoto, G. D. Pavitt and K. Asano (2006). "An eIF5/eIF2 complex antagonizes guanine nucleotide exchange by eIF2B during translation initiation." EMBO J **25**(19): 4537-4546.

Sonenberg, N. and A. G. Hinnebusch (2009). "Regulation of translation initiation in eukaryotes: mechanisms and biological targets." Cell **136**(4): 731-745.

Song, B. B., D. J. Anderson and J. Schacht (1997). "Protection from gentamicin ototoxicity by iron chelators in guinea pig in vivo." J Pharmacol Exp Ther **282**(1): 369-377.

Spahn, C. M., R. Beckmann, N. Eswar, P. A. Penczek, A. Sali, G. Blobel and J. Frank (2001). "Structure of the 80S ribosome from Saccharomyces cerevisiae--tRNA-ribosome and subunit-subunit interactions." Cell **107**(3): 373-386.

Spahn, C. M. and C. D. Prescott (1996). "Throwing a spanner in the works: antibiotics and the translation apparatus." J Mol Med (Berl) **74**(8): 423-439.

Stansfield, I., K. M. Jones, P. Herbert, A. Lewendon, W. V. Shaw and M. F. Tuite (1998). "Missense translation errors in Saccharomyces cerevisiae." J Mol Biol **282**(1): 13-24.

Tatsuta, T. and T. Langer (2008). "Quality control of mitochondria: protection against neurodegeneration and ageing." EMBO J **27**(2): 306-314.

Tirasophon, W., A. A. Welihinda and R. J. Kaufman (1998). "A stress response pathway from the endoplasmic reticulum to the nucleus requires a novel bifunctional protein kinase/endoribonuclease (Ire1p) in mammalian cells." Genes Dev **12**(12): 1812-1824.

Tonin, A. M., A. U. Amaral, E. N. Busanello, M. Grings, R. F. Castilho and M. Wajner (2013). "Long-chain 3-hydroxy fatty acids accumulating in long-chain 3-hydroxyacyl-CoA dehydrogenase and mitochondrial trifunctional protein deficiencies uncouple oxidative phosphorylation in heart mitochondria." J Bioenerg Biomembr **45**(1-2): 47-57.

Tonin, A. M., G. C. Ferreira, M. Grings, C. M. Viegas, E. N. Busanello, A. U. Amaral, A. Zanatta, P. F. Schuck and M. Wajner (2010). "Disturbance of mitochondrial energy homeostasis caused by the metabolites accumulating in LCHAD and MTP deficiencies in rat brain." Life Sci **86**(21-22): 825-831.

Uemura, S., C. E. Aitken, J. Korlach, B. A. Flusberg, S. W. Turner and J. D. Puglisi (2010). "Real-time tRNA transit on single translating ribosomes at codon resolution." Nature **464**(7291): 1012-1017.

Varadarajan, S., S. Yatin, M. Aksenova and D. A. Butterfield (2000). "Review: Alzheimer's amyloid beta-peptide-associated free radical oxidative stress and neurotoxicity." J Struct Biol **130**(2-3): 184-208.

Ventoso, I., A. Kochetov, D. Montaner, J. Dopazo and J. Santoyo (2012). "Extensive translatome remodeling during ER stress response in mammalian cells." PLoS One **7**(5): e35915.

Vicens, Q. and E. Westhof (2001). "Crystal structure of paromomycin docked into the eubacterial ribosomal decoding A site." Structure **9**(8): 647-658.

Vicens, Q. and E. Westhof (2002). "Crystal structure of a complex between the aminoglycoside tobramycin and an oligonucleotide containing the ribosomal decoding a site." Chem Biol **9**(6): 747-755.

Vicens, Q. and E. Westhof (2003). "Crystal structure of geneticin bound to a bacterial 16S ribosomal RNA A site oligonucleotide." J Mol Biol **326**(4): 1175-1188.

Vicens, Q. and E. Westhof (2003). "Molecular recognition of aminoglycoside antibiotics by ribosomal RNA and resistance enzymes: an analysis of x-ray crystal structures." Biopolymers **70**(1): 42-57.

Villalba, J. D., C. Gomez, O. Medel, V. Sanchez, J. C. Carrero, M. Shibayama and D. G. Ishiwara (2007). "Programmed cell death in Entamoeba histolytica induced by the aminoglycoside G418." Microbiology **153**(Pt 11): 3852-3863.

Voigts-Hoffmann, F., S. Klinge and N. Ban (2012). "Structural insights into eukaryotic ribosomes and the initiation of translation." Curr Opin Struct Biol **22**(6): 768-777.

Voorhees, R. M., T. M. Schmeing, A. C. Kelley and V. Ramakrishnan (2010). "The mechanism for activation of GTP hydrolysis on the ribosome." Science **330**(6005): 835-838.

Walter, P. and D. Ron (2011). "The unfolded protein response: from stress pathway to homeostatic regulation." Science **334**(6059): 1081-1086.

Weisser, M., F. Voigts-Hoffmann, J. Rabl, M. Leibundgut and N. Ban (2013). "The crystal structure of the eukaryotic 40S ribosomal subunit in complex with eIF1 and eIF1A." Nat Struct Mol Biol **20**(8): 1015-1017.

West, A. P., G. S. Shadel and S. Ghosh (2011). "Mitochondria in innate immune responses." Nat Rev Immunol **11**(6): 389-402.

Wilhelm, J. M., J. J. Jessop and S. E. Pettitt (1978). "Aminoglycoside antibiotics and eukaryotic protein synthesis: stimulation of errors in the translation of natural messengers in extracts of cultured human cells." Biochemistry **17**(7): 1149-1153.

Wilhelm, J. M., S. E. Pettitt and J. J. Jessop (1978). "Aminoglycoside antibiotics and eukaryotic protein synthesis: structure--function relationships in the stimulation of misreading with a wheat embryo system." Biochemistry **17**(7): 1143-1149.

Wilschanski, M., Y. Yahav, Y. Yaacov, H. Blau, L. Bentur, J. Rivlin, M. Aviram, T. Bdolah-Abram, Z. Bebok, L. Shushi, B. Kerem and E. Kerem (2003). "Gentamicin-induced correction of CFTR function in patients with cystic fibrosis and CFTR stop mutations." N Engl J Med **349**(15): 1433-1441.

Yahata, T., M. P. de Caestecker, R. J. Lechleider, S. Andriole, A. B. Roberts, K. J. Isselbacher and T. Shioda (2000). "The MSG1 non-DNA-binding transactivator binds to the p300/CBP coactivators, enhancing their functional link to the Smad transcription factors." J Biol Chem **275**(12): 8825-8834.

Yamagishi, N., K. Goto, S. Nakagawa, Y. Saito and T. Hatayama (2010). "Hsp105 reduces the protein aggregation and cytotoxicity by expanded-polyglutamine proteins through the induction of Hsp70." Exp Cell Res **316**(15): 2424-2433.

Yamagishi, N., Y. Saito and T. Hatayama (2008). "Mammalian 105 kDa heat shock family proteins suppress hydrogen peroxide-induced apoptosis through a p38 MAPK-dependent mitochondrial pathway in HeLa cells." FEBS J **275**(18): 4558-4570.

Yoshida, H., T. Okada, K. Haze, H. Yanagi, T. Yura, M. Negishi and K. Mori (2000). "ATF6 activated by proteolysis binds in the presence of NF-Y (CBF) directly to the cis-acting element responsible for the mammalian unfolded protein response." Mol Cell Biol **20**(18): 6755-6767.

Zaher, H. S. and R. Green (2009). "Fidelity at the molecular level: lessons from protein synthesis." Cell **136**(4): 746-762.

Zembower, T. R., G. A. Noskin, M. J. Postelnick, C. Nguyen and L. R. Peterson (1998). "The utility of aminoglycosides in an era of emerging drug resistance." Int J Antimicrob Agents **10**(2): 95-105.

Zhang, K. (2010). "Integration of ER stress, oxidative stress and the inflammatory response in health and disease." Int J Clin Exp Med **3**(1): 33-40.

Zhao, H., R. Li, Q. Wang, Q. Yan, J. H. Deng, D. Han, Y. Bai, W. Y. Young and M. X. Guan (2004). "Maternally inherited aminoglycoside-induced and nonsyndromic deafness is associated with the novel C1494T mutation in the mitochondrial 12S rRNA gene in a large Chinese family." Am J Hum Genet **74**(1): 139-152.

Zou, J., Y. Guo, T. Guettouche, D. F. Smith and R. Voellmy (1998). "Repression of heat shock transcription factor HSF1 activation by HSP90 (HSP90 complex) that forms a stress-sensitive complex with HSF1." Cell **94**(4): 471-480.

9 XBP1 mitigates aminoglycoside-induced endoplasmic reticulum stress and neuronal cell death.

Naoki Oishi, Stefan Duscha, Heithem Boukari, Martin Meyer, Jing Xie, Gao Wei, Thomas Schrepfer, Bernd Roschitzki, Erik C. Boettger, and Jochen Schacht

Abstract

Here we study links between aminoglycoside-induced mistranslation, protein misfolding, and neuropathy. We demonstrate that aminoglycosides induce misreading in mammalian cells and assess ER stress and unfolded protein response (UPR) pathways. Genome-wide transcriptome and proteome analyses revealed upregulation of genes related to protein folding and degradation. Quantitative PCR confirmed induction of UPR markers including CHOP, GRP94, BiP, and XBP1 mRNA splicing, which is crucial for UPR activation. We studied the effect of a compromised UPR on aminoglycoside ototoxicity in haploinsufficient XBP1 ($XBP1^{+/-}$) mice. Intra-tympanic aminoglycoside treatment caused high-frequency hearing loss in $XBP1^{+/-}$ mice but not in wild-type littermates. Densities of spiral ganglion cells and synaptic ribbons were decreased in gentamicin-treated $XBP1^{+/-}$ mice, while sensory cells were preserved. Co-injection of the chemical chaperone tauroursodeoxycholic acid attenuated hearing loss. These results suggest that aminoglycoside-induced ER stress and cell death in spiral ganglion neurons is mitigated by XBP1, masking aminoglycoside neurotoxicity at the organismal level.

Introduction

Translational fidelity is maintained throughout all three domains of life (archea, bacteria, eukaryota), suggesting a high selective pressure during evolution to minimize errors in protein synthesis.[1] In bacteria, erroneous protein synthesis induces protein misfolding.[2] In higher eukaryotes, protein misfolding results in endoplasmatic reticulum (ER) stress and initiates the unfolded protein response (UPR), a cascade of integrated pathways regulating gene expression. The UPR^{ER} is mediated by three ubiquitously expressed transmembrane proteins in the ER: inositol-requiring enzyme 1 (IRE1), PKR–like ER kinase (PERK), and activating transcription factor 6 (ATF6).[3-7] Under normal conditions, the luminal domains of IRE1, PERK, and ATF6 are bound by the ER chaperone binding immunoglobulin

protein (BiP) which inhibits self-dimerization and activation of the cytosolic domain.[8,9] Under ER stress, BiP is released resulting in dimerization of IRE1 and ATF6 and multimerization of PERK, initiating the UPR signaling cascades.[8,9] The initial UPR response is protective, increasing the expression of chaperone proteins promoting refolding and, if unsuccessful, the degradation of misfolded proteins.[10-13] Prolonged or severe stress triggers additional pathways that eventually lead to cellular apoptosis.[14-16]

Aminoglycoside antibiotics are well known to affect translational fidelity in bacteria and lower eukaryotes[17-20] but only few reports suggest that aminoglycoside antibiotics may also induce misreading in higher eukaryotes.[21-23] Aminoglycoside-mediated read-through activity has been exploited for therapy of human genetic diseases associated with premature stop codons.[24-27] In addition, aminoglycosides have been shown to induce apoptosis in human cell cultures accompanied by ER stress and mitochondrial cytochrome c release.[28,29] It was suggested that the observed ER stress may be the result of protein misfolding, reflecting aminoglycoside-induced mistranslation.[28] Despite this potential for misreading induced by aminoglycosides in eukaryotes, aminoglycoside treatment in animal models and in patients is well tolerated. Side effects are highly organ-specific, limited to the kidney and the inner ear,[30] while toxicity to the nervous system is not evident even in long-term aminoglycoside treatment.[31] In the case of ototoxicity, the primary drug target are the sensory hair cells, as convincingly demonstrated in various animal models, regardless of whether the drug is given systemically[32] or directly introduced into the cochlea.[33] Degeneration of spiral ganglion cells observed after ototoxic dosages of aminoglycosides are thought to occur only as a sequel to the loss of sensory hair cells in the vast majority of cases. Surprisingly, however, a few analyses of human temporal bones have suggested that spiral ganglia can be affected by aminoglycosides without overt insult to the hair cells.[34,35] This rare pathology, unexplained by the treatment modus, suggests individual variability possibly based on genetic factors.

Prompted by the anecdotal reports of aminoglycoside-induced selective spiral ganglion damage, the objective of this study was to assess the contribution of ER stress to ototoxicity. We first investigated aminoglycoside-induced misreading and UPR responses in HEK293 cells *in vitro*. Next, we examined the role of ER stress in

ototoxicity in cochlear organ cultures of CBA/J mice. Finally, we employed an *in-vivo* mouse model[36] with a compromised ER stress response due to XBP1 haploinsufficiency[37] in order to probe potential links between aminoglycoside neurotoxicity, translation fidelity and protein misfolding.

Results

Aminoglycosides alter translation fidelity. Drug-induced inhibition of translation was used to assess aminoglycoside activity on the eukaryotic ribosome. IC50 values were 0.3 µM for geneticin and 9.8 µM for gentamicin in the cell-free translation assays with rabbit reticulocyte lysate (RRL), and 4.4 µM for geneticin and 812 µM for gentamicin in assays with intact HEK293 cells (Supplementary Figure S1a and b). The ability of the drugs to induce mistranslation was analyzed using sensitive gain-of-function dual-luciferase assays to assess near-cognate misreading and stop-codon read-through. Near-cognate misreading was studied using constructs with substitution of amino acid 245 in the active site of mutated firefly luciferase (wild-type His CAC → near-cognate Arg CGC), which results in loss of enzymatic activity with enzymatic function restored by misreading; stopcodon read-through was determined using constructs with in-frame stop codons abolishing firefly luciferase activity. Both geneticin and gentamicin decreased ribosomal accuracy in cell free translation assays (RRL) and in HEK cells in a dose-dependent manner (Figure 1). Misreading

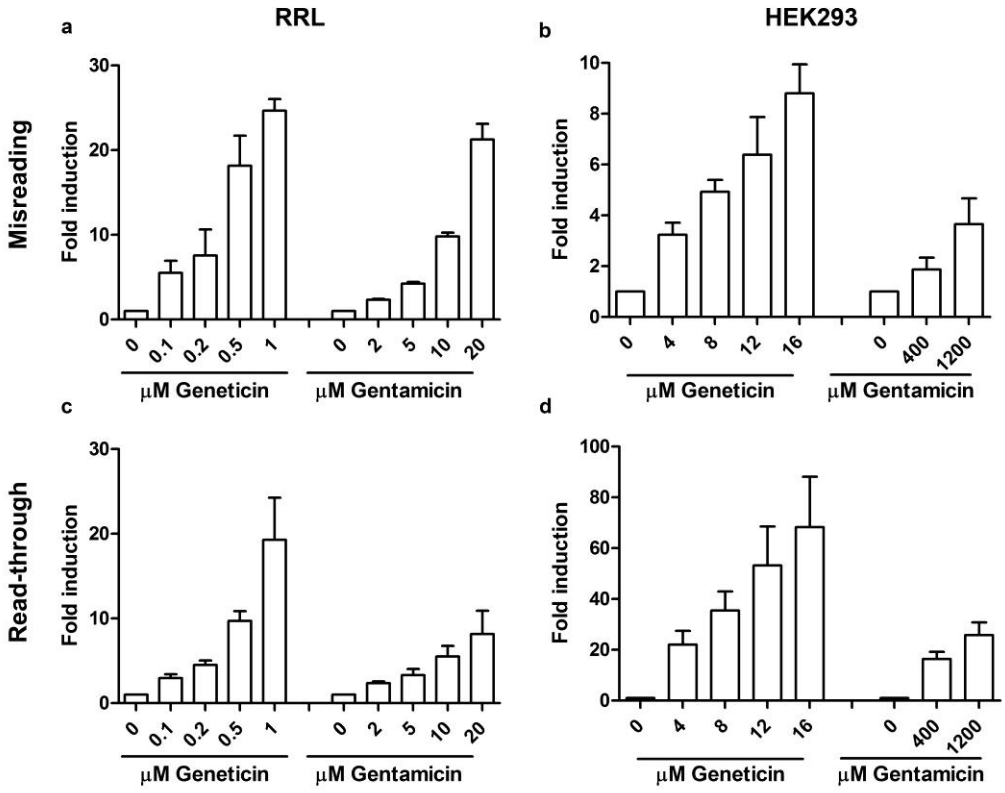

Figure 1 Aminoglycoside-induced mistranslation. (a–b) Misreading and (c–d) read-through measured in rabbit reticulocyte lysate (RRL; a,c) and HEK wild-type cells (b,d). Results are derived from the ratio hFluc/hRluc, given in -fold induction. Untreated samples are set as 1 (*n* = 3; ± SEM).

was induced up to 25-fold in RRL and up to 8.5-fold in HEK cells compared to untreated controls; read-through was induced up to 20-fold in RRL and up to 70-fold in HEK cells compared to untreated controls (Figure 1). In HEK cells transfected with the aminoglycoside phosphotransferase APH(3'), the geneticin-induced but not the gentamicin-induced translation inhibition and mistranslation were abrogated (Supplementary Figure S1c and d), consistent with the selectivity of the enzyme to inactivate geneticin but not gentamicin.[38,39] Aminoglycoside-treated and untreated HEK wild-type cells showed similar metabolic activities and viability (Supplementary Figure S1e and f).

Aminoglycosides induce genome-wide upregulation of cellular folding capacity. In order to study the cellular response to aminoglycoside-induced mistranslation, we used whole genome transcriptomic and proteomic analyses. A microarray analysis of geneticin-treated versus untreated cells revealed a broad transcriptional response totaling 705 genes (selected for a fold change >1.2, Benjamini-Hochberg corrected *p*-value <0.05; Supplementary Figure S2a). Protein folding and transcription were among the most enriched functional ontologies (Supplementary Figure S2b), including the induction of the ER-specific chaperones BiP (HSPA5), glucose-regulated protein 94 (GRP94; HSP90B1), calreticulin (CALR), GRP110 (HYOU1), ERdj3 (DNAJB11), and ERdj6 (DNAJC3), the ER foldases PDIA3 (ERp57), PDIA4 (ERp70), Erp44, and FKBP7, and the N-linked glycosylation factor SDF2L1. Likewise, ER-associated degradation (ERAD) components such as VCP (p97), Derlin2 (DERL2), and Herp (HERPUD1) were significantly upregulated (Supplementary Figure S2c). This transcriptional response indicates a general increased folding and degradation capacity in the ER. In addition, a large number of cytosolic chaperones[40] were upregulated, such as members of the Hsp40, Hsp70, Hsp90, and Hsp110 families and to a lesser extent foldases (peptidyl-prolyl cis/trans isomerases and protein disulfide isomerases; Supplementary Figure S2d and e), indicating an increased folding capacity in the cytosol. Table S1 lists the genes included in the analysis. The microarray data have been deposited in NCBI's Gene Expression Omnibus and are accessible through GEO Series accession number GSE57198 (http://www.ncbi.nlm.nih.gov/geo/query/acc.cgi?acc=GSE57198).

Proteome analysis found 77 proteins to be regulated by geneticin (Bonferroni-corrected *p*-value <0.05). When applying a minimum fold induction of 0.3 (log2 scale)

we identified 35 proteins that were upregulated. Grouping according to function revealed a predominance of proteins involved in protein folding (Figure 2a). Proteins associated with the ER and cytoplasmic UPR, such as BiP, GRP94, calreticulin, foldases, and members of the Hsp70, Hsp90, Hsp110, and Hsp40 families, were also upregulated (Figure 2b). Comparison with corresponding mRNA levels showed an upregulation of the folding machinery both at the transcriptomic and the proteomic level (Figure 2c). The mass spectrometry proteomics data have been deposited to the ProteomeXchange Consortium via the PRIDE partner repository with the dataset identifier PXD000933 and DOI 10.6019/PXD000933.

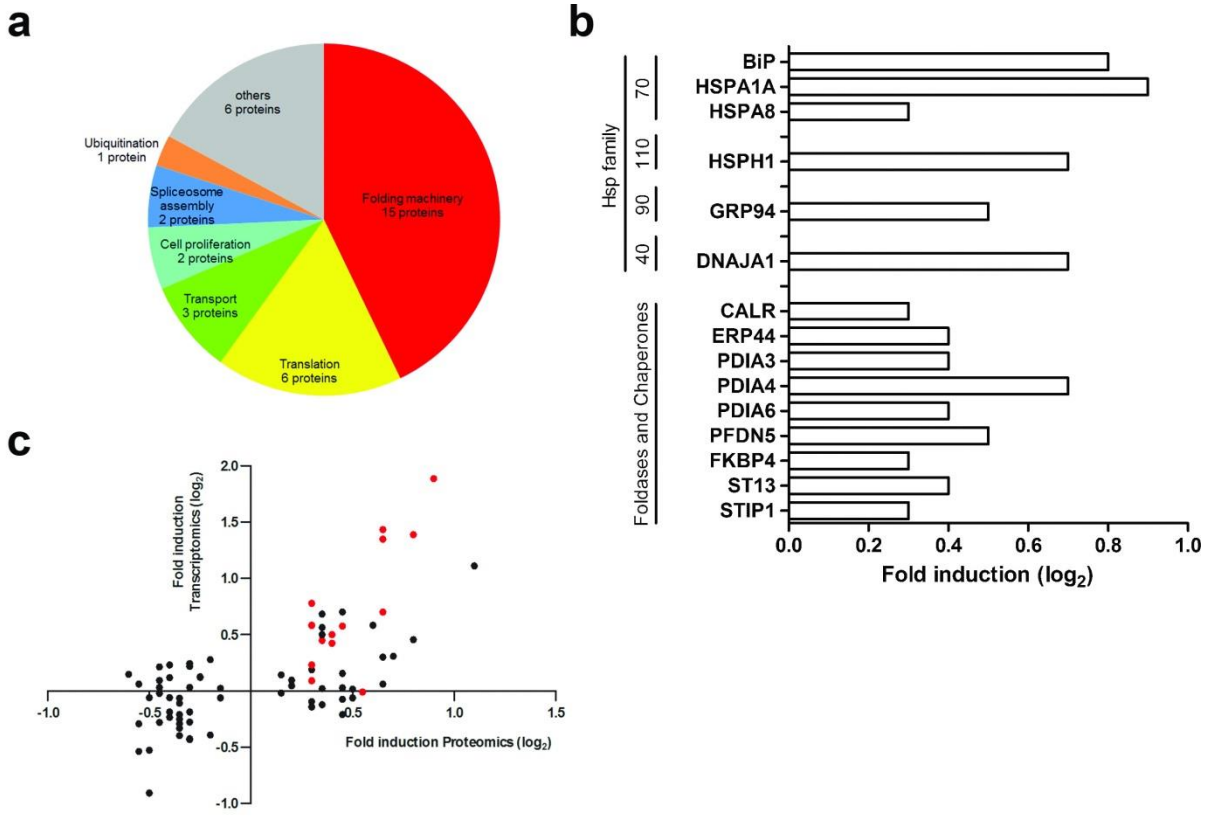

Figure 2 Proteomic analysis of geneticin-treated HEK wild-type cells. (a) Thirty-five upregulated proteins were grouped according to their biological function (Bonferroni corrected p-value < 0.05, $\log_2$ FC > 0.3). (b) Upregulation of the geneticin-induced heat-shock proteins, chaperones, and foldases (Bonferroni corrected p-value < 0.05, $\log_2$ FC > 0.3). (c) Comparison of the significantly regulated proteins (Bonferroni corrected p-value < 0.05) and their corresponding mRNA fold-induction. The upregulated proteins of the folding machinery are shown in red.

Aminoglycosides induce the UPR. To corroborate the results of the microarray analysis, mRNA levels of selected UPR genes were further analyzed by quantitative PCR and corresponding protein levels were assessed by Western blotting. Geneticin

and gentamicin induced mRNA expression of C/EBP homologous protein (CHOP), GRP94, and BiP in a time-dependent manner (Figure 3a–c). Increased protein levels of the two ER chaperones BiP and GRP94 as well as the transcription factor ATF4, which is regulated at the translational level,[41] were observed in geneticin- and gentamicin-treated cells by Western blotting (Figure 3e). As a further element of the UPR, we studied splicing of XBP1 mRNA, which is central for UPR activation[11]. Both geneticin and gentamicin induced XBP1 splicing (Figure 3d). In contrast, XBP1 splicing is induced neither by the non-misreading aminoglycoside hygromycin[42] nor by cycloheximide, an inhibitor of ribosomal translocation,[43] indicating that XBP1 splicing depends on misreading and not on inhibition of translation. Furthermore, the presence of APH(3‘) in HEK cells abrogated geneticin-induced but not gentamicin-induced XBP1 splicing.

The activity of transcription factors XBP1 and ATF6 was examined using reporter plasmids UPRE (p5xATF6-GL3-luc) and ERSE (pGL3-GRP78P(-132)-luc).[44,45] The UPRE reporter is specific for ATF6 activity, the ERSE reporter is regulated by both ATF6 and XBP1.[44,45] Both reporters showed a robust induction by geneticin and gentamicin (Figure 3f and g). Cycloheximide failed to induce any reporter activity consistent with the XBP1 splicing results (Figure 3d, 3f, 3e). The PERK signaling branch was investigated by assessing the formation of stress granules, cytosolic protein aggregates composed of 48S preinitiation complexes and other factors. Stress granules are induced upon activation of PERK and phosphorylation of eIF2α.[46] Treatment of HEK wild-type cells with geneticin for 24 h increased immunostaining of p-eIF2α in a dotted cytosolic distribution indicative of stress granules (Figure 3h). Arsenite treatment served as a positive control. A similar robust induction of UPR by aminoglycosides was observed in Hela cells (Figure S3).

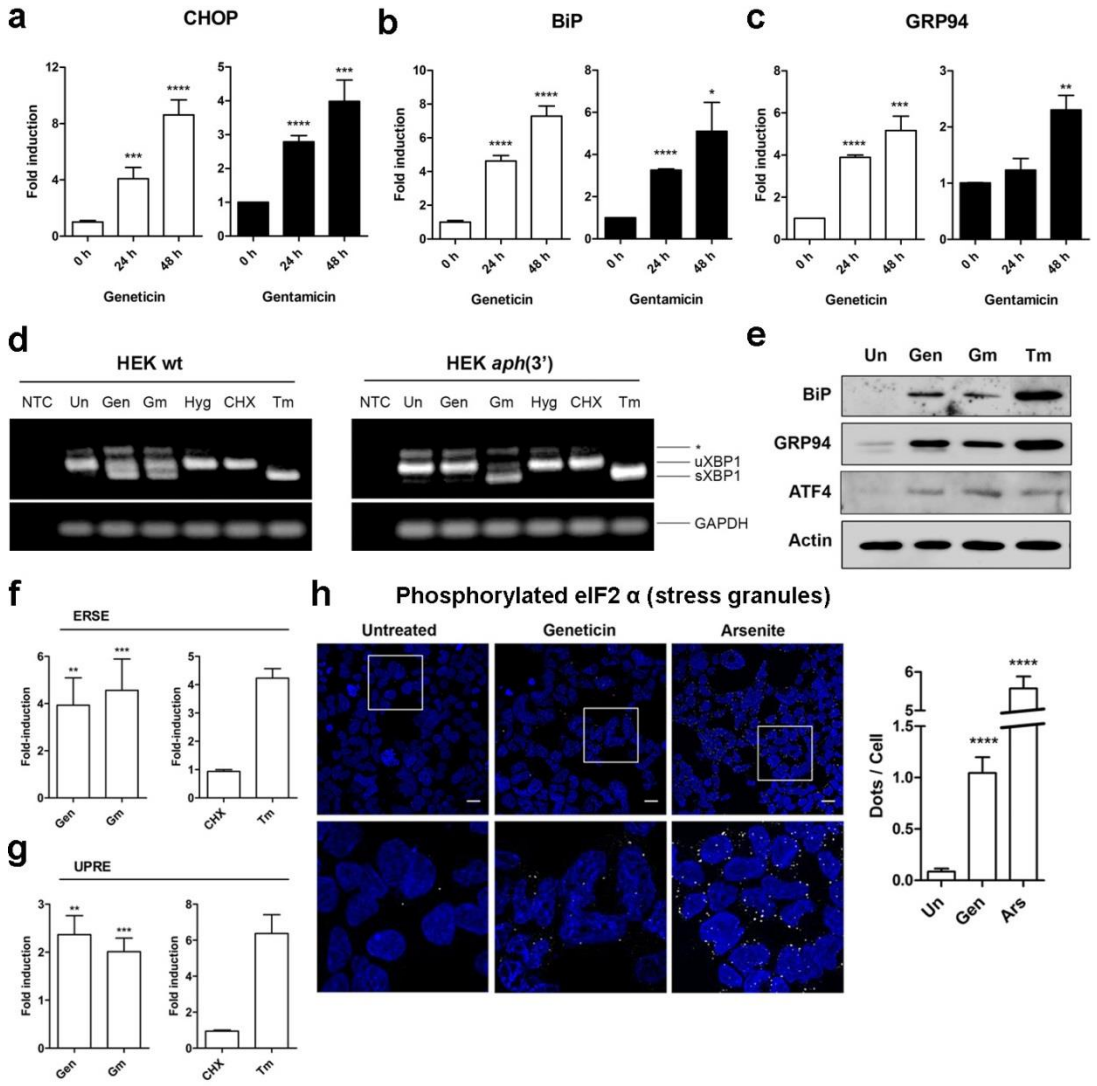

Figure 3 Aminoglycosides induce the UPR. (**a–c**) qPCR analysis. HEK wild-type cells were treated with geneticin (16 µM) or gentamicin (400 µM) and incubated for the indicated times. Expression of CHOP (**a**), BiP (**b**), and GRP94 (**c**) mRNA is shown. Three biological replicates were each run in triplicate assays and means + SD of fold induction relative to 0 h (untreated) sample are presented; **P*<0.05; ***P*<0.01; ****P*< 0.005; *****P*<0.001. (**d**) XBP1 splicing assay. HEK wild-type or HEK *aph*(3') cells were treated with geneticin (16 µM), gentamicin (1250 µM), hygromycin (2 µM), cycloheximide (2 µM), tunicamycin (5 µg/mL) for 24 h or left untreated. NTC: no template control. Products of XBP1 PCR were analyzed by gel electrophoresis; unspliced and spliced versions of XBP1 are indicated. Tunicamycin was a positive control to induce ER stress; GAPDH was a loading control. The asterisk indicates the position of a hybrid amplicon (ref 15). (**e**) Western blot analysis. HEK wild-type cells were treated with geneticin (16 µM) or gentamicin (400 µM) and incubated for 24 h. 10 µg of total protein were loaded and BiP, GRP94 and ATF4 were detected by immunoblotting using specific antibodies. β-actin was used as a loading control. Tunicamycin (2.5 µg/mL) was used as a positive control. (**f-g**) Reporter assays. HEK cells were transfected with luciferase reporter plasmids (**f**) UPRE (reporter for ATF6 activity) or (**g**) ERSE (reporter for ATF6 and XBP1 activity). Cells were treated with geneticin (16 µM) or gentamicin (800 µM) for 24 h. Cycloheximide (16 µM) was used as a negative control, tunicamycin (2.5 µg/mL) was used as a positive control for UPR. Luciferase activities were determined and the Fluc/Rluc ratios were calculated. Untreated samples are set as 1 and fold inductions are given (n = 3-6, ± SEM). **P<0.01, ***P<0.005. (**h**) Stress granule formation. HEK wild-type cells were treated with geneticin (16 µM) for 24 h or arsenite (0.5 mM) for 1 h as a positive control. Phosphorylated eIF2α was detected by immunofluorescence. Scale bars: 40 µm. The lower panels show insets in higher magnification. Bar graph indicates quantification of peIF2α immunofluorescence (n number of cells; $n_{untreated}$ = 540; $n_{geneticin}$ = 249; $n_{arsenite}$ = 648); *****P*<0.001. Gen: Geneticin; Gm: Gentamicin; Hyg: Hygromycin; Tm: Tunicamycin; CHX: Cycloheximide; Ars: Arsenite; Un: Untreated.

Gentamicin induces ER stress in spiral ganglion cells but not in auditory hair cells. To study the response of auditory hair cells to ER stress, we first employed tunicamycin, an established ER stress-inducer in early post-natal cochlear explants of the CBA/J mouse, a common strain for auditory research. Preliminary experiments (data not shown) with hair cell counts on surface preparations had established incubation with 0.07 µg/mL tunicamycin as a suitable treatment with hair cell death beginning at 48 h and progressing to 50% of cells by 72 h. The ER-stress-associated pro-apoptotic factor CHOP already appeared after 8 h of incubation with tunicamycin and was expressed in the nuclei of most hair cells by 24 h (Figure 4a and Supplementary Figure S4). Staining mostly had disappeared at 48 h (Supplementary Figure S4) when loss of hair cells became apparent, implicating CHOP in hair cell death. In the same explant model, treatment with gentamicin caused significant loss of hair cells with the pattern of loss showing the typical progression of aminoglycoside damage[47] with most destruction in the base (Supplementary Figure S5) while inner hair cells were mostly spared. Despite continuing and increasing cell death, CHOP was not observed throughout the entire time course up to 72 h (Figure 4a).

The response of ganglion neurons to ER stress was studied in spiral ganglion cells (SGCs) that were harvested from the base to the middle of the modiolus of cochlear explants and similarly treated with tunicamycin or gentamicin (Figure 4b). As expected from its activity as an ER stressor, tunicamycin induced CHOP in the nuclei of SGCs within 24 h. In contrast to its effect on hair cells, gentamicin increased the immunoreactivity to CHOP in SGCs, evident after 48 h of incubation.

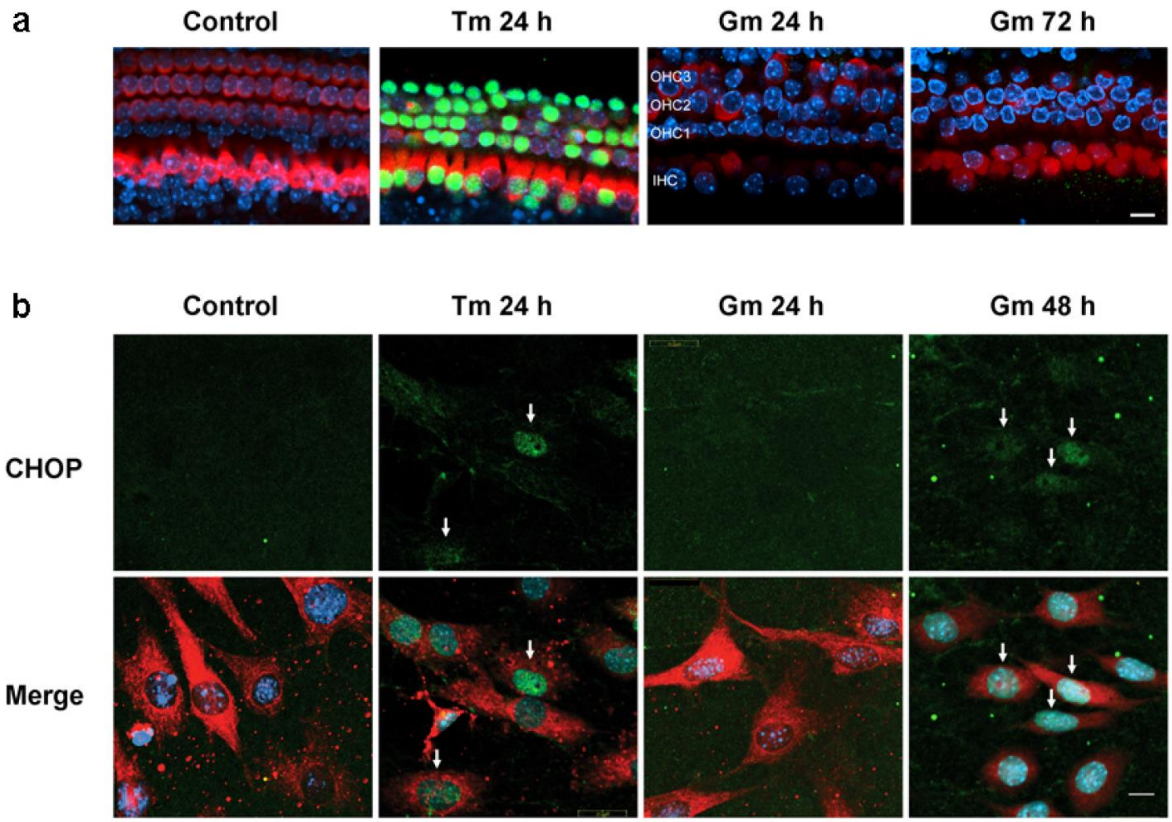

Figure 4 ER stress in cochlear tissues. (a) Tunicamycin but not gentamicin causes ER stress in hair cells. Tunicamycin (0.07 µg/mL) induced the specific ER stress-associated pro-apoptotic factor, CHOP (green), in the nuclei of hair cells in organ of Corti explants by 24 h but was not observed in any part of the organ of Corti throughout the entire time course of gentamicin treatment (3.5 µM) until hair cell death. Segments shown are from the basal turn. Green: CHOP, red: Myo 7a, blue: Hoechst 33342 staining for nuclei. The figure represents three different explants at each time point; focal plane is the nuclear level of outer hair cells. Scale bar (Gm): 10 µm. (b) Gentamicin induces ER stress in spiral ganglion cells (SGCs). Tunicamycin (0.07 µg/mL) treatment for 24 h induced CHOP in the nuclei of SGCs (arrows). With gentamicin (3.5 µM) treatment, CHOP appeared in the nuclei of SGCs by 48 h (arrows). Green: CHOP, red: neuronal class III β-tubulin staining for SGCs, blue: Hoechst 33342 staining for nuclei. The figure represents three different explants at each time point. Scale bar, 10 µm.

Gentamicin reduces spiral ganglion cells and synaptic ribbons but not hair cells in XBP1$^{+/-}$ mice *in vivo*. In wild-type strains such as the CBA/J mouse, the OHCs are the primary target of chronic aminoglycoside ototoxicity *in* and very little direct effect—if any—can be observed on SGCs. In view of the modest but significant gentamicin-induced CHOP expression in SGCs of cochlear explants, we investigated potential gentamicin-induced ER stress in a model of compromised UPR, an XBP1-haploinsufficient mouse. The local route of drug administration to the middle ear, chosen for this study, is able to isolate effects to the auditory periphery while avoiding

adverse complications associated with systemic gentamicin treatment in the mouse.[30]

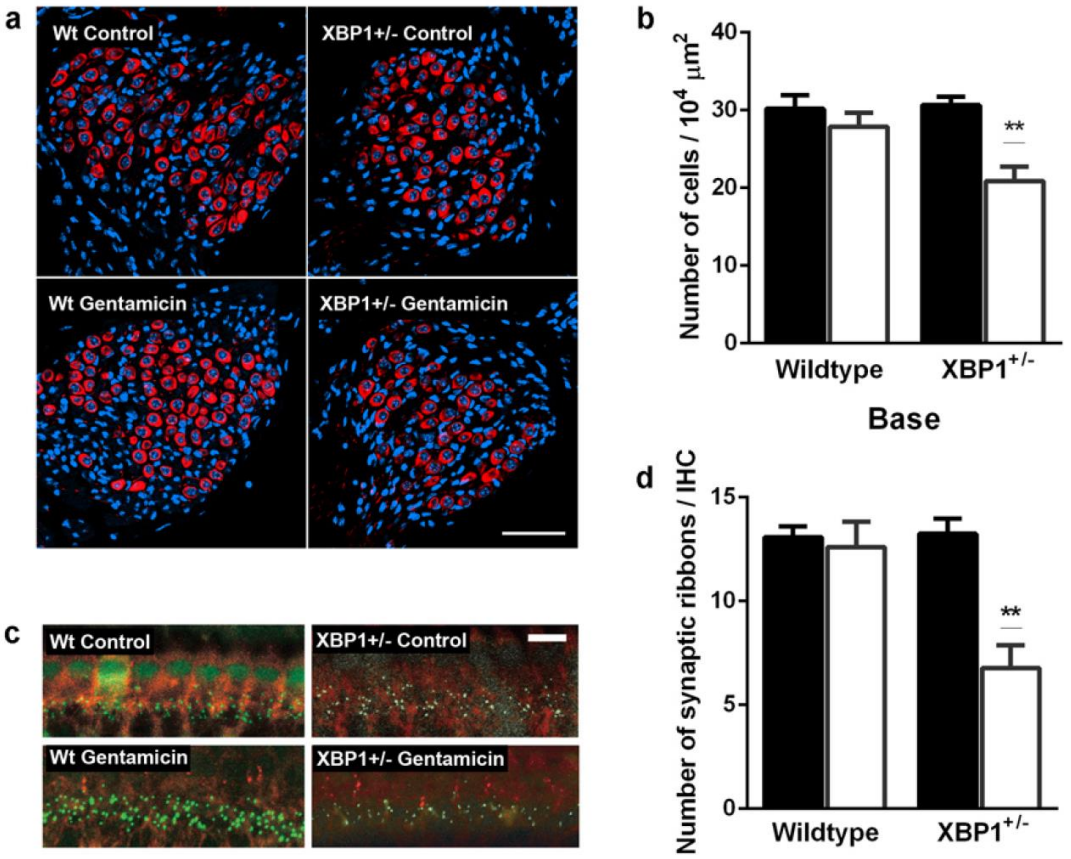

Figure 5 Gentamicin reduces the number of SGCs and IHC synapses in XBP1$^{+/-}$ mice. Gentamicin (0.56 M) was locally injected into the middle ear through the bulla as described in the Methods section "Drug administration *in vivo*." (a,b) Gentamicin reduces SGCs in XBP1$^{+/-}$ but not in wild-type (XBP1$^{+/+}$) littermates. (a) The number of SGCs was counted from high-magnification images of Rosenthal's canal of saline- and gentamicin-injected wild-type and XBP1$^{+/-}$ mice. Red: neuronal class III β-tubulin staining for neural cells, blue: Hoechst 33342 staining for nuclei. The figure represents five different animals at each condition. Scale bar: 50 µm. (b) Quantitative evaluation revealed that SGC density in the basal turn of XBP1$^{+/-}$ mice but not in wildtype mice was significantly decreased by gentamicin. Filled bars, controls; open bars, gentamicin treatment. n = 5 in each group; $^{**}P<0.01$. Middle and apical turns were not affected. (c,d) Gentamicin reduces synaptic ribbons in XBP1$^{+/-}$ but not in wild-type mice. (c) Hair cells were stained with anti-Myo7 antibodies (red) and synaptic ribbons with antibodies to CtBP2 (green). The number of synaptic ribbons per IHC in the basal turn was quantified from 3-D images created by using Imaris software. Staining of some nuclei is consistent with a partial nuclear localization of this protein,[66] which has also been confirmed for IHCs.[67] The figure represents three different animals at each condition. Scale bar: 20 µm. (d) Quantitative evaluation demonstrated that synaptic ribbon density of XBP1$^{+/-}$ mice but not of wildtype littermates was diminished by local injection of gentamicin. Filled bars, controls; open bars, gentamicin treatment. n = 3 in each group; $^{**}P<0.01$

Preliminary experiments with a series of gentamicin concentrations starting at 0.09 M established 0.56 M as a suitable dose that caused a moderate threshold shift while avoiding major pathology (data not shown).

Surface preparations from XBP1$^{+/-}$ and wild-type littermates treated with gentamicin *in vivo* were examined from base to apex three weeks after drug injection. OHCs were present in all parts of the cochlea in both wild-type and XBP1$^{+/-}$ mice except for scattered loss at the very end of the basal turn (Supplementary Figure S5c). Quantitation of hair cell loss along the entire cochlea confirmed only minor damage at the extreme the basal turn with no difference between wild-type and XBP1$^{+/-}$ mice.

In the absence of any discernible defects on hair cell integrity and prompted by the in-vitro results, we then analyzed spiral ganglion density and synaptic connections. Three weeks after gentamicin injection, the SGCs were counted on mid-modiolar cryosections stained for β-tubulin and nuclei. There was a significant reduction in spiral ganglion density in the basal turn of the cochlea in XBP1$^{+/-}$ mice but not in wild-type littermates (Figures 5a and 5b). The innervation of hair cells by the spiral ganglion was assessed by staining synaptic ribbons with antibody to CtBP2, a constituent of the ribbon protein RIBEYE. The number of synaptic ribbons per IHC was reduced by approximately 50% in the basal turn of the cochlea of the XBP1$^{+/-}$ mice but not of corresponding wild-type littermates (Figures 5c and 5d).

Auditory physiology corroborates auditory pathology and ER stress. In order to assess the impact of the observed pathology on auditory function, we measured auditory brain stem responses (ABR) and distortion product otoacoustic emissions (DPOAE). ABR provides information on the ascending auditory pathway reflecting synaptic and neuronal activity, while DPOAE probes the functional integrity of outer hair cells. Deterioration of auditory thresholds was apparent one week after the injection of gentamicin and remained stable for up to three weeks, the latest time point studied (Figure 6a). Large threshold shifts were observed at 32 kHz in XBP1$^{+/-}$ mice but not in wild-type littermates, which were little affected. Consistent with the morphological observations of intact outer hair cells, DPOAE remained unaffected by gentamicin treatment (Supplementary Figure S6).

Finally, in order to validate the potential contribution of protein misfolding to the changes in auditory thresholds, we treated animals with TUDCA, a clinically used

chemical chaperone. Systemic TUDCA co-administration significantly attenuated gentamicin-induced ototoxicity in the XBP1$^{+/-}$ mice (Figure 6b) as measured by ABR three weeks after the drug treatment.

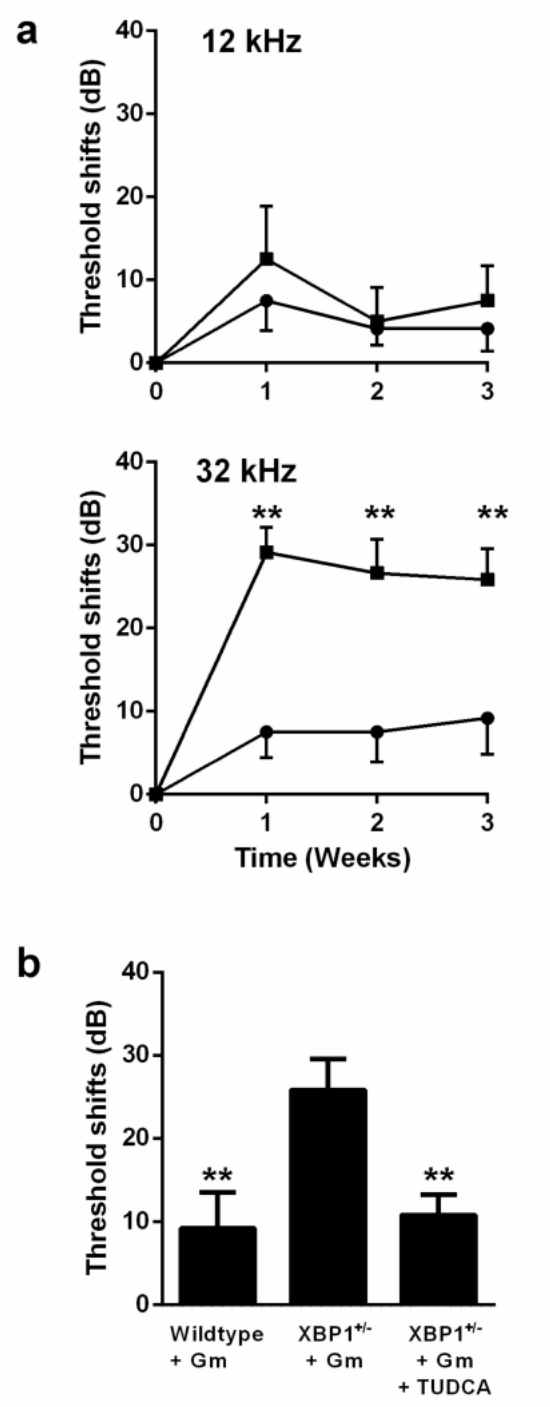

Figure 6 Auditory threshold shifts induced by gentamicin. (a) Gentamicin (0.56 M) was locally injected into the middle ear through the bulla as described in 'Methods'. Three weeks after treatment, large threshold shifts had developed at 32 kHz in XBP1$^{+/-}$ mice (square symbols) but not in wild-type littermates (circles). Data are presented as mean + SD for XBP1$^{+/-}$ mice and mean - SD for wild-types. *n* = 6 in each group; ***P*<0.01. (b) TUDCA attenuates gentamicin ototoxicity in XBP1$^{+/-}$ mice. Animals in all three groups received the local injection of gentamicin and, as indicated, TUDCA co-treatment (500 mg/kg i.p. at 6 d, 3 d, and 3 h before gentamicin injection). Data are presented as means + SD of threshold shifts at 32 kHz, determined three weeks after treatment. *n* = 6 in each; ***P*<0.01

Discussion

Aminoglycoside-induced loss of translational fidelity in eukaryotes is evident from our experiments on HEK293 cells and, moreover, is clearly linked to the ribosomal activity of the drugs. We have primarily chosen HEK293 cells for study as these cells are readily transfected, facilitating the use of reporter constructs to study drug-induced misreading.[49] However, we have obtained similar results in human Hela cells. The known misreading-inducers geneticin and gentamicin, but not hygromycin or cycloheximide, elicit a UPR. Gentamicin was selected as a classical clinical aminoglycoside to bridge the findings from our *in-vitro* studies to the animal model. Geneticin was included because its inactivation by the APH(3‘) enzyme allowed to control for the specificity of drug action.[39] Modification of geneticin by APH(3‘) (which abrogates its anti-ribosomal activity by phosphorylation of the 3‘ OH group) eliminates the ability of geneticin to cause both misreading and ER stress. In contrast, APH(3‘) did not affect the misreading activity of gentamicin, which lacks the 3‘ OH group and thus is not a target for APH(3‘). The finding that the cell viability and the metabolic activity of HEK wild-type cells remain intact despite drug-induced mistranslation attests to the protective efficacy of cellular homeostatic responses such as the UPR and allows us to extrapolate that the UPR, at least in part, mitigates mistranslation induced by aminoglycosides in eukaryotic organisms.

Consistent with this notion, $XBP1^{+/-}$ haploinsufficient mice but not wild-type mice sustain gentamicin-induced loss of SGCs. XBP1 is one of the central components in the three main pathways of the UPR, regulating molecular chaperones and promoting ER-associated degradation.[50] The crucial function of XBP1 for cell survival is indicated by embryonic lethality of homozygous XBP1 knock-out mice.[37] Haploinsufficient mice are viable but are less capable of inducing chaperones and promoting ERAD under ER stress conditions.[51] Consequently, ER stress is prone to damage cells in $XBP1^{+/-}$ but not in wild-type mice.

Oxidative stress is a major factor in the pathomechanism of aminoglycoside ototoxicity,[48] but evidence for an involvement of ER stress has been only indirect or lacking. Upregulation of heat shock proteins protects the mouse cochlea in part from aminoglycoside-induced ototoxicity *in vivo*.[52] However, the ER stress marker m-calpain is unaffected by aminoglycoside treatment in the mouse cochlea *in vivo*.[53] Despite the extensive loss of hair cells that gentamicin can cause in cochlear

explants, no ER stress marker develops there. This is in contrast to their induction with the ER stressor tunicamycin, a finding consistent with previous observations of tunicamycin-induced hearing loss in the rat.[54] Further distinguishing the pathological effects of the two drugs, the damage caused by tunicamycin broadly encompasses all regions of the cochlea while the pattern of gentamicin-induced damage in the explants follows the base-to-apex gradient characteristic of aminoglycosides.[48]

Our results clarify that aminoglycoside-induced ER stress in the cochlea is limited to neurons of the spiral ganglion. In the *in-vivo* model, the local application of a single low dose of gentamicin does not lead to hair cell death. However, spiral ganglion cells were significantly reduced in the base of the cochlea, corroborating the *in-vitro* results on ER stress in the nerve but not in hair cells. Gentamicin-induced ER stress has also been observed in rat kidneys *in vivo* as part of its nephrotoxic actions,[55] a result in agreement with our findings that aminoglycosides are capable of inducing ER stress in mammalian tissues. In accord with a gentamicin-reduced density of spiral ganglion cells, synaptic connections to hair cells are lost, providing an explanation for the observed high-frequency hearing loss.

The selective actions of gentamicin on spiral ganglion cells and synapses suggest a heightened sensitivity to neurodegeneration in the XBP1$^{+/-}$ haploinsufficient mice in contrast to the more common pathology of hair cell loss. It is interesting in this context that a loss of afferent nerve terminals and subsequent degeneration of the cochlear nerve has also been observed after moderate noise exposure that leaves the sensory cells intact.[56]

On a mechanistic level, disruption of translational fidelity causes protein misfolding and aggregation. The ability of XBP1 to maintain cell integrity upon drug-induced mistranslation appears to be mediated by induction of ER chaperones such as BiP, which we also find to be upregulated in response to aminoglycoside challenge. On an organismal level, protein misfolding has been associated with a variety of disorders collectively termed conformational diseases.[57] Presumably, cell-type specific differences in the buffering capacity of the proteostasis network account for the cell- or organ-selectivity in some of these diseases.[58] Aminoglycoside-induced death of hair cells has previously been associated with inhibition of host-cell protein synthesis[47,59] and oxidative stress.[48] The hypothesis presented here that aminoglycoside-induced loss of SGCs in XBP1$^{+/-}$ haploinsufficient mice is conferred

by the drug‘s misreading activity is supported by the observation that administration of a chemical chaperone significantly alleviated the hearing loss. Specifically, we postulate that the UPR is normally able to maintain a protein folding equilibrium in the presence of aminoglycoside-induced mistranslation in SGCs. However, when the UPR system is compromised, e.g. by genetic haploinsufficiency of XBP1, aminoglycoside-induced mistranslation can manifest as neuropathology.

EXPERIMENTAL PROCEDURES

Materials and sources. Monoclonal anti-GADD 153 antibody, Santa Cruz Biotechnology (Dallas, TX, USA); polyclonal antibody against neuronal class III β-Tubulin, Covance (Princeton, NJ, USA); monoclonal anti-CtBP2 antibody, BD Biosciences (San Jose, CA, USA); polyclonal antibody against p-eIF2α, Cell Signaling (Danvers, MA, USA); polyclonal anti-myosin7a antibody (Proteus Biosciences, Ramona, CA, USA); secondary goat anti-rabbit antibody conjugated with Texas Red, Abcam (Cambridge, MA, USA); rhodamine phalloidin, Invitrogen (Life Technologies, Carlsbad, CA, USA); HEK293 cells, Innoprot (Biscay, Spain); geneticin, gentamicin, tunicamycin, cycloheximide, arsenite, saponin, and HEK *aph*(3') cells, Sigma Aldrich (St. Louis, MO, USA); hygromycin, PAA Laboratories (Cansera, Canada); nucleotide primers, Microsynth (Balgach, Switzerland); cell culture media and trypsin, Life Technologies (Carlsbad, CA, USA).

Assessment of mistranslation. Misreading and stop-codon read-through were assessed in gain-of-function dual luciferase assays.[60,61] For translation in rabbit reticulocyte lysates (RRL, Promega, Madison, WI, USA), luciferase mRNA was produced *in vitro* using T7 RNA polymerase (Thermo Scientific, Waltham, MA, USA) and plasmids pGL4.14 (firefly luciferase, hFluc) and pGL4.75 (renilla luciferase, hRluc; both from Promega), where the mammalian promoter was replaced by the T7 bacteriophage promoter. For misreading, we replaced residue His245 (CAC codon) with Arg245 (CGC near-cognate) in the hFluc protein by site-directed mutagenesis. Read-through was assessed with a fusion construct in which hRluc and hFluc were fused by a 27-nucleotide linker encoding the polypeptide STCDQPFGF, using overlap PCR mutagenesis to result in the pT7 hRluc-hFluc vector; a UGA nonsense-codon was introduced at the glutamine residue (wild-type CAA) of the linker sequence by site-directed PCR mutagenesis. A cell-free luciferase translation assay was performed as described.[51] Mistranslation in HEK cells was determined using the pRM hRluc-hFluc H245R vector, where His245 (CAC codon) was replaced by Arg245 (CGC codon) in the pRM hRluc-hFluc vector. Read-through was determined by pRM hRluc-hFluc D357X, where Asp357 (GAC codon) was replaced by a UGA nonsense-codon in the firefly luciferase transcript. Both constructs were designed by site-directed PCR mutagenesis. HEK wild-type cells were transfected with reporter plasmid using TurboFect (Fermentas) according to the manufacturer's protocol. After

a 24-h incubation, medium was replaced by F10 with 15 µg/mL saponin. Aminoglycoside antibiotics were added and cells were incubated for another 24 h. Cells were lysed and luciferase activities determined; hRluc mRNA was used as an internal control and misreading and read-through were quantified by calculating mutant firefly/renilla activities. The basal error frequency of the eukaryotic ribosome is 4 x 10^{-4} to 10^{-5}.[62] For each set of replicates, the hFluc/hRluc ratio of the untreated samples were set as 1, which reflects this basal error frequency. Luminescence was measured in a luminometer FLx800 (Bio-Tek Instruments, Winooski, VT).

Viability assay. HEK cells were grown to 70% confluence and treated with 16 µM geneticin or 400 µM gentamicin in F10 medium with 15 µg/mL saponin for the indicated time. Ten-percent Alamar Blue solution was added (v/v) for 3 h and fluorescence was monitored at 530 nm for excitation and 590 nm for emission. The fluorescence level of the control sample (untreated) was set as 100% after subtraction of background fluorescence, measured in cell-free wells.

Sytox dead cell stain. HEK cells were grown to 60% confluence in DMEM with 10% FBS. Medium was changed to F10 with 15 µg/mL saponin and aminoglycoside antibiotics were added and cells were incubated for 24 h or 48 h. Cells were detached by adding 100 µL accutase (Life Technologies) and were resuspended in 400 µL FACS buffer (1x PBS, 2% FBS) and transferred to FACS tubes. Sytox Red (Life Technologies) was added to the cell suspension. The nucleic acid stain penetrates cells with compromised plasma membranes but will not cross uncompromised cell membranes. The samples were then analyzed with a BD FACS Canto II and the FlowJo data analysis software.

Microarray analysis. See legend to Supplemental Figure S2.

Proteome analysis. Cell samples were incubated with lysis buffer (150 mM NaCl, 0.1% SDS, 0.5% Na-deoxycholate, 50 mM Tris pH 7.5, and 1× complete protease inhibitor (Roche)) for 10 min at RT on a shaking mixer. The lysate was ultrasonicated for 10 min and centrifuged for 20 min at 16,000 × *g* at 4 °C. Eighty micrograms of protein of each sample were used for iTRAQ labeling (AB SCIEX).

Each iTRAQ 4-plex experiment was carried out with two biological replicates of untreated HEK wild-type cells (114 and 116 label) and two biological replicates of cells treated with 16 µM geneticin for 32 h (115 and 117 label) following the

manufacturer's protocol. iTRAQ samples were pooled, dried, reconstituted in solvent A (5% ACN, 8 mM KH_2PO_4, pH 4.5), and fractionated by HILIC-HPLC (Pack Polyamine II, 250 × 4 mm, 120 Å S-5 µm, YMC). The column was equilibrated with solvent A. Peptides were eluted using solvent B (5% ACN, 100 mM KH_2PO_4, pH 4.5) by a gradient of: 0–7.5 min, 0% B; 7.5–37.5 min, 0–50% B; 37.5–42.5 min, 50–100% B; 42.5–47.5 min, 100% B at a flow rate of 0.4 mL/min. The resulting 13 fractions were desalted using ZipTips (Millipore) according to the manufacturer's protocol and reconstituted in solvent C (3% ACN and 0.1% formic acid) for LC-MS/MS analysis. Samples were auto-injected into an Eksigent-nano-HPLC system and separated on a custom reverse phase tip column (75 µm × 150 mm) packed with C_{18} material (3 µm, 200 Å, AQ, Bischoff GmbH). The column was equilibrated with solvent C and 5% solvent D (0.2% FA in ACN). For elution, a flow rate of 300 nL/min was used and a gradient of 0–70 min, 5–25% D; 70–85 min, 25–50% D; 85–88 min, 50–98% D. High accuracy mass spectra were acquired with an AB SCIEX 5600 mass spectrometer (AB SCIEX) in the range of 385–1250 m/z. Up to 36 data-dependent MS/MS were recorded in high sensitivity mode of the most intense ions with charge states 2+, 3+, and 4+ using collision-induced dissociation. Target ions already selected for MS/MS were dynamically excluded for 90 s after three occurrences. MS/MS data were analyzed using Mascot 2.4 (Matrix Science) and searched against a decoyed human database from Swissprot (release December 2012) concatenated with an in-house build contaminant database. The search parameters were: precursor ion mass tolerance of 20 ppm, fragment ion mass tolerance of 0.05 Da, trypsin digestion, fixed modifications of MMTS-labeled cysteine, 4-plex iTRAQ modifications of free amines at the N-termini and of lysine, and variable modification 4-plex iTRAQ of tyrosine. Peptides without 4-plex iTRAQ labelling at the N-terminus or at a lysine were excluded from the analysis. Scaffold_4.1 (Proteome Software Inc., Portland, OR) was used to validate MS/MS-based peptide and protein identifications. We identified and quantified 1,785 proteins (protein prophet probability 95%, minimum two peptides for identification of a protein, and minimum Mascot Ionscore of 40). After the permutation test and further amendment of the *p*-value with the Bonferroni correction, 77 proteins were found to be regulated (p-value < 0.05). Thirty-five proteins were upregulated based on a threshold of 0.3 ($\log_2$-scale).

XBP1-splicing assay and qPCR. RNA samples from HEK cells were prepared using Trizol extraction (Life Technologies) and were reverse transcribed using a

ThermoScript RT-PCR System (Life Technologies) according to the manufacturer‘s instructions. The XBP1 splicing assay employed XBP1-specific primers that amplify spliced (-26 nt) and unspliced XBP1 mRNA (forward 5‘-TTACGAGAGAAAACTCATGGCC-3’, reverse 5’-GGGTCCAAGTTGTCCAGAATGC-3’). PCR products were analyzed on a 2.7% agarose gel. Amplification of GAPDH cDNA served as loading control. For qPCR the Quantitect SYBR Green PCR Kit (Qiagen) was used together with the 7500 Fast Real-Time PCR System (Applied Biosystems). The primers were CHOP: forward 5‘-GCGCATGAAGGAGAAAGAAC-3‘, reverse 5‘-CCAATTGTTCATGCTTGGTG-3‘; BiP: forward 5‘-TTTCTGCCATGGTTCTCACTAAAA-3‘, reverse 5‘-AACATTTAGGCCAGCAATAGTTCC-3‘; GAPDH: forward 5‘-ACCCACTCCTCCACCTTTGA-3‘, reverse 5‘-CTGTTGCTGTAGCCAAATTCGT-3‘; GRP94 forward 5‘-TGGGAAGAGGTTCCAGAATG-3‘, reverse 5‘-GTTGCCAGACCATCCGTACT-3‘. For relative quantification, GAPDH mRNA served as a reference. Measured quantification cycles were analyzed according to Pfaffl[63], comparing treated with untreated samples. Three biological replicates were run in triplicates each and means and standard deviations were calculated.

Western Blot. HEK cells were grown to 60% confluence in DMEM with 10% FBS. Medium was changed to F10 with 15 µg/mL saponin and aminoglycoside antibiotics were added and cells were incubated for 24 h. Cells were lysed in hypotonic buffer (20 mM HEPES pH 7.5, 10 mM KCl, 3 mM Mg Acetate, 1 mM DTT and 10 µg/ml DNase I) and ultrasonicated. Lysates were centrifuged (13.000 rpm, 10 min) and protein concentration in the supernatant was measured by the Micro BCA Protein Assay Kit (Thermo). Ten µg of total protein were resolved on 10% SDS-polyacrylamide gels and blotted on nitrocellulose membranes, which were probed with specific antibodies. Amersham ECL Prime Western Blotting Detection Reagent (GE Healthcare, RPN2232) was used as a substrate for the horseradish peroxidase (HRP). The specific antibodies used in this study were: anti-BiP antibody (Abcam, ab21685); anti-GRP94 antibody (Abcam, ab87886); anti-ATF4 antibody (Abcam, ab23760); anti-β-actin antibody (Sigma, A1978-200UL); HRP-conjugated goat anti-rabbit (Invitrogen, G-21234) and goat anti-mouse antibodies (Invitrogen, A10551).

UPR reporter assay. Reporter plasmids UPRE (p5xATF6-GL3) and ERSE (pGL3-GRP78P(-132)-luc) carrying luciferase under the control of UPR-specific cis-acting

elements were kind gifts from Kazutoshi Mori (Kyoto University, Japan). HEK cells were grown to 60% confluence and co-transfected with reporter constructs and pGL4.75 (Rluc) using TurboFect reagent (Fermentas) according to the manufacturer's protocol. After a 24-h incubation medium was replaced by F10 with 15 µg/mL saponin. Aminoglycosides were added and cells were incubated for another 24 h. Cells were lysed and luciferase activities determined. Normalization of luciferase activities was performed as described above. Cycloheximide was used as a mistranslation negative control and tunicamycin was used as a positive control for UPR.

P-eIF2α immunofluorescence assay. HEK cells grown on poly-D-lysine (Sigma)-coated cover slips (Thermo Scientific) were treated for 24 h with geneticin in F10 medium with 15 µg/mL saponin, or with arsenite for 1 h (positive control). Cells were then fixed with 4% paraformaldehyde and methanol and incubated with blocking solution (1× PBS with 1% BSA and 0.5% saponin) for 1 h at RT. Immunostaining used a rabbit polyclonal antibody against p-eIF2α (1:250) and a secondary goat anti-rabbit antibody conjugated with Texas Red (1:250) diluted in blocking solution. Cover slips were mounted on glass slides (VWR) using Dapi fluoromount (Southern Biotech), and cells were imaged using a Lyca Sp2 confocal microscope and a 63× objective. p-eIF2α and nuclear signals were quantified using Imaris software (Bitplane) and the dots-per-cell ratio was calculated.

Animals. Male and female CBA/J mice were purchased from Harlan Sprague-Dawley Co. (http://www.harlan.com/products_and_services/research_models_and_services/research_models/cbaj_inbred_mice.hl) at an age of 6–8 weeks and bred in-house in order to obtain pups for organotypic cultures of the post-natal organ of Corti and SGCs (see next section). $XBP1^{+/-}$ mice, originally derived from D3 embryonic stem cells, were from a stock kindly provided by Dr. Laurie H. Glimcher[31] and received via Dr. Randal J. Kaufman, University of Michigan. Littermates served as wild-type ($XBP1^{+/+}$) controls. Animals were kept on a 12-h light/12-h dark cycle with free access to water and diet (Purina 5001) and used in the *in-vivo* studies at an age of 3–4 months. Experimental protocols were approved by the University of Michigan Committee on the Use and Care of Animals and animal care was under the supervision of the University of Michigan's Unit for Laboratory Animal Medicine.

Organotypic cultures of post-natal organ of Corti and spiral ganglion cells. The procedures were as described previously.[64] Mice at post-natal day 2–3 (p2–3) were euthanized and cochleae dissected in cold Hank's Balanced Salt Solution to isolate the organ of Corti; spiral ganglion cells (SGCs) were dissected from the base to the middle of the modiolus. Explants were placed onto a culture dish in 2 mL of medium consisting of Basal Medium Eagle, 1% serum-free supplement (Gibco #51500-056, Life Technologies), 1% bovine serum albumin, 5 mg/mL glucose and 10 U/mL penicillin G, allowed to settle for 4 h (37 °C, 5% CO_2) and incubated for 2 d to mitigate dissection stress. Medium was then exchanged for new media with or without drugs and incubation continued. For immunofluorescent labeling, explants were fixed with 4% paraformaldehyde overnight at 4 °C and permeabilized for 30 min with 3% Triton X-100 in phosphate buffered saline (PBS) at room temperature. After three washes with PBS and blocking with 10% goat serum for 30 min at RT, incubation with the primary antibodies followed at 4 °C for 72 h. After three washes with PBS, secondary antibodies were applied (Alexa Fluor 488-conjugated goat anti-mouse and Alexa Fluor 546-conjugated goat anti-rabbit antibody; 1:200 in PBS) at 4 °C overnight in darkness. After several rinses, specimens were mounted on a slide with Prolong Gold anti-fade reagent (Life Technologies) and imaged with an Olympus Fluoview Confocal Laser Scanning Microscope-FV500 (Olympus America, Center Valley, PA). For staining of hair cells, specimens were incubated at RT with rhodamine phalloidin (1:100) for 1 h; or for staining of nuclei with Hoechst 33342 (2 µg/mL in PBS) for 40 min. Presence or absence of OHCs and IHCs was determined on a Leitz Orthoplan microscope (Leica, Wetzlar, Germany) whose right objective had a 0.19-mm scale imposed on the field. Successive 0.19-mm fields were evaluated beginning at the apex by observers blinded to the experimental conditions. Cell counts were compared to a normative database (KHRI Cytocochleogram, version 3.0.6, Kresge Hearing Research Institute, University of Michigan, Ann Arbor, MI, USA).

Drug administration *in vivo*. Gentamicin was locally delivered as previously described.[65] Mice were anesthetized with an intra-peritoneal injection of xylazine (7 mg/kg) and ketamine (90 mg/kg) and body temperature was maintained. The temporal bone was approached via a retro-auricular incision and a small hole was made in the thin part of the bulla with a 30-G needle. Surgical tubing was inserted through the hole, and 10 µL of 0.56 M gentamicin dissolved in saline was slowly

injected. The skin incision was closed with tissue adhesive. TUDCA (Calbiochem, EMD Millipore, Billerica, MA, USA) was dissolved in 0.15 M $NaHCO_3$ (adjusted to pH 7.4) and injected subcutaneously at 500 mg/kg body weight 6 d, 3 d, and 3 h before gentamicin administration. Injections of 0.15 M $NaHCO_3$ served as vehicle controls. Injection of TUDCA did not cause any apparent side effects.

Hair cell counts in adult mice. Three weeks after injections, cochleae were fixed as described above. The apical bony capsule was removed and the cochlea decalcified in 4% sodium EDTA (adjusted to pH 7.4) for 7 d at 4 °C. Subsequently, cochleae were dissected into apical, middle, and basal segments. Segments were permeabilized in 3% Triton X-100 for 30 min at room temperature, washed three times with PBS, and incubated with rhodamine phalloidin (1:100) at room temperature for 1 h. The procedures for cell counting were the same as for explants.

Quantification of spiral ganglion cells and synaptic ribbons. Following decalcification with 4% EDTA, cochleae were cryo-sectioned. Sections of 8 µm thickness were incubated in 0.3% Triton X-100 in PBS for 30 min at room temperature, blocked with 10% goat serum for 30 min, followed by incubation with anti-neuronal class III β-Tubulin antibody (1:2,000) for 48 h at 4 °C. After three rinses in PBS, sections were incubated with a secondary antibody (Alexa Fluor 546-conjugated; 1:500) at 4 °C overnight in darkness. After three washes with PBS, sections were stained with Hoechst 33342 (2 µg/mL in PBS) for 40 min at room temperature. After a final wash, the slides were mounted with Prolong Gold anti-fade reagent. Controls were processed without primary antibody. The number of SGCs in Rosenthal's canal was quantified using ImageJ software (National Institutes of Health, Bethesda, MD) by counting the β-tubulin- and Hoechst-positive cells on images taken with an Olympus laser confocal microscope. Two mid-modiolar sections, separated by 40 to 50 µm, were used to obtain the average for each animal. For synaptic ribbon counts, cryo-sections were incubated for 30 min at room temperature with 5% donkey serum in PBS with 0.3% Triton X-100 and overnight in darkness at 4 °C with antibodies against CtBP2 (1:200) and Myo7a (1:200). After three washes in PBS (15 min each), tissues were incubated with secondary antibodies (Alexa Fluor 488- and Alexa Fluor 546-conjugated; 1:1,000) at room temperature for 1 h. After three washes, the epithelia were mounted and images taken on an Olympus laser confocal microscope. Images were reconstructed 3-

dimensionally using Imaris software (Bitplane). The number of synaptic ribbons was quantified per IHC based on an average of 14 IHCs per sample.

Auditory function measurements. For auditory brainstem responses (ABR), animals were anesthetized with an intra-peritoneal injection of xylazine (7 mg/kg), ketamine (65 mg/kg), and acepromazine (2 mg/kg), and placed in a sound-isolated and electrically shielded booth (Acoustic Systems, Austin, TX, USA). Body temperature was maintained near 37 °C with a heating pad. Acoustic stimuli were delivered monaurally to a Beyer earphone attached to a speculum inserted into the left ear canal. Sub-dermal electrodes were inserted at the vertex of the skull, under the left ear, and under the right ear (ground). ABRs were measured at 12 kHz and 32 kHz using Tucker Davis Technology (TDT) System III hardware and SigGen/Biosig software to present the stimuli (15 ms tone bursts, 1 ms rise-fall time) and record up to 1024 responses for each stimulus level. Thresholds were determined by reducing the intensity in 10-dB increments and then in 5-dB steps until no organized responses were detected. Threshold shifts were calculated for individual animals as the difference in auditory thresholds between ABR measurements before and at the end of the studies. For the DPOAE procedure, see the legend to Supplementary Figure S6.

Statistical analysis. Data were evaluated by one-way ANOVA followed by Tukey's Honestly Significant Difference tests using JMP version 8.0.1 (SAS Institute Inc.) or Student's t-test. All tests were two-sided with significance set at $P<0.05$.

Conflict of Interest. The authors declare no conflicts of interest.

Acknowledgements. The data discussed in this publication have been deposited in NCBI's Gene Expression Omnibus and are accessible through GEO Series accession number GSE57198 (http://www.ncbi.nlm.nih.gov/geo/query/acc.cgi?acc=GSE57198).

The mass spectrometry proteomics data have been deposited to the ProteomeXchange Consortium via the PRIDE partner repository with the dataset identifier PXD000933 and DOI 10.6019/PXD000933.

We thank Ariane Kanicki and the Histology Core at KHRI for valuable help with cochlear histology. We thank Christian Trachsel, Jonas Grossman and Claudia Fortes from the FGCZ proteomics team for technical help and advice, and Christele Thibault and Doulaye Dembele from the Microarray and Sequencing Platform of the IGBMC, Illkirch, France, for help with the microarray analysis.

The project was supported by grant R01 DC-003685 and core grant P30 DC-05188 from the National Institute on Deafness and Other Communication Disorders, National Institutes of Health to JS.

Author contributions: JS, NO, and ECB designed the study. All authors discussed the data. NO, SD, HB, JS, and ECB wrote the paper with input from all authors.

Personal contributions: SD performed the mistranslation assays, conducted the iTRAQ experiment, interpreted the proteome data and executed with HB the XBP1 splicing assay and the Western Blots.

References

1. Drummond DA, Wilke CO. Mistranslation-induced protein misfolding as a dominant constraint on coding-sequence evolution. *Cell* 2008; **134:** 341-352.

2. Goltermann L, Good L, Bentin T. Chaperonins fight aminoglycoside-induced protein misfolding and promote short-term tolerance in Escherichia coli. *J Biol Chem* 2013; **288**:10483-10489.

3. Prostko CR, Brostrom MA, Malara EM, Brostrom CO. Phosphorylation of eukaryotic initiation factor (eIF) 2 alpha and inhibition of eIF-2B in GH3 pituitary cells by perturbants of early protein processing that induce GRP78. *J Biol Chem* 1992; **267:** 16751-16754.

4. Shi Y, Vattem KM, Sood R, An J, Liang J, Stramm L*, et al.* Identification and characterization of pancreatic eukaryotic initiation factor 2 alpha-subunit kinase, PEK, involved in translational control. *Mol Cell Biol* 1998; **18:** 7499-7509.

5. Tirasophon W, Welihinda AA, Kaufman RJ. A stress response pathway from the endoplasmic reticulum to the nucleus requires a novel bifunctional protein kinase/endoribonuclease (Ire1p) in mammalian cells. *Genes Dev* 1998; **12:** 1812-1824.

6. Haze K, Yoshida H, Yanagi H, Yura T, Mori K. Mammalian transcription factor ATF6 is synthesized as a transmembrane protein and activated by proteolysis in response to endoplasmic reticulum stress. *Mol Biol Cell*. 1999; **10**: 3787-3799.

7. Yoshida H, Okada T, Haze K, Yanagi H, Yura T, Negishi M*, et al.* ATF6 activated by proteolysis binds in the presence of NF-Y (CBF) directly to the cis-acting element responsible for the mammalian unfolded protein response. *Mol Cell Biol* 2000; **20:** 6755-6767.

8. Shen J, Chen X, Hendershot L, Prywes R. ER stress regulation of ATF6 localization by dissociation of BiP/GRP78 binding and unmasking of Golgi localization signals. *Dev Cell.* 2002; **3**: 99-111.

9. Bertolotti A1, Zhang Y, Hendershot LM, Harding HP, Ron D. Dynamic interaction of BiP and ER stress transducers in the unfolded-protein response. *Nat Cell Biol*. 2000; **2**: 326-32.

10. Schroder M, Kaufman RJ. The mammalian unfolded protein response. *Annu Rev Biochem* 2005; **74:** 739-789.

11. Zhang K, Kaufman RJ. The unfolded protein response: a stress signaling pathway critical for health and disease. *Neurology* 2006; **66:** S102-109.

12. Hetz C. The unfolded protein response: controlling cell fate decisions under ER stress and beyond. *Nat Rev Mol Cell Biol* 2012; **13:** 89-102.

13. Travers KJ, Patil CK, Wodicka L, Lockhart DJ, Weissman JS, Walter P. Functional and genomic analyses reveal an essential coordination between the unfolded protein response and ER-associated degradation. *Cell* 2000; **101:** 249-258.

14. Yoshida H, Matsui T, Hosokawa N, Kaufman RJ, Nagata K, Mori K. A time-dependent phase shift in the mammalian unfolded protein response. *Dev Cell.* 2003; **4**: 265-271.

15. Lin JH, Li H, Yasumura D, Cohen HR, Zhang C, Panning B*, et al.* IRE1 signaling affects cell fate during the unfolded protein response. *Science* 2007; **318:** 944-949.

16. Haynes CM, Titus EA, Cooper AA. Degradation of misfolded proteins prevents ER derived oxidative stress and cell death. *Mol Cell* 2004; **15:** 767-776.

17. Edelmann P, Gallant J. Mistranslation in E. coli. *Cell* 1977; **10:** 131-137.

18. Palmer E, Wilhelm JM. Mistranslation in a eucaryotic organism. *Cell* 1978; **13:** 329-334.

19. Palmer E, Wilhelm JM, Sherman F. Phenotypic suppression of nonsense mutants in yeast by aminoglycoside antibiotics. *Nature* 1979; **277:** 148-150.

20. Stansfield I, Jones KM, Herbert P, Lewendon A, Shaw WV, Tuite MF. Missense translation errors in Saccharomyces cerevisiae. *J Mol Biol* 1998; **282:** 13-24.

21. Wilhelm JM, Pettitt SE, Jessop JJ. Aminoglycoside antibiotics and eukaryotic protein synthesis: structure--function relationships in the stimulation of misreading with a wheat embryo system. *Biochem* 1978; **17:** 1143-1149.

22. Buchanan JH, Stevens A, Sidhu J. Aminoglycoside antibiotic treatment of human fibroblasts: intracellular accumulation, molecular changes and the loss of ribosomal accuracy. *Eur J Cell Biol* 1987; **43:** 141-147.

23. Abraham AK, Pihl A. Effect of protein synthesis inhibitors on the fidelity of translation in eukaryotic systems. *Biochim Biophys Acta* 1983; **741:** 197-203.

24. Burke JF, Mogg AE. Suppression of a nonsense mutation in mammalian cells in vivo by the aminoglycoside antibiotics G-418 and paromomycin. *Nucleic Acids Res* 1985; **13:** 6265-6272.

25. Howard M, Frizzell RA, Bedwell DM. Aminoglycoside antibiotics restore CFTR function by overcoming premature stop mutations. *Nat Med* 1996; **2:** 467-469.

26. Bedwell DM, Kaenjak A, Benos DJ, Bebok Z, Bubien JK, Hong J, et al. Suppression of a CFTR premature stop mutation in a bronchial epithelial cell line. *Nat Med* 1997; **3**: 1280-1284.

27. Nudelman I, Rebibo-Sabbah A, Shallom-Shezifi D, Hainrichson M, Stahl I, Ben-Yosef T, *et al.* Redesign of aminoglycosides for treatment of human genetic diseases caused by premature stop mutations. *Bioorg Med Chem Lett* 2006; **16:** 6310-6315.

28. Jin QH, Zhao B, Zhang XJ. Cytochrome c release and endoplasmic reticulum stress are involved in caspase-dependent apoptosis induced by G418. *Cell Mol Life Sci*. 2004; **61**:1816-1825.

29. Quiros Y, Vicente-Vicente L, Morales AI, López-Novoa JM, López-Hernández FJ. An integrative overview on the mechanisms underlying the renal tubular cytotoxicity of gentamicin. *Toxicol Sci*. 2011; **119**: 245-256.

30. Forge A, Schacht J. Aminoglycoside antibiotics. *Audiol Neurootol* 2000; **5:** 3-22. 25.

31. Kass JS, Shandera WX. Nervous system effects of antituberculosis therapy. *CNS drugs* 2010; **24:** 655-667.

32. Tan J, Shepherd RK. Aminoglycoside-induced degeneration of adult spiral ganglion neurons involves differential modulation of tyrosine kinase B and p75 neurotrophin receptor signaling. *Am J Pathol* 2006; **169:** 528-543.

33. Jeong SW, Kim LS, Hur D, Bae WY, Kim JR, Lee JH. Gentamicin-induced spiral ganglion cell death: apoptosis mediated by ROS and the JNK signaling pathway. *Acta Otolaryngol* 2010; **130:** 670-678.

34. Hinojosa R, Lerner SA. Cochlear neural degeneration without hair cell loss in two patients with aminoglycoside ototoxicity. *J Infect Dis* 1987; **156:** 449-455.

35. Sone M, Schachern PA, Paparella MM. Loss of spiral ganglion cells as primary manifestation of aminoglycoside ototoxicity. *Hear Res* 1998, **115:** 217-223.

36. Wu WJ, Sha SH, McLaren JD, Kawamoto K, Raphael Y, Schacht J. Aminoglycoside ototoxicity in adult CBA, C57BL and BALB mice and the Sprague-Dawley rat. *Hear Res* 2001; **158:** 165-178.

37. Reimold AM, Etkin A, Clauss I, Perkins A, Friend DS, Zhang J*, et al.* An essential role in liver development for transcription factor XBP-1. *Genes Dev* 2000; **14:** 152-157.

38. Southern PJ, Berg P. Transformation of mammalian cells to antibiotic resistance with a bacterial gene under control of the SV40 early region promoter. *J Mol Appl Genet* 1982; **1:** 327-341.

39. Takano M, Okuda M, Yasuhara M, Hori R. Cellular toxicity of aminoglycoside antibiotics in G418-sensitive and -resistant LLC-PK1 cells. *Pharm Res* 1994; **11:** 609-615.

40. Kampinga HH, Hageman J, Vos MJ, Kubota H, Tanguay RM, Bruford EA*, et al.*Guidelines for the nomenclature of the human heat shock proteins. *Cell Stress Chaperones* 2009; **14:** 105-111.

41. Harding HP, Novoa I, Zhang Y, Zeng H, Wek R, Schapira M, Ron D. Regulated translation initiation controls stress-induced gene expression in mammalian cells. *Mol Cell.* 2000; **6**: 1099-1108.

42. Manuvakhova M, Keeling K, Bedwell DM. Aminoglycoside antibiotics mediate contextdependent suppression of termination codons in a mammalian translation system. *Rna* 2000; **6:** 1044-1055.

43. Schneider-Poetsch T, Ju J, Eyler DE, Dang Y, Bhat S, Merrick WC*, et al.* Inhibition of eukaryotic translation elongation by cycloheximide and lactimidomycin. *Nat Chem Biol* 2010; **6:** 209-217.

44. Wang, Y., Shen, J., Arenzana, N., Tirasophon, W., Kaufman, R. J., and Prywes. Activation of ATF6 and an ATF6 DNA Binding Site by the Endoplasmic Reticulum Stress Response. R. *J Biol Chem.* 2000; **275**: 27013-27020.

45. H. Yoshida, K. Haze, H. Yanagi, T. Yura, and K. Mori. Identification of the *cis*-acting endoplasmic reticulum stress response element responsible for transcriptional induction of mammalian glucose-regulated proteins; involvement of basic leucine zipper transcription factors. *J Biol Chem*. 1998; **273**: 33741-33749.

46. Anderson P, Kedersha N. Stressful initiations. *J Cell Sci* 2002; **115:** 3227-3234.

47. Shulman E, Belakhov V, Wei G, Kendall A, Meyron-Holtz EG, Ben-Shachar D*, et al.* Designer aminoglycosides that selectively inhibit cytoplasmic rather than mitochondrial ribosomes show decreased ototoxicity: a strategy for the treatment of genetic diseases. *J Biol Chem* 2014; **289:** 2318-2330.

48. Xie J, Talaska AE, Schacht J. New developments in aminoglycoside therapy and ototoxicity. *Hear Res* 2011; **281:** 28-37.

49. Geisse S, Voedisch B. Transient expression technologies: past, present, and future. *Methods Mol Biol* 2012; **899:** 203-219.

50. Walter P, Ron D. The unfolded protein response: from stress pathway to homeostatic regulation. *Science* 2011; **334:** 1081-1086.

51. Ozcan U, Cao Q, Yilmaz E, Lee AH, Iwakoshi NN, Ozdelen E*, et al.* Endoplasmic reticulum stress links obesity, insulin action, and type 2 diabetes. *Science* 2004; **306:** 457-461.

52. Taleb M, Brandon CS, Lee FS, Harris KC, Dillmann WH, Cunningham LL. Hsp70 inhibits aminoglycoside-induced hearing loss and cochlear hair cell death. *Cell Stress Chaperones* 2009; **14:** 427-437.

53. Jiang H, Sha SH, Forge A, Schacht J. Caspase-independent pathways of hair cell death induced by kanamycin in vivo. *Cell Death Differ* 2006; **13:** 20-30.

54. Fujinami Y, Mutai H, Mizutari K, Nakagawa S, Matsunaga T. A novel animal model of hearing loss caused by acute endoplasmic reticulum stress in the cochlea. *J Pharmacol Sci* 2012; **118**: 363-372.

55. Peyrou M, Hanna PE, Cribb AE. Cisplatin, gentamicin, and p-aminophenol induce markers of endoplasmic reticulum stress in the rat kidneys. *Toxicol Sci* 2007; **99**: 346-353.

56. Kujawa SG, Liberman MC. Adding insult to injury: cochlear nerve degeneration after—temporaryll noise-induced hearing loss. *J Neurosci* 2009; **29**: 14077-14085.

57. Carrell RW, Lomas DA. Conformational disease. *Lancet* 1997; **350:** 134-138.

58. Gidalevitz T, Kikis EA, Morimoto RI. A cellular perspective on conformational disease: the role of genetic background and proteostasis networks. *Curr Opin Struct Biol* 2010; **20:** 23-32.

59. Francis SP, Katz J, Fanning KD, Harris KA, Nicholas BD, Lacy M, Pagana J, Agris PF, Shin JB. A novel role of cytosolic protein synthesis inhibition in aminoglycoside ototoxicity. *J Neurosci* 2013; **33**: 3079-3093.

60. Matt T, Ng CL, Lang K, Sha SH, Akbergenov R, Shcherbakov D*, et al.* Dissociation of antibacterial activity and aminoglycoside ototoxicity in the 4-monosubstituted 2-deoxystreptamine apramycin. *Proc Natl Acad Sci* 2012; **109:** 10984-10989.

61. Salas-Marco J, Bedwell DM. Discrimination between defects in elongation fidelity and termination efficiency provides mechanistic insights into translational readthrough. *J Mol Biol* 2005; **348:** 801-815.

62. Kramer EB, Vallabhaneni H, Mayer LM, Farabaugh PJ. A comprehensive analysis of translational missense errors in the yeast Saccharomyces cerevisiae. *Rna* 2010; **16:** 1797-1808.

63. Pfaffl MW. A new mathematical model for relative quantification in real-time RT-PCR. *Nucleic Acids Res* 2001; **29:** e45.

64. Oishi N, Kendall A, Schacht J. Metformin protects against gentamicin-induced hair cell death in vitro but not ototoxicity in vivo. *Neurosci Lett* 2014; **583**: 65-69.

65. Oishi N, Chen FQ, Zheng HW, Sha SH. Intra-tympanic delivery of short interfering RNA into the adult mouse cochlea. *Hear Res* 2013; **296:** 36-41.

66. Zhao LJ, Subramanian T, Zhou Y, Chinnadurai G. Acetylation by p300 regulates nuclear localization and function of the transcriptional corepressor CtBP2. *J Biol Chem* 2006; **281:** 4183-4189.

67. Tong M, Brugeaud A, Edge AS. Regenerated synapses between postnatal hair cells and auditory neurons. *J Assoc Res Otolaryngol* 2013; **14:** 321-329.

Supplementary Information

Figure S1 Translation and viability assays

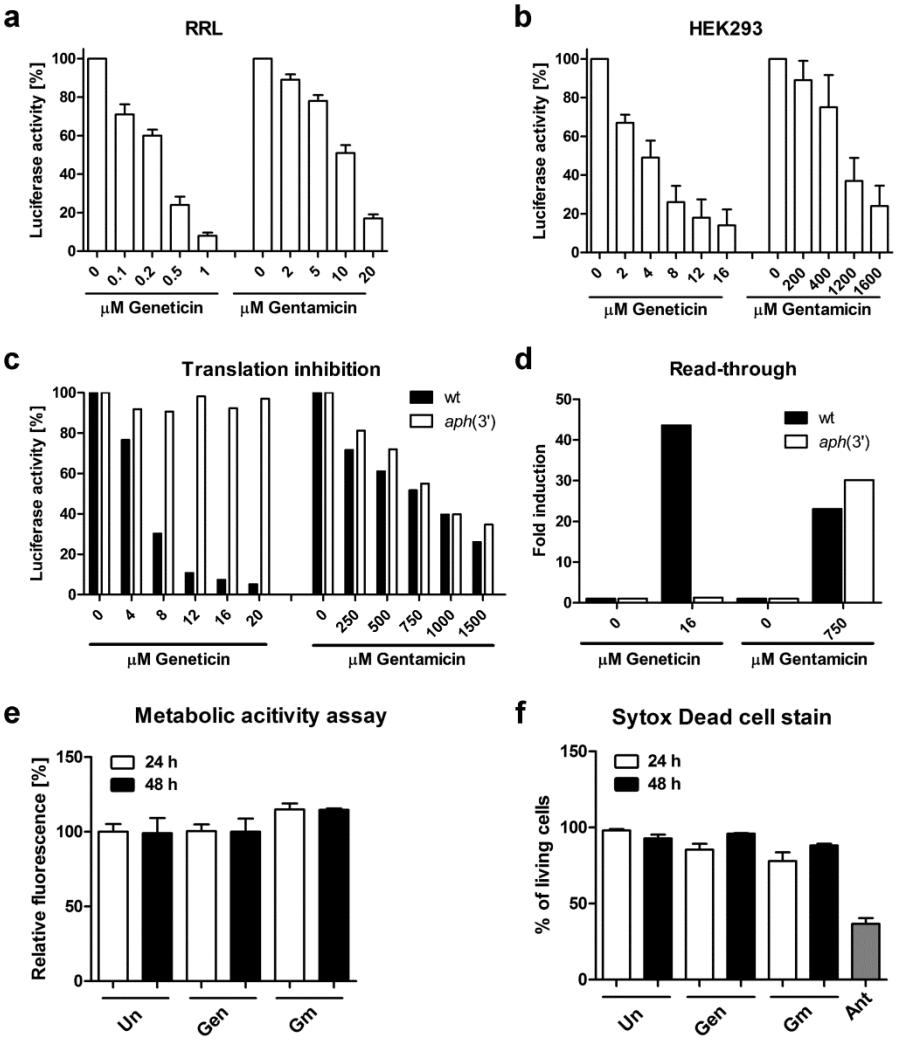

(**a–c**) Aminoglycoside-induced translation inhibition in (**a**) Rabbit reticulocyte lysate (RRL), (**b**) HEK wild-type cells, (**c**) HEK wild-type versus HEK *aph*(3') cells. Translation inhibition is measured by hRluc activity; hRluc signals of untreated samples are set as 100% luciferase activity. (**d**) Read-through, measured in HEK wild-type versus HEK *aph*(3') cells, indicated by the ratio hFluc/hRluc and given as fold induction. Untreated samples are set as 1. (**e**) Metabolic activity assay. HEK wild-type cells were treated with geneticin (16 µM) or gentamicin (400 µM). The Alamar Blue fluorescence level of the untreated samples average was set as 100%. No statistical difference was observed between treated and untreated controls. (**f**) Sytox Dead cell stain. HEK wild-type cells were treated with geneticin (16 µM) or gentamicin (400 µM), stained with Sytox Red and analyzed by FACS. Antimycin (20 µg/mL for 8 h) was used as positive control for cell death. The fluorescence level of the untreated samples average was set as 100% and percentage of living cells are presented. Treatment with geneticin and gentamicin slightly decreased cell viability by 5-15% ($p<0.05$) (**a,b,e,f**) Data are presented as means + SEM (n = 3). Gen: Genteicin; Gm: Gentamicin; Ant: Antimycin; Un: Untreated.

Figure S2 Transcriptome analysis of geneticin-treated HEK wild-type cells

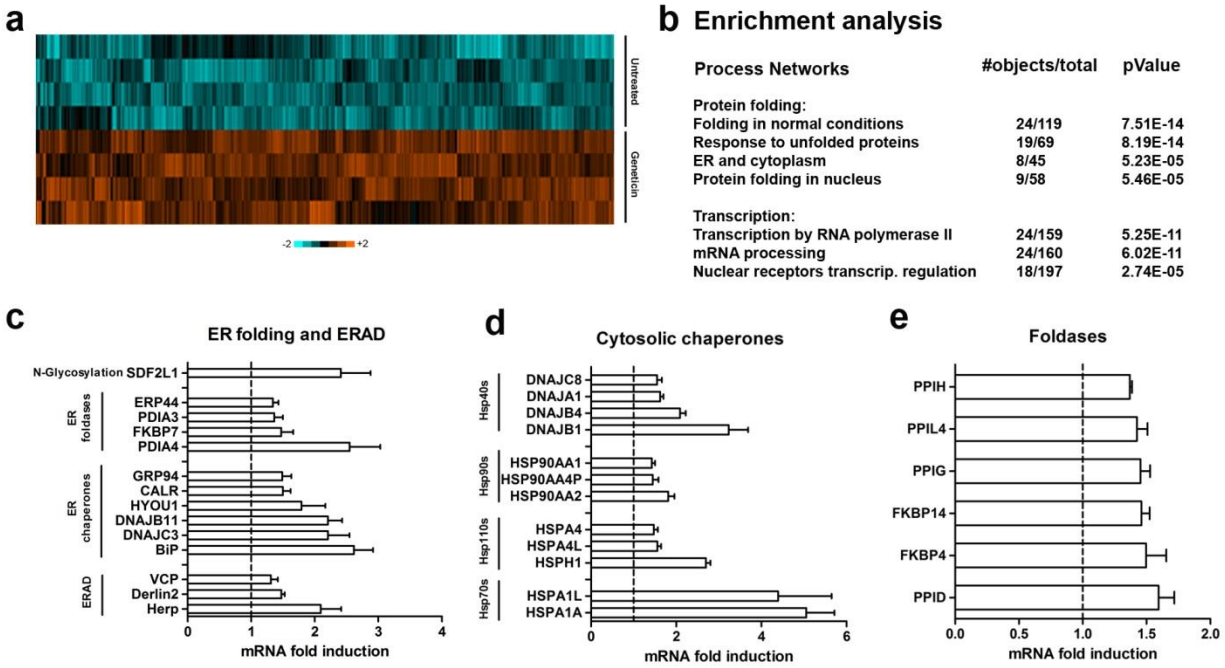

(**a**) A comparison of microarray analyses of four geneticin-treated biological replicates against four untreated biological replicates revealed 705 genes induced by geneticin (*Benjamini-Hochberg* corrected p-value < 0.05, FC > 1.2). The figure represents a heat map of the genes. (**b**) Functional ontology enrichment analysis indicating the most significantly enriched networks (p-value < 0.0001) of the 705 up-regulated genes. (**c, d, e**) mRNA fold induction of individual ER folding machinery and ERAD components(**c**), chaperones of the Hsp70, Hsp90, Hsp110, and Hsp40 protein families (**d**), and foldases (**e**) (*Benjamini-Hochberg* corrected p-value < 0.05).

Methods HEK cells were treated with 16 µM geneticin in F10 medium with 15 ug/mL saponin at 37 °C for 32 h. RNA was extracted from four independent samples for each condition (geneticin-treated, untreated). Biotinylated single-strand cDNA targets were prepared from 200 ng of total RNA, using the Ambion WT Expression Kit and the Affymetrix GeneChip WT Terminal Labeling Kit according to the manufacturer's protocols. Following fragmentation and end-labeling, 1.9 µg of cDNAs were hybridized for 16 h at 45 °C on GeneChip Human Gene 1.0 ST arrays (Affymetrix) interrogating 28,869 genes represented by approximately 27 probes spread across the full length of the gene. The chips were washed and stained in the GeneChip Fluidics Station 450 (Affymetrix) and scanned with the GeneChip® Scanner 3000 7G (Affymetrix) at a resolution of 0.7 µm. Raw data (.CEL intensity files) were extracted from the scanned images using the Affymetrix GeneChip Command Console, version 3.2. CEL files were further processed with Affymetrix Expression Console software version 1.1 to calculate probe set signal intensities using Robust Multi-array Average algorithms with default settings. Hierarchical clustering was performed using Cluster and TreeView software (http://www-microarrays.u-strasbg.fr). Functional ontology enrichment of process networks was analysed with the MetaCore software (GeneGo, Thomson Reuters). Significance of the difference in expression of each gene between treated and untreated samples was tested using the TREAT method and the correction of Benjamini-Hochberg for multiple testing was applied in order to take into account the number of tests performed. Corrected p-values < 0.05 were considered as significant.

Figure S3 Aminoglycoside-induced UPR in Hela cells.

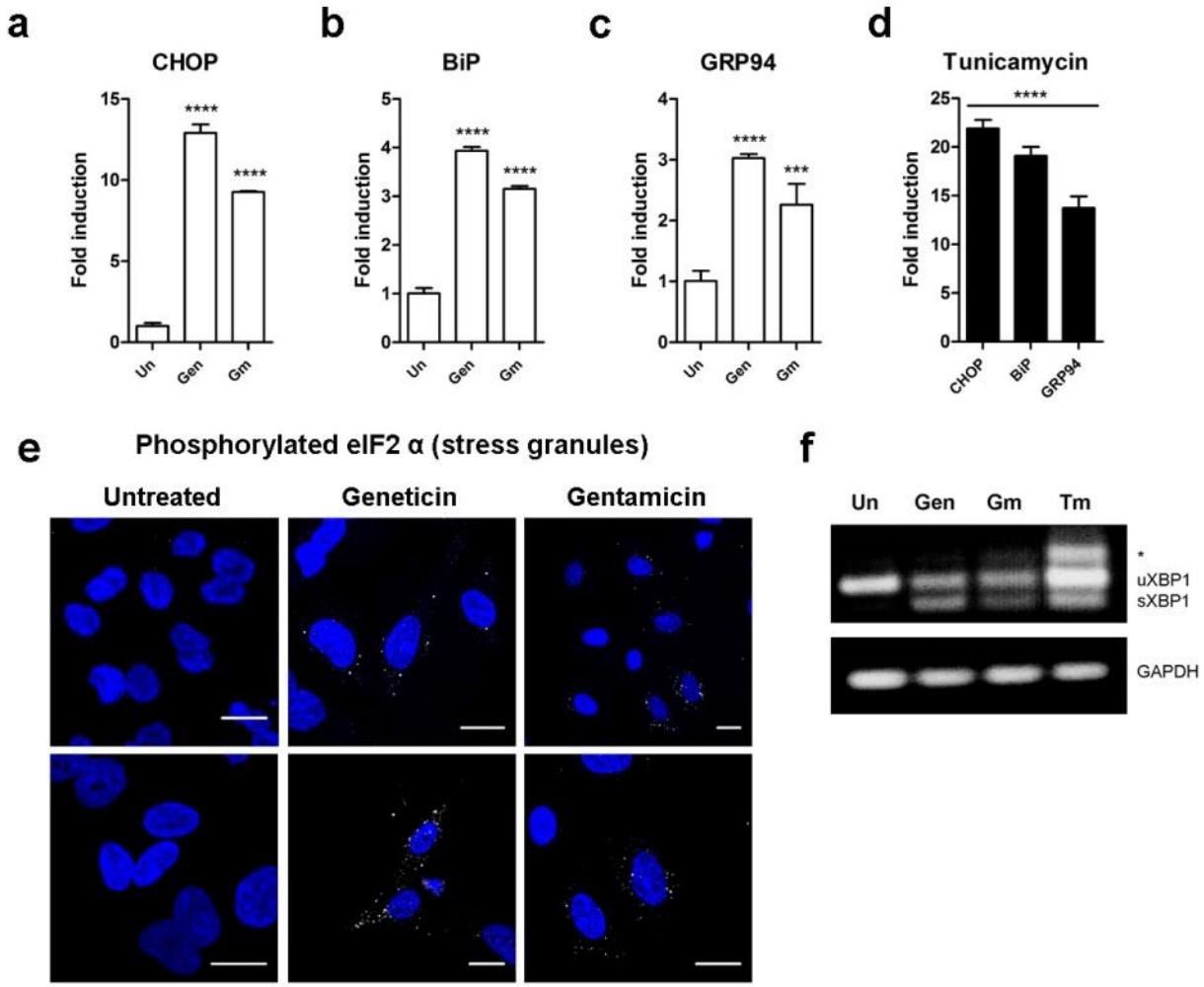

(**a–d**) qPCR analysis. Hela wild-type cells were treated with geneticin (16 µM) or gentamicin (400 µM) and incubated for 24 h. Expression of CHOP (**a**), BiP (**b**), and GRP94 (**c**) mRNA is shown. (**d**) Tunicamycin was use as positive control. Experiments were run in triplicates and means + SD of fold induction relative to untreated samples are presented; ***P< 0.005; ****P<0.001. (**e**) Stress granule formation. Hela wild-type cells were treated with geneticin (16 µM) or gentamicin (400 µ M) for 24 h. Phosphorylated eIF2α was detected by immunofluorescence. Scale bars: 20 µm. Two representative pictures shown for each sample. (**f**) XBP1 splicing assay. Hela wild-type cells were treated with geneticin (16 µM) or gentamicin (400 µM) for 24 h, or left untreated. Products of XBP1 PCR were analyzed by gel electrophoresis; unspliced (uXBP1) and spliced (sXBP1) versions of XBP1 are indicated. Tunicamycin (2.5 µg/mL) was a positive control to induce ER stress; GAPDH was a loading control. The asterisk indicates the position of a hybrid amplicon (ref 15). Gen: Geneticin; Gm: Gentamicin; Tm: Tunicamycin; UN: Untreated.

Figure S4 Effect of tunicamycin on cochlear explants

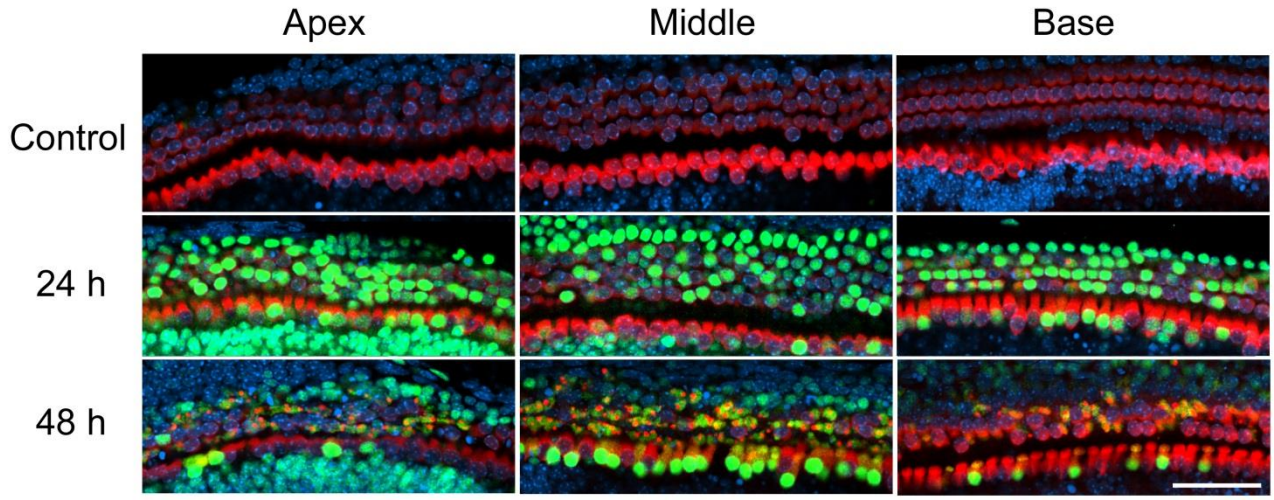

Control: The specific ER stress-associated pro-apoptotic factor, CHOP (green) is absent from untreated organ of Corti explants of CBA/J mice (P2–3). **24 h:** After a 24-h incubation, tunicamycin (0.07 µg/mL) induced CHOP in the nuclei of most hair cells from base to apex of the organ of Corti. **48 h:** Loss of staining consistent with beginning hair cell death. Green: CHOP, red: Myo 7a stain for hair cells, blue: Hoechst 33342 staining for nuclei. The figure represents three different explants at each time point. Scale bar: 50 µm.

Figure S5 Effect of gentamicin on hair cells *in vitro* and *in vivo*

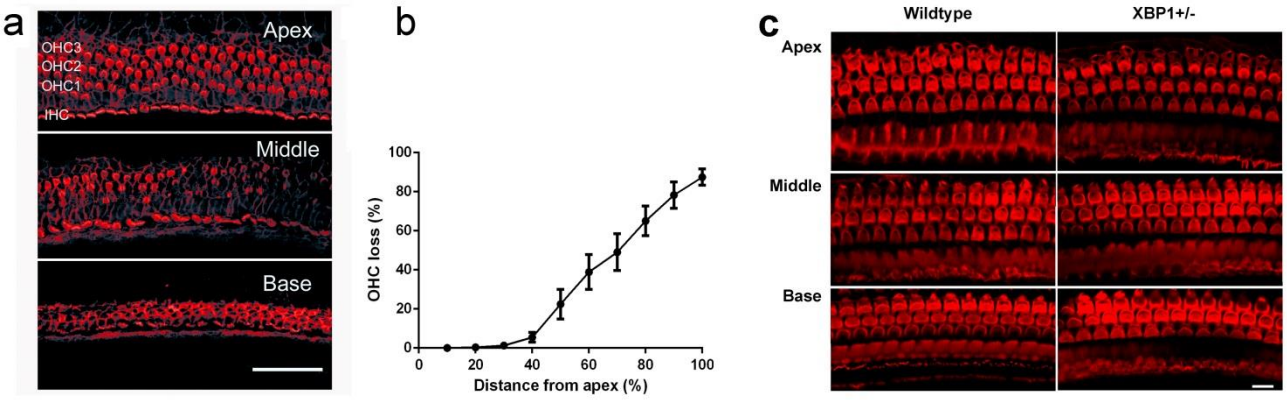

a, b: Effect of gentamicin on hair cells in cochlear explants. (**a**) Loss of OHCs due to gentamicin treatment (3.5 µM for 72 h) showed the typical base-to-apex gradient with most destruction in the base. The figure represents six different explants from CBA/J mice. (**b**) Complete quantification of hair cell loss from apex to base of the explant. Data are mean ± SD. Red: rhodamine phalloidin to outline hair cell structure. Scale bar: 50 µm.

c: Effect of intratympanic application of gentamicin. Surface preparations from adult wild-type and XBP1$^{+/-}$ mice previously treated with intratympanically applied gentamicin were examined from base to apex. Actin staining (red) showed the presence of OHC cuticular plates and stereocilia in all parts of the cochlea, except for minor scattered loss at the base. Five wildtype and five XBP1$^{+/-}$ mice were treated with gentamicin; the images are representative samples. Scale bar: 10 µm.

Figure S6 Distortion product otoacoustic emissions (DPOAE) remain unaltered by intratympanic gentamicin treatment

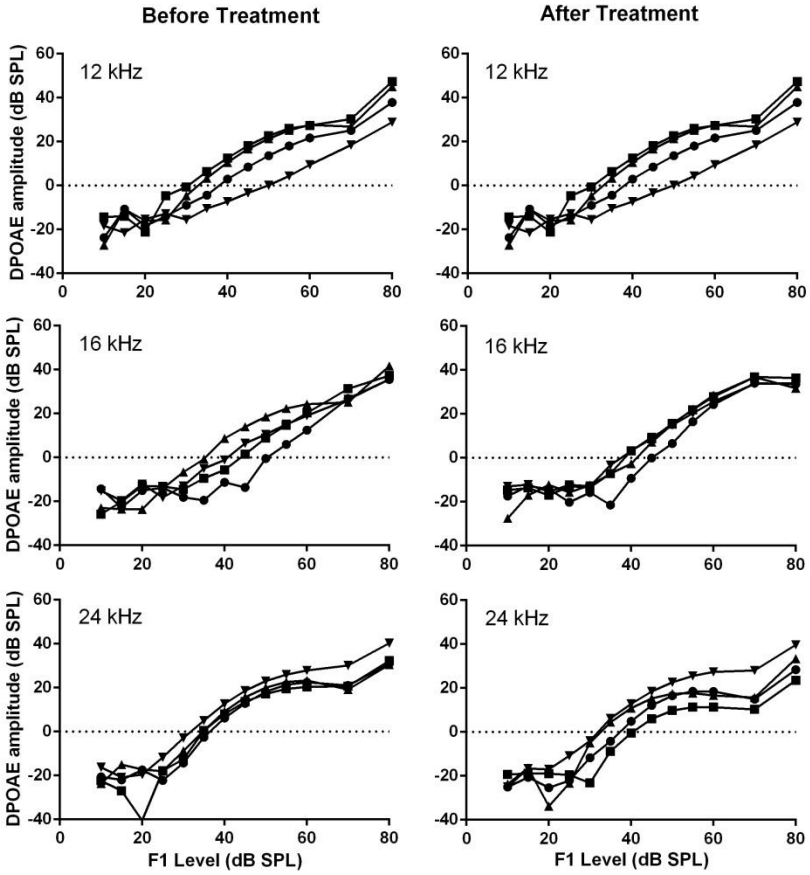

Animals were anesthetized with ketamine 65 mg/kg, xylazine 3.5 mg/kg, and acepromazine 2 mg/kg and body temperature was maintained. The primary tones, F1 and F2, were set at a F2/F1 ratio of 1.2. The intensity of F1 (L1) was varied in 5- or 10-dB steps (with the intensity of F1 ranging from 10–80 dB SPL), and the intensity of F2 (L2) was maintained 10 dB lower than L1. DPOAE were measured at 2F1 - F2. Tones were presented via two EC1 drivers (TDT) connected through an electret condenser microphone (Knowles Acoustics, type FG-23329-P07). TDT System III hardware and SigGen/BioSig software were used to present the stimuli and record responses. DPOAE responses in four adult $XBP1^{+/-}$ mice were measured before and after gentamicin treatment. Lines for the four animals are distinguished by different symbols.

Supplementary Table 1.

List of analyzed UPR and ER folding machinery genes and human chaperones and foldases.
* Genes considered significantly regulated (p-value ≤ BH correction)

Gene symbol	Other symbols	Fold change	P-value	BH correction
UPR(Lecca, Wagner et al. 2005, Sharma, Jiang et al. 2007, Hetz 2012) UPR sensors				
ERN1	IRE1	0.88	0.193	0.013
EIF2AK3	PERK	1.26	0.033	0.006
ATF6		1.03	0.778	0.034
ATF6B		0.68	0.001*	0.001
UPR Transcription factors				
ATF3		0.99	0.898	0.041
ATF4		0.82	0.013	0.004
ATF6		1.03	0.778	0.034
ATF6B		0.68	0.001*	0.001
XBP1		1.30	0.012	0.004
DDIT3	CHOP	1.51	0.020	0.005
ERAD(Araki and Nagata 2011) Processing and targeting				
EDEM1		0.97	0.913	0.042
EDEM2		1.04	0.806	0.036
EDEM3		1.12	0.182	0.012
PDIA2	PDI, PDIP, PDIR	0.91	0.458	0.022
HSPA5	BiP, GRP78	2.62	<0.001*	<0.001
HSP90B1	GRP94	1.49	<0.001*	<0.001
DNAJB9	ERdj4, MDG1	1.78	0.003	0.002
DNAJC10	ERdj5, JPD1	0.82	0.015	0.004
FOXRED2	ERFAD	0.74	<0.001*	<0.001
PPIB	CyclophilinB, CYPB	1.00	0.987	0.049
OS9	ERLEC2	0.96	0.724	0.032
ERLEC1	XTP3-B	1.21	0.037	0.006
SEL1L		1.25	0.061	0.007
Possible retrotranslocation channel				
SEC61A1	SEC61	1.03	0.845	0.038
SEC61A2		1.13	0.300	0.017
SEC61B		1.14	0.141	0.011
SEC61G		1.57	0.001*	0.001
DERL1	Derlin 1	1.08	0.458	0.022
DERL2	Derlin 2	1.48	<0.001*	<0.001
DERL3	Derlin 3	1.43	0.008	0.003
Other possible component or regulator				
HERPUD1	HERP, Mif1, SUP	2.10	<0.001*	<0.001

VIMP	SELS	1.43	0.004	0.002
BCAP31	BAP31	1.09	0.442	0.021
JKAMP	HSPC213, JAMP	1.20	0.011	0.004
DNAJB12	DJ10	0.99	0.961	0.046
HM13	SPP	0.99	0.949	0.045
SSR1	TRAP alpha	0.87	0.114	0.010
SSR2	TRAP beta	1.00	0.984	0.049
SSR3	TRAP gamma	0.97	0.828	0.037
SSR4	TRAP delta	0.88	0.176	0.012
TICAM2	TRAM	1.17	0.082	0.008
AUP1		1.22	0.002	0.002
SVIP		1.15	0.212	0.013
E2 ubiquitin-conjugating enzyme				
UBE2K	UBC1, HIP2	1.20	0.008	0.003
UBE2D1	UBCH5	1.42	<0.001*	<0.001
UBE2J1	UBC6	0.96	0.725	0.032
UBE2J2		1.14	0.154	0.011
UBE2G1	UBC7	1.04	0.788	0.035
UBE2G2		1.17	0.090	0.009
UBE2N	UBC13	1.11	0.233	0.014
E3 ubiquitin-ligase				
NEDD4L	NEDD4-2	1.15	0.135	0.011
PARK2	PDJ	0.67	0.001*	0.001
RNF5	RMA1	1.34	0.001*	0.001
AMFR	RNF45, GP78	0.95	0.638	0.028
SYVN1	HRD1, DER3	1.28	0.007	0.003
MARCH6	TEB4, DOA10	0.96	0.772	0.034
RNF139	HRCA1, TRC8	1.27	0.006	0.003
TRIM13	CAR, RNF77	1.01	0.971	0.047
RNF103	KF1	1.09	0.343	0.018
RNF19A	RNF19	1.12	0.212	0.013
RNF121		1.36	0.003	0.002
STUB1	CHIP	0.95	0.679	0.030
SKP1-CUL1-F-box (SCF) E3				
SKP1	OCP	1.36	0.006	0.003
CUL1	cullin-1	1.23	0.004	0.002
FBXO2	FBG1	0.88	0.160	0.011
FBXO6	FBG2	0.91	0.247	0.015
RBX1	RNF75, ROC1	1.09	0.357	0.018
E4 ubiquitin-conjugating enzyme				
UBE4B	UFD2	0.90	0.240	0.014
Substrate extraction and recruiting				
VCP	p97, ALS14	1.31	0.001*	0.002
UFD1L	UFD1	1.30	0.003	0.002
NPLOC4	NPL4	1.13	0.187	0.012

UBXD family protein				
UBXN6	UBXD1	1.02	0.905	0.042
UBXN4	UBXD2	1.12	0.226	0.014
UBXN7	UBXD7	1.31	0.010	0.003
FAF2	UBXD8	1.47	<0.001*	0.001
UBXN1	UBXD10	1.02	0.844	0.038
Deglycosylating enzyme				
NGLY1	PNGase	1.11	0.270	0.015
DUB (deubiquitination)				
VCPIP1	DUBA3, VCIP135	1.21	0.011	0.004
YOD1	DUBA8, YOD1	1.57	<0.001*	<0.001
ATXN3	Ataxin-3	1.12	0.259	0.015
USP19		1.19	0.071	0.008
Shuttle protein				
UBQLN1	Ubiquilin1	1.18	0.017	0.004
RAD23A	HR23A	0.78	0.004	0.003
RAD23B	HR23B	0.91	0.382	0.019
Ubiquitin receptor				
PSMD4	Rpn10	0.86	0.159	0.011
PSMC3	Rpt5	0.95	0.686	0.030
ADRM1	Rpn13	1.13	0.247	0.015
ER Chaperones(Lecca, Wagner et al. 2005, Hebert and Molinari 2007, Araki and Nagata 2011)				
DNAJC1	ERdj1, MTJ1	0.97	0.834	0.037
SEC63	ERdj2, DNAJC23	0.91	0.343	0.018
DNAJB11	ERdj3, HEDJ, ERj3	2.21	<0.001*	<0.001
DNAJB9	ERdj4, MDG1	1.78	0.003	0.002
DNAJC10	ERdj5, JPD1	0.82	0.015	0.004
TOR1A	Torsin A	1.05	0.636	0.028
SIL1	BAP, ULG5	1.02	0.886	0.040
HYOU1	GRP170	1.79	<0.001*	0.001
HSP90B1	GRP94	1.49	<0.001*	<0.001
HSPA5	BiP	2.62	<0.001*	<0.001
CALR	Calreticulin	1.50	<0.001*	0.001
CANX	Calnexin	1.10	0.310	0.017
SERPINH1	HSP47	1.24	0.024	0.005
LRPAP1	RAP	1.07	0.558	0.025
LEPRE1	P3H1	0.95	0.641	0.028
P4HB	P4H, ERP59, PDIA1	0.95	0.668	0.029
DNAJC3	ERdj6	2.21	<0.001*	<0.001
ER foldases(Lecca, Wagner et al. 2005, Schroder and Kaufman 2005, Hebert and Molinari 2007, Bernasconi and Molinari 2011)				
PDIA3	ERP57, ERP61, ERP60	1.36	0.001*	0.002
PDIA4	ERP70, ERP72	2.55	<0.001*	<0.001

DNAJC10	ERdj5	0.82	0.015	0.004
PDIA5	PDIR	0.97	0.832	0.037
MUTED	ERP46, PDIA15	0.98	0.903	0.042
PDIA2	PDI, PDIp, PDIr	0.91	0.458	0.022
PDILT	PDIA7	0.93	0.507	0.024
ERP44	PDIA10, TXNDC4	1.34	0.001*	0.001
TXNDC12	ERP18, PDIA16, ERP19	1.17	0.035	0.006
TMX1	TMX, PDIA11	1.06	0.589	0.026
TMX2	PDIA12	1.26	0.021	0.005
TMX3	PDIA13	0.96	0.755	0.033
TMX4	PDIA14	0.90	0.297	0.016
PDIA6	P5, ERP5, TXNDC7	1.42	0.002	0.002
ERO1LB	ERO1B	1.60	0.003	0.002
ERO1L	ERO1A	0.79	0.004	0.002
P4HB	PDIA1, ERP59	0.95	0.668	0.029
ERP29	PDIA9, ERP28, ERP31	0.67	<0.001*	0.001
PPIB	CyclophilinB, CYPB	1.00	0.987	0.049
FKBP2	FKBP13	1.05	0.717	0.032
FKBP7	FKBP23	1.47	<0.001*	0.001
FKBP10	FKBP65	0.74	0.002	0.002
FKBP11	FKBP19	1.14	0.370	0.019
N-linked Glycosylation(Lecca, Wagner et al. 2005, Schroder and Kaufman 2005)				
UGGT1	UGT1	1.00	0.973	0.047
UGGT2	UGT2	1.09	0.478	0.023
SDF2		1.50	0.003	0.002
SDF2L1		2.41	<0.001*	<0.001
MOGS	alpha glucosidase I	1.11	0.366	0.019
GANAB	alpha glucosidase II	0.80	0.006	0.003
MAN1A1	alpha mannosidase I	0.99	0.953	0.046
MAN2A1	alpha mannosidase II	0.81	0.023	0.005
ALG12		1.29	0.008	0.003
ALG5		1.30	0.006	0.003
PIGA	GPI3	1.35	0.012	0.004
PIGB		0.87	0.169	0.012
RPN1	OST1	1.01	0.942	0.045
STT3A	STT3, ITM1	0.90	0.226	0.014
DDOST	WBP1	0.95	0.653	0.029
Human Chaperones(Kampinga, Hageman et al. 2009) HSPA (Hsp70 chaperones)				
HSPA1A		5.05	<0.001*	<0.001
HSPA1L		4.40	<0.001*	<0.001
HSPA2		1.37	0.005	0.003
HSPA5	BiP, GRP78	2.62	<0.001*	<0.001
HSPA6		1.65	0.004	0.002
HSPA7		1.65	0.004	0.002
HSPA8		1.17	0.021	0.005
HSPA9		1.00	0.977	0.048

HSPA12A		0.92	0.381	0.019
HSPA12B		0.96	0.680	0.030
HSPA13		1.05	0.715	0.031
HSPA14		1.26	0.007	0.003
HSPH (Hsp110 chaperones)				
HYOU1	GRP170	1.79	<0.001*	0.001
HSPH1		2.70	<0.001*	<0.001
HSPA4		1.48	<0.001*	<0.001
HSPA4L		1.56	<0.001*	<0.001
HSPC (Hsp 90 chaperones)				
HSP90AA1		1.43	<0.001*	<0.001
HSP90AA2		1.81	<0.001*	<0.001
HSP90AB1		1.06	0.651	0.029
HSP90B1	GRP94	1.49	<0.001*	<0.001
TRAP1		0.82	0.016	0.004
DnaJA (Hsp40 co-chaperones)				
DNAJA1		1.62	<0.001*	<0.001
DNAJA2		1.14	0.121	0.010
DNAJA3		1.12	0.169	0.012
DNAJA4		0.99	0.938	0.044
DnaJB (Hsp40 co-chaperones)				
DNAJB1		3.23	<0.001*	<0.001
DNAJB2		0.90	0.376	0.019
DNAJB3		0.93	0.517	0.024
DNAJB4		2.09	<0.001*	<0.001
DNAJB5		1.10	0.321	0.017
DNAJB6		1.22	0.018	0.004
DNAJB7		0.99	0.921	0.043
DNAJB8		0.90	0.217	0.014
DNAJB9		1.78	0.003	0.002
DNAJB11		2.21	<0.001*	<0.001
DNAJB12		0.99	0.961	0.046
DNAJB13		1.00	0.963	0.047
DNAJB14		1.04	0.721	0.032
DnaJC (Hsp40 co-chaperones)				
DNAJC1		0.97	0.834	0.037
DNAJC2	MPP11	1.19	0.021	0.005
DNAJC3	ERdj6	2.21	<0.001*	<0.001
DNAJC4		0.82	0.020	0.005
DNAJC5		1.05	0.693	0.030
DNAJC5B		0.99	0.946	0.045
DNAJC5G		1.00	0.984	0.049
DNAJC6		1.31	0.006	0.003
DNAJC7		1.10	0.223	0.014

DNAJC8		1.55	0.001*	0.001
DNAJC9		1.22	0.028	0.005
DNAJC10	ERdj5	0.82	0.015	0.004
DNAJC11		1.38	0.008	0.003
DNAJC12		1.11	0.372	0.019
DNAJC13		0.96	0.781	0.035
DNAJC14		1.01	0.924	0.043
DNAJC15		0.98	0.874	0.040
DNAJC16		0.80	0.015	0.004
DNAJC17		#N/A	#N/A	#N/A
DNAJC18		0.75	0.001*	0.001
DNAJC19	TIMM14	0.98	0.897	0.041
DNAJC21		1.03	0.769	0.034
DNAJC22		0.98	0.868	0.039
DNAJC24	DPH4	1.15	0.112	0.010
DNAJC25		1.19	0.023	0.005
DNAJC27		1.12	0.349	0.018
DNAJC28		0.96	0.703	0.031
DNAJC30		0.99	0.972	0.047
HSCB		1.04	0.776	0.034
SEC63	ERdj2	0.91	0.343	0.018
GAK	DNAJC26	1.06	0.638	0.028
SACS	DNAJC29	1.10	0.328	0.017
HspB (small heat shock proteins)				
HSPB1	HSP25	1.90	0.001*	0.001
HSPB2	HSP27	0.93	0.532	0.024
HSPB3	HSPL27	1.07	0.611	0.027
HSPB6	HSP20	#N/A	#N/A	#N/A
HSPB7		0.92	0.466	0.022
HSPB8		1.42	0.121	0.010
HSPB9		0.91	0.356	0.018
HSPB11		1.11	0.290	0.016
HSPBAP1		1.18	0.049	0.007
CRYAA		0.88	0.224	0.014
CRYAB		1.03	0.811	0.036
Chaperonin (Hsp10 and 60)				
HSPD1	HSP60, GROEL	1.15	0.036	0.006
HSPD1P1		1.36	0.010	0.003
HSPE1	HSP10, GROES	1.58	<0.001*	<0.001
MKKS		0.99	0.940	0.045
BBS10		1.30	0.012	0.004
BBS12		1.15	0.260	0.015
Chaperone regulator				
STIP1		1.72	<0.001*	<0.001
CLIPs (ribosome-associated chaperones)				
TCPA1		1.19	0.005	0.003

CCT2		1.07	0.525	0.024
CCT3		1.13	0.133	0.010
CCT4		1.10	0.264	0.015
CCT5		1.14	0.047	0.007
CCT6A		1.26	<0.001*	0.001
CCT6B		0.97	0.855	0.039
CCT7		1.13	0.089	0.009
CCT8		1.10	0.292	0.016
PFDN1		1.22	0.007	0.003
PFDN2		1.15	0.088	0.009
VBP1		1.29	0.009	0.003
PFDN4		1.21	0.048	0.007
PFDN5		0.99	0.963	0.047
PFDN6		1.48	<0.001*	0.001
DNAJC2		1.19	0.021	0.005
HSPA14		1.26	0.007	0.003
BTF3		1.01	0.956	0.046
NACA		1.01	0.955	0.046
Peptidylprolyl cis-trans Isomerases (PPI)(Gerard, Deleersnijder et al. 2011, Benham 2012)				
FKBP1A		1.04	0.056	0.007
FKBP1B		1.14	0.197	0.013
FKBP2		1.05	0.717	0.032
FKBP3		1.04	0.723	0.032
FKBP4		1.50	<0.001*	0.001
FKBP5		1.27	0.003	0.002
FKBP6		0.88	0.206	0.013
FKBP7		1.47	<0.001*	0.001
FKBP8		0.97	0.817	0.036
FKBP9		0.83	0.060	0.007
FKBP9L		0.81	0.023	0.005
FKBP10		0.74	0.002	0.002
FKBP11		1.14	0.370	0.019
FKBP14		1.46	0.001*	0.001
FKBPL		1.02	0.843	0.038
PIN1		1.15	0.073	0.008
PIN1P1		#N/A	#N/A	#N/A
PIN4		1.18	0.154	0.011
PPIA		1.08	0.418	0.020
PPIAL4A		1.02	0.927	0.044
PPIAL4B		1.00	0.927	0.044
PPIAL4C		1.00	0.927	0.044
PPIAL4D		#N/A	#N/A	#N/A
PPIAL4E		1.00	0.927	0.044
PPIAL4F		1.00	0.927	0.044
PPIAL4G		0.97	0.908	0.042
PPIB	CyclophilinB, CYPB	1.00	0.987	0.049
PPIC		0.92	0.432	0.021
PPID		1.59	<0.001*	0.001

PPIE		1.19	0.077	0.008
PPIEL		1.04	0.949	0.045
PPIF		1.00	0.992	0.049
PPIG		1.45	<0.001*	0.001
PPIH		1.37	<0.001*	<0.001
PPIL1		1.17	0.045	0.007
PPIL2		0.82	0.010	0.003
PPIL3		0.91	0.304	0.017
PPIL4		1.42	0.001*	0.001
PPIL6		0.85	0.095	0.009
PPWD1		1.10	0.325	0.017
Protein Disulfide Isomerases (PDI)[11]				
PDIA2		0.91	0.458	0.022
PDIA3		1.36	0.001*	0.002
PDIA4		2.55	<0.001*	<0.001
PDIA5		0.97	0.832	0.037
PDIA6		1.42	0.002	0.002
PDILT		0.93	0.507	0.024
PDIK1L		0.93	0.502	0.023
P4HB		0.95	0.668	0.029
ERP27		0.97	0.880	0.040
ERP29		0.67	<0.001*	0.001
ERP44		1.34	0.001*	0.001
TMX1		1.06	0.589	0.026
TMX2		1.26	0.021	0.005
TMX3		0.96	0.755	0.033
TMX4		0.90	0.297	0.016
TXNDC5		1.21	0.274	0.016
TXNDC12		1.17	0.035	0.006
AGR2		1.07	0.528	0.024
AGR3		0.97	0.898	0.041
DNAJC10		0.82	0.015	0.004
CASQ1		0.98	0.930	0.044
CASQ2		0.92	0.397	0.020

References

Araki, K. and K. Nagata (2011). "Protein folding and quality control in the ER." Cold Spring Harb Perspect Biol **3**(11): a007526.

Benham, A. M. (2012). "The protein disulfide isomerase family: key players in health and disease." Antioxid Redox Signal **16**(8): 781-789.

Bernasconi, R. and M. Molinari (2011). "ERAD and ERAD tuning: disposal of cargo and of ERAD regulators from the mammalian ER." Curr Opin Cell Biol **23**(2): 176-183.

Gerard, M., A. Deleersnijder, J. Demeulemeester, Z. Debyser and V. Baekelandt (2011). "Unraveling the role of peptidyl-prolyl isomerases in neurodegeneration." Mol Neurobiol **44**(1): 13-27.

Hebert, D. N. and M. Molinari (2007). "In and out of the ER: protein folding, quality control, degradation, and related human diseases." Physiol Rev **87**(4): 1377-1408.

Hetz, C. (2012). "The unfolded protein response: controlling cell fate decisions under ER stress and beyond." Nat Rev Mol Cell Biol **13**(2): 89-102.

Kampinga, H. H., J. Hageman, M. J. Vos, H. Kubota, R. M. Tanguay, E. A. Bruford, M. E. Cheetham, B. Chen and L. E. Hightower (2009). "Guidelines for the nomenclature of the human heat shock proteins." Cell Stress Chaperones **14**(1): 105-111.

Lecca, M. R., U. Wagner, A. Patrignani, E. G. Berger and T. Hennet (2005). "Genome-wide analysis of the unfolded protein response in fibroblasts from congenital disorders of glycosylation type-I patients." FASEB J **19**(2): 240-242.

Schroder, M. and R. J. Kaufman (2005). "The mammalian unfolded protein response." Annu Rev Biochem **74**: 739-789.

Sharma, R., H. Jiang, L. Zhong, J. Tseng and A. Gow (2007). "Minimal role for activating transcription factor 3 in the oligodendrocyte unfolded protein response in vivo." J Neurochem **102**(5): 1703-1712.

10 List of publications

(1) **Decoding and deafness: Two sides of a coin.** Akbergenov, R., D. Shcherbakov, T. Matt, **S. Duscha**, M. Meyer, D. Perez-Fernandez, R. Pathak, S. Harish, I. Kudyba, S. R. Dubbaka, S. Silva, M. del Carmen Riuz, S. Salian, A. Vasella, E. C: Böttger. In: Ribosomes: Structure, Function and Dynamics, Eds: M. V. Rodnina, W. Wintermeyer, R. Green, Springer Verlag Vienna Austria. 2011, 249-261 ISBN 978-3-7091-0214-5.

(2) **Molecular basis for the selectivity of antituberculosis compounds capreomycin and viomycin.** Akbergenov, R., D. Shcherbakov, T. Matt, **S. Duscha**, M. Meyer, D. N. Wilson and E. C. Bottger. *Antimicrob Agents Chemother.* 2011, 55(10): 4712-4717.

(3) **Dissociation of antibacterial activity and aminoglycoside ototoxicity in the 4-monosubstituted 2-deoxystreptamine apramycin.** Matt, T., C. L. Ng, K. Lang, S. H. Sha, R. Akbergenov, D. Shcherbakov, M. Meyer, **S. Duscha**, J. Xie, S. R. Dubbaka, D. Perez-Fernandez, A. Vasella, V. Ramakrishnan, J. Schacht and E. C. Bottger. *Proc Natl Acad Sci U S A.* 2012, 109(27): 10984-10989.

(4) **Structure-activity relationships among the kanamycin aminoglycosides: role of ring I hydroxyl and amino groups.** Salian, S., T. Matt, R. Akbergenov, S. Harish, M. Meyer, **S. Duscha**, D. Shcherbakov, B. B. Bernet, A. Vasella, E. Westhof and E. C. Bottger. *Antimicrob Agents Chemother.* 2012, 56(12): 6104-6108.

(5) **4'-O-substitutions determine selectivity of aminoglycoside antibiotics.** Perez-Fernandez, D., D. Shcherbakov, T. Matt, N. C. Leong, I. Kudyba, **S. Duscha**, H. Boukari, R. Patak, S. R. Dubbaka, K. Lang, M. Meyer, R. Akbergenov, P. Freihofer, S. Vaddi, P. Thommes, V. Ramakrishnan, A. Vasella and E. C. Bottger. *Nat Commun*. 2014, 5: 3112.

(6) **Importance of the 6'-hydroxy group and its configuration for apramycin activity.** Mandhapati, A. R., D. Shcherbakov, **S. Duscha**, A. Vasella, E. C. Bottger and D. Crich. *ChemMedChem.* 2014, 9(9): 2074-2083.

(7) **Identification and evaluation of improved 4'-O-(alkyl) 4,5-disubstituted 2-deoxystreptamines as next-generation aminoglycoside antibiotics**. **Duscha, S.*****, H. Boukari*, D. Shcherbakov*, S. Salian*, S. Silva*, A. Kendall*, T. Kato*, R. Akbergenov, D. Perez-Fernandez, B. Bernet, S. Vaddi, P. Thommes, J. Schacht, D. Crich, A. Vasella and E. C. Bottger. 2014, *MBio* 5(5): e01827-01814.

(8) **XBP1 mitigates aminoglycoside-induced endoplasmic reticulum stress and neuronal cell death.** Oishi, N.*, **S. Duscha***, H. Boukari*, M. Meyer, J. Xie, G. Wei, B. Roschitzki, Boettger, E. C., Schacht, J.
Accepted for publication in Cell Death and Disease

(9) **Aminomethyl Spectinomycins as Therapeutics for Drug Resistant Respiratory Tract and Sexually Transmitted Bacterial Infections.** Bruhn, D. F:, S. L. Waidyarachchi, D. B. Madhura, D. Shcherbakov, Z. Zheng, J. Liu, Y. M. Abdelrahman, A. P. Singh, **S. Duscha**, C. Rathi, R. B. Lee, R. J. Belland, B. Meibohm, J. W. Rosch, E. C. Böttger, R. E. Lee

Accepted for publication in Science Translational Medicine

* equal contribution

11 Conference presentations

2010 **5th International Conference on the Ribosome, Orvieto, Italy**
Reconstruction of the *in vivo* Evolution of Aminoglycoside Resistance in *Mycobacterium tuberculosis* by Directed 16S rRNA Mutagenesis. **S. Duscha,** M. Meyer, D. Shcherbakov, E.C. Böttger

Aminoglycosides, Ototoxicity and Malfunction of the Mitoribosome: Towards Synthesis of New Compounds with Altered Drug-Target Interaction. E.C. Böttger, T. Matt, R . Akbergenov, D. Sherbakov, **S. Duscha**, M. Meyer, D. Perez-Fernandez, S.R: Dubakka, A. Vasella

2011 **EMBO Protein synthesis and translational control, Heidelberg, Germany**
Molecular Basis for the Selectivity of Antituberculosis Compounds Capreomycin and Viomycin. M. Meyer, R. Akbergenov, **S. Duscha**, D. N. Wilson, E. C. Böttger

2012 **EMBO Quality Control – From Molecules to Organelles, Heidelberg, Germany**
Mitochondrial DNA Positions 1555 and 1494 Control Quality of Mitoribosomal Protein Biogenesis. D. Shcherbakov, H. Boukari, R. Akbergenov, T. Matt, **S. Duscha**, M. Mayer, P. Freihofer, E.C. Böttger

2013 **6th International Conference on the Ribosome, Napa Valley, USA**

Dissociation of Antibacterial Activity and Aminoglycoside Ototoxicity in the 4-monosubstituted 2-deoxystreptamine Apramycin. **S. Duscha**, T. Matt, M. Meyer, C. L. Ng, K. Lang, S.H. Sha,R. Akbergenov, D. Shcherbakov, S. R. Dubbaka, J. Xie, A. Vasella, V. Ramakrishnan, J. Schacht, and E. C. Böttger

Synthesis of 4'-O-substituted Aminoglycosides and Selectivity of Antiribosomal Activity at the Drug Target Level. H. Boukari, D. Shcherbakov, P. Freihofer, D. Perez-Fernandez, C. L. Ng, I. Kudyba, R. Patak, K. Lang, M. Meyer, **S. Duscha**, V. Ramakrishnan, A. Vasella, E. C. Böttger